Magmatic olivine as a tool to investigate geochemical mantle heterogeneities beneath Iceland

Maja Bar Rasmussen

Faculty of Earth Sciences
University of Iceland
2021

Magmatic olivine as a tool to investigate geochemical mantle heterogeneities beneath Iceland

Maja Bar Rasmussen

Dissertation submitted in partial fulfillment of a
Philosophiae Doctor degree in Geology

PhD Committee
Sæmundur A. Halldórsson
Sally A. Gibson
Guðmundur H. Guðfinnsson

Opponents
Abigail K. Barker
Kevin W. Burton

Faculty of Earth Sciences
School of Engineering and Natural Sciences
University of Iceland
Reykjavik, January 2021

Magmatic olivine as a tool to investigate geochemical mantle heterogeneities beneath Iceland
Dissertation submitted in partial fulfillment of a *Philosophiae Doctor* degree in Geology

Faculty of Earth Sciences
School of Engineering and Natural Sciences
University of Iceland
Sturlugata 7
101, Reykjavik
Iceland

Telephone: 525 4000

Bibliographic information:
Maja Bar Rasmussen, 2021, *Magmatic olivine as a tool to investigate geochemical mantle heterogeneities beneath Iceland*, PhD dissertation, Faculty of Earth Sciences, University of Iceland, 127 pp.

Author ORCID: 0000-0002-1579-2966
ISBN: 978-9935-9555-1-7

Printing: Háskólaprent
Reykjavik, Iceland, January 2021

Abstract

The extent of compositional and lithological heterogeneity in Earth's convecting mantle, caused by the recycling of oceanic and continental lithosphere, has long been a subject of interest to geochemists and geophysicists. A fundamental outstanding question that is still widely debated is: how is recycling of crustal material preserved in ocean island basalts?

Olivine is usually the first mineral to crystallise during the ascent of mantle-derived melts and is stable over a large range in pressure, temperature, and melt composition. Because of this, the chemistry of olivine is often used as a proxy for primitive melt compositions prior to secondary modifications occurring in the uppermost part of the mantle and the crust. Iceland is the largest subaerial section of the global mid-ocean-ridge system and reflects the current location of the Iceland mantle plume. Previous work has shown that the mantle beneath Iceland is chemically heterogenous, and this has been attributed in part to the presence of recycled crust entrained within the upwelling plume. The recognition of a chemically heterogenous plume, together with the widespread occurrence of primitive basalts, makes Iceland an ideal location to identify the properties of recycled crust in a mantle plume from the chemical composition of high-forsterite olivine.

This thesis is in three parts where I present a detailed study of high-forsterite olivine from the active rift and flank zones as well as older crust in Iceland. I apply a combination of *in-situ* and bulk digestion analytical techniques to produce an internally-consistent, high-precision dataset for distinguishing mantle-derived variability from the effect of secondary processes, such as fractional crystallisation and assimilation. In the first part of the thesis, I use minor and trace elements in olivine and previously published He isotopes to show, that the geochemical heterogeneity beneath Iceland is mainly caused by the Iceland plume entraining pyroxene-rich mantle components, formed from recycled oceanic crust. In the second part, I use oxygen isotopic ratios in the same olivine crystals to show, that the amount of entrained recycled crust has increased since the initiation of the plume (~ 60 Ma). This is related to an increase in plume flux and melt production, which was likely facilitated by the coincidence of the Iceland mantle plume and the North Atlantic Rift starting at ~ 25 Ma and resulted in the formation of the Iceland plateau around the same time. In the final part, I explore the use of bulk digestion methods to determine Mg and Fe isotopic ratios in olivine from the same samples of Icelandic basalts to further assess the nature of this recycled component. Here, I find that variations in Mg and Fe isotopes in Icelandic olivine are mostly controlled by magma transport timescales which, going forward, could enable us to estimate residence times for olivine in the various volcanic regions.

Útdráttur

Vel er þekkt að sökk úthafsfleka niður í möttulinn á niðurstreymisflekamótum leiðir til aukins breytileika í efna- og steindasamsetningu möttuls jarðar. Hinsvegar hefur fræðasamfélagið lengi deilt um hvert umfang slíks endurunnis efnis sé í jarðmöttlinum og að hve miklu leyti og á hvaða hátt það skilar sér aftur til yfirborðs í gegnum djúpættaðar rætur úthafseyja.

Steindin ólívín er að öllu jöfnu meðal fyrstu fasa sem kristallast úr möttulættaðri bergbráð á leið til yfirborðs. Hún er stöðug yfir langt hita- og þrýstingsbil ásamt því að efnasamsetning hennar ræðst af þeirri bráð sem hún kristallast úr. Þannig hefur verið sýnt fram á að nota megi aðal- og snefilefnasamsetningu ólivínkristalla til að endurskapa þær frumbráðir sem ólivínið kristallaðist úr og að efnasamsetningin markist lítt af seinni kvikuferlum. Ísland er óvenjulega umfangsmikil landspilda þar sem úthafshryggur liggur ofansjávar. Ástæða þess er sú að Ísland er heitur reitur sem talinn er stafa af djúpstæðum möttulstrók sem flytur varma og efni í átt að yfirborði. Á grundvelli áratuga rannsókna á íslensku basalti hefur sýnt fram á að möttullinn undir Íslandi er efnafræðilega misleitur og úr honum verði til margvíslegar bráðir. Einnig hafa verið leiddar að því líkur að meginhluta þessarar misleitni í möttli megi rekja til bráðnunar á úthafsflekaefni sem orðið er hluti af íslenska möttulstróknum eftir að hafa sokkið í niðurstreymisbeltum. Á Íslandi eru frumstæðar bergtegundir sem í má finna ólivínkristalla nokkuð algengar. Því eru hér kjöraðstæður til þess að kanna frekar umfang endurunnis efnis í möttli og hvernig ummerki um það varðveitast í ólivínkristöllum.

Í þessari ritgerð eru lagðar fram þrjár greinar þar sem frumstæðir ólivínkristallar er rækilega kannaðir með þessar hugmyndir að leiðarljósi. Hágæðagögnum, sem samanstanda aðallega af örgreiningum á kristöllum ásamt heildarefnagreiningum á stökum kristöllum, var safnað og þau túlkuð með það að markmiði að endurskapa sem best efnasamsetningar möttulættaðra bráða. Í fyrsta kafla eru kynntar niðurstöður örgreininga á aðal- og snefilefnum með áður birtum helíumsamsætugögnum. Samtúlkun þessara ólíku gagnasafna varpar ljósi á uppbyggingu íslenska möttulstróksins og umfang endurunnis efnis sem finna má í honum. Í kafla tvö notfæri ég mér súrefnissamsætugreiningar á sömu kristöllum, gerðar með jónaprób/örgreini, til að kanna vensl súrefnissamsæta, samsetningu kristalla og helíumsamsæta. Súrefnissamsætur gera okkur kleyft að meta enn betur umfang endurunnis efnis sem íslenski möttulstrókurinn dregur með sér. Samtúlkun með helíumsamsætum sýnir jafnframt fram á hvernig riskraftur og afl íslenska möttulstróksins jókst samhliða opnun Norður-Atlantshafssins og myndun Íslandshásléttunnar. Í þriðja kafla kanna ég möguleika á að nota Mg- og Fe-samsætugreininga á stökum kristöllum til skorða betur efnaeiginleika endurunna efnisins sem finna má í íslenska möttlinum. Sýnt er fram á að samhliða risi bráða og efnasveimi, sem á sér stað milli bráðar og nærliggjandi kristalla, eyðast flestöll ummerki þessa eiginleika möttulefnisins. Hinsvegar benda þessar niðurstöður til þess að vensl séu milli dvalartíma kristalla og samsætuhlutfalla, sem opnar á þann möguleika að nota megi Mg- og Fe-samsætugreiningar til að leggja mat á dvalartíma bráða.

This thesis is dedicated to my dearest mor and aba who are still insisting on picking me up in the airport even though it has become a regular ordeal. There is no better way of showing someone you love them than that. Thank you!

Preface

This thesis presents work carried out at the University of Iceland from December 2016 until October 2020. The work was funded by the Nordic Volcanological Center and the Icelandic Research Fund (Grant #196084-051 and Grant #196139-051). The work has resulted in three manuscripts of which one is published, one is submitted and one is under preparation at the time of submission of this thesis:

Rasmussen, M. B., Halldórsson, S. A., Gibson, S. A., & Guðfinnsson, G. H. (2020). Olivine chemistry reveals compositional source heterogeneities within a tilted mantle plume beneath Iceland. *Earth and Planetary Science Letters*, **531**, 116008.

Rasmussen, M. B., Halldórsson, S. A., Jackson, M. G., Bindeman, I. B., & Whitehouse, M. J. (*submitted*). Formation of the Iceland Plateau by enhanced plume flux and entrainment of deeply stored domains. Submitted to *Proceedings of the National Academy of Sciences* (*PNAS*)

Rasmussen, M. B., Williams, H. M., Tipper, E. T., Reekie, C. D. J. & Halldórsson, S. A. (*in prep*). Evaluation of source and magmatic process-derived Mg and Fe isotope characteristics of Icelandic olivine crystals. To be submitted to *Geochimica et Cosmochimica Acta* or a similar journal.

Table of Contents

List of Figures

List of Tables

Abbreviations

MORB	Mid-ocean ridge basalt
OIB	Ocean island basalt
DM	Depleted mantle
EM	Enriched mantle
HIMU	High-μ mantle where μ is defined as the Pb/U ratio of the initial reservoir
FOZO	Focal Zone
PREMA	Prevalent mantle
Ma	Million (10^6) years ago
Ga	Billion (10^9) years ago
Fo	Forsterite content (Mg/[Mg+Fe] in mol%)
Ol	olivine
ERZ	Eastern Rift Zone
NRZ	Norther Volcanic Zone
WRZ	Western Volcanic Zone
SIVZ	South Iceland Volcanic Zone
SNS	Snæfellsnes (Volcanic Zone)
ÖVZ	Öræfajökull
TER	Tertiary lavas
HRP	Hreppar Formation
R_A	$^3He/^4He$ relative to that of air
$\delta^{18}O$	relative difference between sample and standard $^{18}O/^{16}O$ ratios in ‰
ROL	Recycled oceanic lithosphere
IP	Iceland Plateau
$\delta^{26}Mg$	relative difference between sample and standard $^{26}Mg/^{24}Mg$ ratios in ‰
$\delta^{56}Fe$	relative difference between sample and standard $^{56}Fe/^{54}Fe$ ratios in ‰

EMPA	Electron MicroProbe Analyser
LA-ICP-MS	Laser Ablation Inductively Coupled Plasma Mass Spectrometry
SIMS	Secondary Ion Mass Spectrometry
LF	Laser Fluorination oxygen isotope measurements
MC-ICP-MS	Multi Collector-Inductively Coupled Plasma Mass Spectrometer
SD	Standard deviation

Acknowledgements

Firstly, I would like to thank my supervisor and my program committee. Thanks for taking me on, Sæmi, and for providing me with motivational science talks when I would get stuck over the years. Thanks for teaching me how to think out of the box, for including me in field work, and for introducing me to some incredible people, most of whom are now part of, if I may say so myself, my impressive list of co-authors. Thank you, Sally, for being a very inspiring voice throughout this project. I am always looking forward to seeing you and thank you for taking me in when I first arrived in Cambridge and to Andy too for taking me on a bike ride that I will never forget. Thank you, Gummi, for being a tower of knowledge. I always know, that when something has passed you it is in an appropriate shape. Also thank you Enikő for always being ready to help me out with lab or modelling issues and for making me feel part of a group when you and Gummi invited me to some amazing evenings of delicious food and strong Hungarian alcohol.

Thank you, Thomas Kokfelt and Paul Martin Holm, for initiating the contact that led me to Iceland and for being an initial part of this project. I have very much appreciated all you have done for me and for this project to become a reality. I would also like to thank all my co-authors for sharing your expertise with me and for the huge amount of work that you have all put into helping me with the papers that constitute this thesis. I would like to give a special thanks to Matt Jackson for showing me how one can also be a scientist and for joining Eemu and I on that trip to Askja.

Thank you a million to Rikke, who is the main reason that I ever made it to Iceland. You have been the solid and caring rock that made me feel like I was never alone through these last four years and you are one of the coolest people I know! I will always feel very lucky to have been a part of the Nordvulk family and for the various amazing fellows that have passed through since 2016. A special thank you to you, Maria, for picking me up every morning at 9.30 for a morning tea/coffee – those coffee walks made me get up every morning.

A big thank you goes out to my family, who have been extremely patient with me and my crazy idea to live overseas. I could not have lived my life as it is without the love and support that you provide me with every day! A special thanks goes to my grandfather Peter Rasmussen for sharing his nerdiness with me. Thank you for always being ready to discuss science and for helping me getting the most out of whichever school project was at hand. Thank you to my friends back in Denmark who have been as patient with me as my family has and who have insisted on keeping me as a natural part of their lives despite me being away for so long. I am so grateful to you all and I cannot wait to become a more regular physical presence once again in all of your lives.

Barbara, I cannot thank you enough for being my friend. How lucky I was that you and I had to go shopping together for Friday coffee snacks. I have said it before, and I will say it again: Iceland would not be what it is if I had not me you. Thank you for putting up with me and for being my family away from home. You are an inspiration both professionally and personally and I am so very lucky for having you and for being your friend. And thank you, Ed, for taking good care of her and for being just the most awesome person, lockdown-family and friend! I have learned so much from you on both a personal and scientific level. My sanity would not have been intact without the two of you.

Eemu, thank you so much for being an exceptional office- and science teammate for the last three years. Thanks for listening to my complaining and strange stories, for having my back even when I probably did not deserve it and for being the most fun Swede/Finn I have ever met. You are full of amazing traits that everyone could learn from, especially me, and I will miss our multiple daily coffee walks and weird office chats.

It is hard to adequately thank everyone who has been a part of these last four years where I have met so many amazing people both in Reykjavik but also in Cambridge. Thank you to the best flatmates I could have ever wished for, Deirdre, Paavo, Gadi and Chloé. Thank you to the lunch group that have made lunch my favorite part of every day. Thank you to Charlotte, Simon, Dave and Callum for welcoming me and making me feel ‘at home’ in Cambridge. And thank you to all the other amazing people that I have met while living on this beautiful island and working in this strangely designed building. If it had not been for you, I would not be writing this acknowledgement, so thank you!

1 Chapter 1 Introduction

1.1 The concept of mantle heterogeneity

Soon after the publication and acceptance of the theory of plate tectonics (McKenzie, 1966), the first applications of radiogenic isotopes to distinguish melt sources revealed that the Earth's mantle is isotopically heterogenous (e.g., Gast, 1960; Tatsumoto, 1966; Faure & Hurley, 1963). These investigations also showed that several distinct mantle components must be responsible for generating the isotopic array displayed by mid-ocean ridge basalts (MORBs) and ocean island basalts (OIBs). Since then, many studies have attempted to identify the nature of these heterogeneities and constrain the distribution of the various isotopic components within the mantle. This has resulted in the identification of at least four isotopically distinct mantle end-members to explain the geochemical array presented by global MORBs and OIBs (Figure 1.1) including (i) depleted mantle (DM), characterised by low $^{206}Pb/^{204}Pb$, $^{207}Pb/^{204}Pb$ and $^{208}Pb/^{204}Pb$ (from now on simply referred to as Pb isotope ratios), low $^{87}Sr/^{86}Sr$ and high $^{143}Nd/^{144}Nd$; (ii) enriched mantle (EMI and EMII), characterised by intermediate Pb isotope ratios, high $^{87}Sr/^{86}Sr$ and low $^{143}Nd/^{144}Nd$; (iii) High-μ mantle (HIMU, where μ is defined as the Pb/U ratio of the initial reservoir) characterised by high Pb isotope ratios, low $^{87}Sr/^{86}Sr$ and high $^{143}Nd/^{144}Nd$; and finally (iv) a component characterised by intermediate Pb isotope ratios and intermediate $^{87}Sr/^{86}Sr$ and $^{143}Nd/^{144}Nd$, sometimes denoted FOZO (focal zone) or PREMA (prevalent mantle), and referring to the proposed location of the component within the mantle or the notion that most magmas tend to plot in this field (Hart *et al.*, 1992; Stracke, 2012; Stracke *et al.*, 2005; Zindler & Hart, 1986; Jackson *et al.*, 2007).

Depleted mantle represents the residue left behind after the extraction of melts from the primitive mantle and likely constitutes the most abundant material in Earth's mantle (e.g., O'Nions *et al.*, 1979; Zindler & Hart, 1986; Stracke *et al.*, 2019). Pure DM is exclusively sampled (when defined by radiogenic isotopes) by 'normal' mid-ocean ridge basalts (N-MORBs) but is mostly likely present to variable degrees in the source of all MORBs and OIBs, while the other three components are associated with enriched MORBs (E-MORBs), intraplate magmas and OIBs. The nature, origin and location of the enriched mantle components, and the processes responsible for the geochemical anomalies that they imprint on their derivative basalts, are still heavily debated (e.g., Zindler & Hart, 1986; Stracke *et al.*, 2005; Stracke, 2012). The most popular explanation for mantle heterogeneity and the presence of enriched mantle components is subduction of oceanic lithosphere into the mantle. Thus, the resulting chemical anomalies are controlled by which part of this lithosphere has been recycled (Stracke, 2012; Chauvel & Hémond, 2000; Jackson *et al.*, 2007).

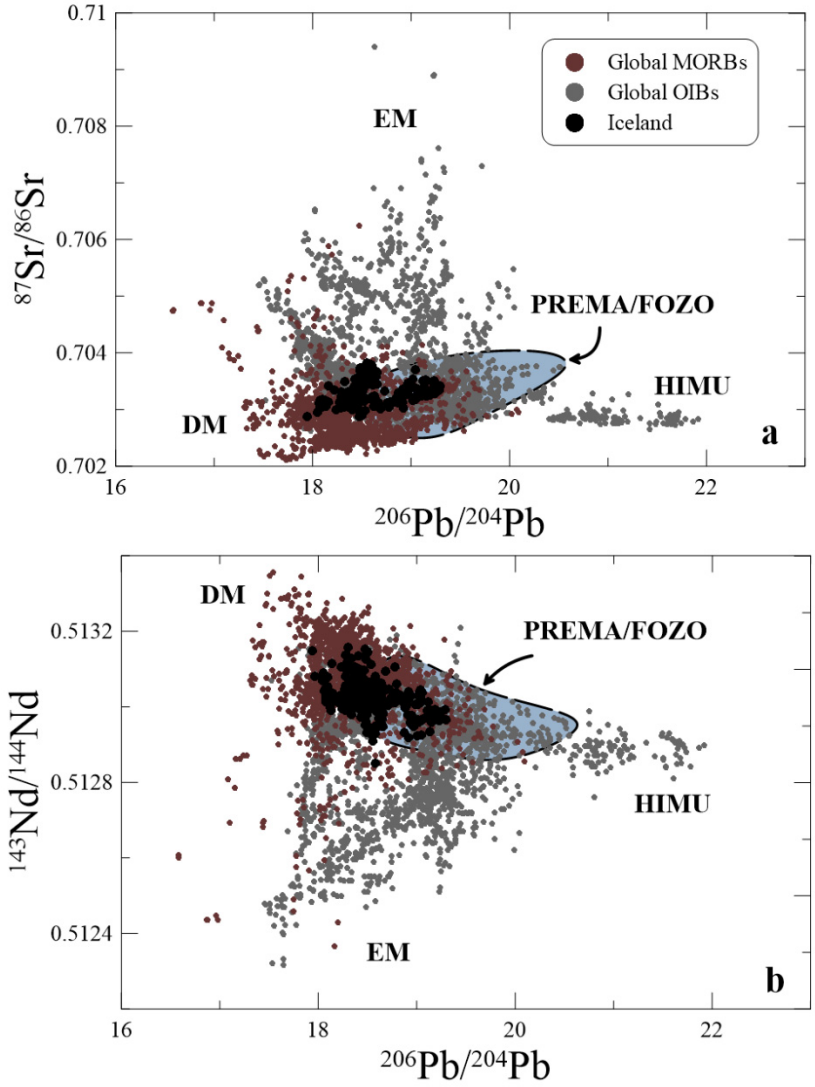

*Figure 1.1 Radiogenic isotope ratios of global OIBs and MORB**s** along with the four main mantle endmember types inferred to generate the observed array. (a) $^{87}Sr/^{86}Sr$ versus $^{206}Pb/^{204}Pb$; (b) $^{143}Nd/^{144}Nd$ versus $^{206}Pb/^{204}Pb$. Iceland (black symbols) plots in the FOZO/PREMA field with spread towards the EM and DM members, suggesting significant mantle heterogeneity. The Iceland data is from Harðardóttir (2020) and the compiled OIB and MORB data is from Stracke et al. (2012).*

When cold dense oceanic lithosphere enters the mantle through subduction, it sinks. Depending on the density of the downgoing slab, and the temperature and density of the ambient mantle, the slab can stagnate at various depths in Earth's mantle. The presence of high-velocity domains in the lower mantle has been suggested as evidence that slabs can accumulate as far down as the core-mantle boundary (e.g., Dziewonski, 1984; Kellogg *et al.*, 1999; Figure 1.2). What happens to the subducted slabs after they stagnate within the mantle is still a topic of discussion, but the most popular explanation is that they are cycled through the solid mantle and entrained by the mantle plumes responsible for the presence of ocean islands, such as Hawaii and Iceland. But how does the crustal material become entrained and remelted in these mantle plumes? Is it through direct melting of various sections of these plates (e.g., Chauvel & Hémond, 2000)? Is it through secondary processes in which

fluids/melts derived from the recycled plate overprint the surrounding mantle's radiogenic fingerprint, thereby being preserved as a 'phantom' of the recycled crust (e.g., Herzberg *et al.*, 2014)? Or do these fluids/melts alter the surrounding mineralogy (e.g., Sobolev *et al.*, 2005)? How can we with the geochemical tools currently at hand unravel this recycling process? And what geochemical observations can be used to trace the relative contribution from different mantle components generated by this recycling process? These are all questions that I have attempted to answer in this thesis by studying primitive olivine chemistry from Iceland.

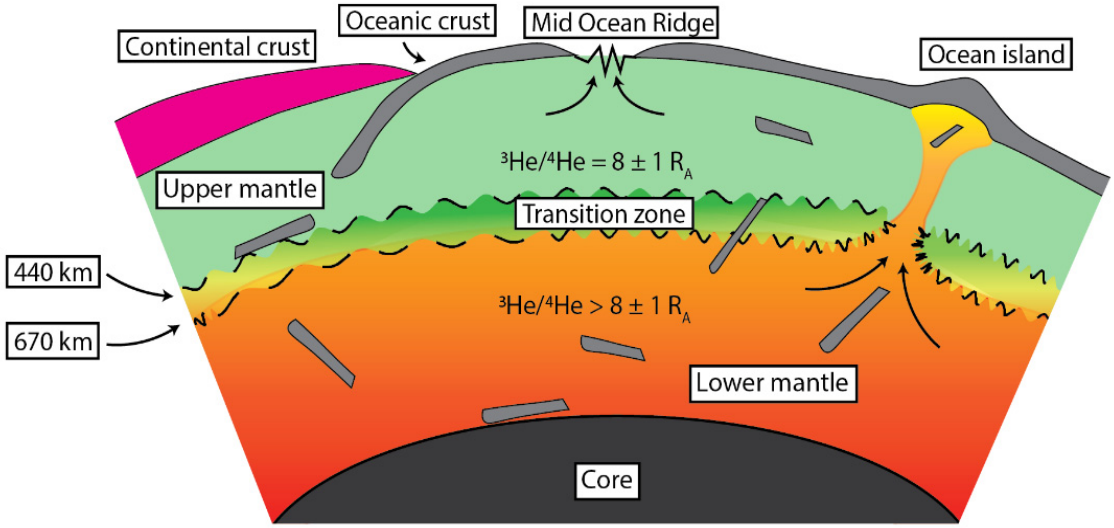

Figure 1.2 Simplified model of the mantle dynamics causing chemical heterogeneity in the Earth's mantle. Oceanic crust is generated at mid-ocean ridges from upper mantle material. Oceanic crust gets reintroduced into the mantle through subduction by which it sinks and eventually stagnates (grey pieces). The depth of stagnation is controlled by parameters such as the temperature and density of the subducting plate and the surrounding mantle. Whole-mantle convection means subducted oceanic crust is capable of reaching the lower mantle and the core-mantle boundary. Recycling of subducted oceanic crust is likely to occur in high-$^3He/^4He$ mantle plumes, originating in the lower mantle, feeding ocean islands such as Hawaii and Iceland. The high $^3He/^4He$ (characteristic of dense lower mantle material) of these plumes implies that the plumes are capable of entraining denser material, possibly incorporating cold subducted oceanic crust along the way (Jackson et al., 2017). The figure and relative sizes of the various reservoirs are not to scale.

1.2 The Iceland plateau and chemical heterogeneity in the underlying mantle

The Iceland plateau, as we know it today, represents the largest subaerial section of the global mid-ocean ridge system. This unique feature is a result of unusually high melt production caused by the coincidence of the Iceland plume and the North Atlantic mid-ocean ridge (e.g., Sigmundsson *et al.*, 2020). Based on radiogenic isotopic compositions of Icelandic basalts (e.g., Harðardóttir, 2020 and references therein), the Iceland plume appears to be tapping PREMA/FOZO components with additions from EM and DM components characteristic of plume-influenced melts (Figure 1.1). The presence of the plume beneath the Iceland plateau is, moreover, evident in several chemical tracers (e.g., Sigmarsson *et al.*, 2008), such as Sr and Pb isotope ratios. These systems show a shift from relatively depleted $^{87}Sr/^{86}Sr$ and $^{206}Pb/^{204}Pb$ values, characteristic of MORB, at latitude around 60° N along the Mid-Atlantic Ridge to an enriched $^{87}Sr/^{86}Sr$ and intermediate $^{206}Pb/^{204}Pb$ signature between ~ 64-67° N, characteristic of OIB-like melts (Figure 1.3). This shift is mirrored in He isotope ratios, from those typical of MORBs ($^{3}He/^{4}He = 8 \pm 1$ R_A, where 1 R_A represent air, Graham, 2002) to high $^{3}He/^{4}He$ values up to 34 R_A in central Iceland (e.g., Harðardóttir *et al.*, 2018; Hilton *et al.*, 2000), characteristic of modern plume involvement.

Helium-3 is a primordial isotope, meaning that the abundance present in the mantle is almost exclusively controlled by the ^{3}He budget of the Earth at the time of formation, as ^{3}He cannot be generated by processes generally occurring in the mantle. Thus, $^{3}He/^{4}He$ values above those presented by MORB, a product of melting of the upper mantle, have been attributed to sampling of a less or completely undegassed primordial lower-mantle reservoir (Figure 1.2). However, abundant evidence from seismic tomographic, gravity studies and dynamic models of mantle convection reveal that mantle convection cells, responsible for transporting subducted crust to the core-mantle boundary, operate across the transition zone located at about 410-660 km depth (Figure 1.2). This zone was previously thought to prevent mixing between the upper and lower mantle, and material transport across this boundary means that upper versus lower mantle heterogeneity cannot be preserved over a longer timescale (e.g., van Keken *et al.*, 2002). Various models have been put forward to explain the preservation of high $^{3}He/^{4}He$ in a convective mantle, such as chemical dilution leading to decreasing rates of lower mantle degassing through chemical diffusion (Gonnermann & Mukhopadhyay, 2009), contribution of primordial He stored in the core (e.g., Bouhifd *et al.*, 2020; Roth *et al.*, 2019) or the presence of stable lower-mantle structures of high viscosity bridgmanite-enriched ancient mantle structures (BEAMS), essentially preventing complete mantle mixing (Ballmer *et al.*, 2017). But common for these models is that plumes characterised by $^{3}He/^{4}He$ values above MORB, such as Iceland, must be sourced from the lower mantle, thus constraining the origin of the Iceland plume.

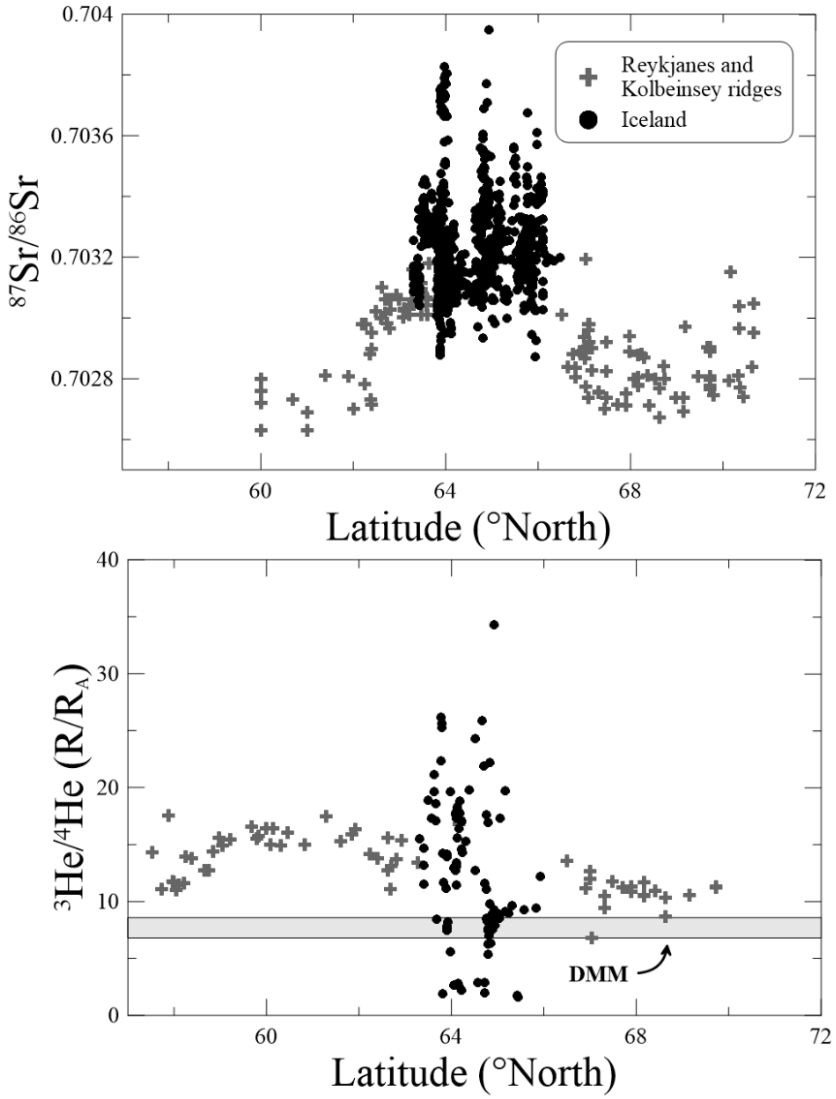

Figure 1.3 Chemical tracers of the involvement of a mantle plume beneath Iceland. The increase in $^{87}Sr/^{86}Sr$ at the location of the Iceland plateau suggests that the plume beneath Iceland is more enriched than the mantle sampled south and north of the plateau. This increase is mirrored in He isotopes where $^{3}He/^{4}He$ up to 34 R_A in central Iceland reflects the involvement of a mantle plume originating in the lower mantle. The latitude for individual Sr isotope values along the Reykjanes Ridge is estimated from the sample map presented in Hart et al. (1973). The He isotopes were measured in volcanic glasses from Reykjanes and Kolbeinsey ridge, but various kinds of materials from within Iceland (see Harðardóttir, 2020). The data used for Iceland is from Harðardóttir (2020). The data for Kolbeinsey and Reykjanes ridge was downloaded from the PetDB database (www.earthchem.org/petdb) on the October 9th, 2020 using the search criteria presented in data supplement for Chapter 1. The literature from which this data was compiled is also presented in data supplement for Chapter 1.

Subaerial and subglacial rock formations in Iceland are dominated by hyaloclastites, pillow lavas and lava flows of tholeiitic basalts in the active rift zones, while transitional alkalic to alkalic products dominate in the flank and off-rift zones (Jakobsson *et al.*, 2008, Figure 1.4). These basalts display spatially controlled isotopic and trace element patterns, which are

consistent with varying contributions from enriched and depleted components in the Iceland mantle (e.g., Sigmarsson *et al.*, 2008; Kokfelt *et al.*, 2006), and the likely intermingling of the Iceland plume and the surrounding upper-mantle material (e.g., Harðardóttir *et al.*, 2018; Rasmussen *et al.*, 2020). Several studies have shown how chemical signatures of enriched source components (e.g., more radiogenic Pb isotope ratios and higher La/Y and Sm/Y) in the Iceland mantle become stronger away from the inferred plume centre (e.g., Sigmarsson *et al.*, 2008; Kokfelt *et al.*, 2006). This effect has been attributed to the increased lithospheric thickness away from the plume centre and active rifting zones, leading to shorter melting columns that are truncated at greater depths, enhancing the geochemical signal of recycled crustal material (e.g., Kokfelt *et al.*, 2006; Sigmarsson *et al.*, 2008). Pb isotopes have also been used to show that the signature of certain mantle components sampled in the western and eastern rift zones (Figure 1.4) is completely lacking in melts in the northern rift zone (Peate et al., 2010), implying that the compositional heterogeneity in the mantle beneath Iceland exists not only vertically, but also laterally.

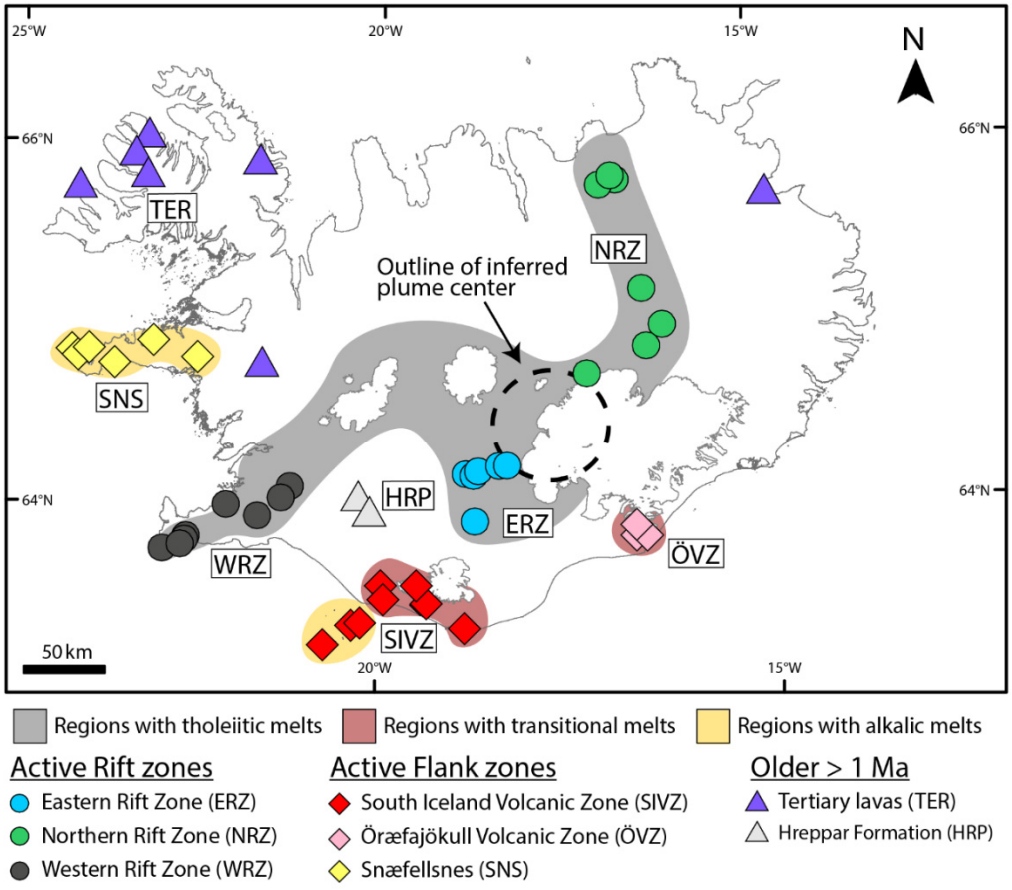

Figure 1.4 Map of Iceland with the sample localities targeted for this thesis. The dominating magma types (tholeiitic, transitional or alkalic) and the distribution of these are controlled by the location of the various volcanic systems on-rift or off-rift. Radiogenic Pb isotopes and tracers of chemical enrichment, such as La/Y, increases with an increasing distance to the plume center with an inferred location below the Eastern part of Vatnajökull. The marked abbreviations and symbols used to represent the various volcanic zones will be used throughout this thesis.

1.3 Oxygen isotopes as a tracer of mantle heterogeneity

Oxygen is the most abundant element in the silicate part of Earth and represents 45 % of the mass of the mantle and crust. The oxygen isotopic value ($\delta^{18}O$, defined as the relative difference between sample and standard mean ocean water $^{18}O/^{16}O$ ratios in ‰) for the Earth's upper and lower mantle has proven overall homogenous (at 5.2 ± 0.3 ‰; Eiler, 2001). Despite this, variations in $\delta^{18}O$ especially occur in OIBs and are often associated with the presence of recycled crustal material or secondary crustal processes, such as assimilation (e.g, Workman *et al.*, 2008; Wang & Eiler, 2008).

Fractionation of stable isotopes is negligible at high temperatures, such as those present in the mantle and during the crystallisation of basalts; therefore, only slight oxygen isotopic fractionation occurs between silicate melt and the crystallising phases (e.g., $\Delta_{melt\text{-}olivine} \sim 0.5$ ‰, Eiler, 2001). However, as the temperature decreases fractionation increases (Urey, 1947; Chacko *et al.*, 2001) and at surface conditions, fractionation of oxygen isotopes can be several 10s per mil. Because of this, oxygen is an ideal tracer for the presence of material that experienced oxygen isotopic fractionation close to the surface prior to incorporation in the mantle source of OIBs.

$\delta^{18}O$ values of Icelandic basalts are notably low compared to the canonical mantle value of 5.2 ‰. Two prevailing hypotheses have been put forward to account for this: interaction with low- $\delta^{18}O$ altered crust or the presence of a low-$\delta^{18}O$ mantle source (Muehlenbachs *et al.*, 1974). Meteoric water in Iceland has exceptionally low $\delta^{18}O$ (down to -14 ‰; Sveinbjörnsdóttir *et al.*, 2020), which is a result of the high-latitude location of the island. Interaction between this water and the Icelandic crust has resulted in crustal $\delta^{18}O$ values down to -10 ‰ measured in hydrothermally altered basalt from Krafla (Hattori & Muehlenbachs, 1982). The interaction and assimilation of this material into ascending melts could lower the $\delta^{18}O$ of the resulting melt, and this process has indeed been shown to cause $\delta^{18}O_{melt}$ values down to 3 ‰ in large-volume tholeiites from the active rift zones (e.g., Bindeman *et al.*, 2008; Halldórsson *et al.*, 2018).

While previous studies have suggested the presence of a mantle component beneath Iceland — characterised by $\delta^{18}O$ values up to ~ 1 ‰ below that of the normal mantle — most of these have been based on bulk measurements of single or multiple crystals of mainly olivine (e.g., Macpherson *et al.*, 2005; Thirlwall *et al.*, 2006). These measurements cannot, however, resolve intra-crustal variations caused by growth of olivine in equilibrium with an evolving melt affected by assimilation processes (Bindeman *et al.*, 2008). Rather, bulk measurements of olivine with chemical zonation in $\delta^{18}O$, reflecting both source and crustal-derived $\delta^{18}O$ values, would be skewed relative to the primary value of the source component (Bindeman *et al.*, 2008). Thus, *in-situ* or 'spot' analyses of individual olivines are needed to distinguish $\delta^{18}O$ values representative of the Icelandic mantle and $\delta^{18}O$ values resulting from assimilation of low-$\delta^{18}O$ crust.

1.4 Advantages of using olivine as a proxy for mantle-source compositions

The composition of primary melts resulting from adiabatic decompression (or partial melting) of the mantle is rarely preserved at the surface. Rather, erupted magmas have typically been subjected to secondary processes, such as melt mixing (e.g., Winpenny & Maclennan, 2011; Maclennan, 2008), assimilation of wall-rock (e.g., Bindeman *et al.*, 2008) and melt evolution through fractional crystallisation. These processes can all overprint mantle-derived variability, and assumptions must therefore be made when recreating the composition of the mantle from which these melts were sourced. Extensive melt mixing is well-documented in lavas from the northern volcanic zone in Iceland (e.g., Maclennan, 2008) and, as discussed in the previous section, assimilation of low-$\delta^{18}O$ crust has been shown to result in $\delta^{18}O$ compositions skewed towards a crustal rather than source-derived values (Bindeman *et al.*, 2008). So how do we confidently distinguish between crustal- versus source-derived fingerprints on the chemical variation observed in Icelandic basalts? The answer to this question might very well be found in the study of olivine chemistry.

Olivine represents one of the first phases to crystallise from a mantle-derived melt. This high-forsterite (high Mg/Fe) olivine often crystallises prior to most secondary processes, such as melt mixing, assimilation and melt evolution that can modify melt compositions in the crust. As olivine reflects the composition of the magma at the time of crystallisation, this makes it an ideal proxy for primary melt compositions, especially in settings where secondary processes are likely to modify source-derived melt variabilities or in locations where primitive glasses are unavailable.

Olivine macrocrysts in Icelandic basalts are generally too primitive to be in equilibrium with their carrier melts, meaning that they likely crystallised from a magma that was more primitive than the host magma (Thomson & Maclennan, 2013). This apparent crystal-melt disequilibrium has been linked to accumulation processes occurring in magma storage zones at various depths, supporting the need for a stacked-sill model to describe the Iceland magmatic system (Maclennan, 2019). Here, mantle melts crystallise mafic phases, such as olivine, that are later incorporated into more evolved magmas. The rims of these crystals are often in equilibrium with their more evolved carrier melt (e.g., Hansen & Grönvold, 2000), highlighting the need for spatial control when targeting primitive olivine compositions.

Minor and trace elemental variations in olivine have proven a useful tool for identifying lithological variability in the source. Sobolev *et al.* (2005) proposed that the exceptionally high Ni content and correspondingly low Mn and Ca contents of magmatic olivine could be used to infer the presence of pyroxenite lithologies in the mantle, representing the incorporation of recycled oceanic crust. This secondary 'reaction' pyroxenite, referred to as olivine-free mantle lithologies, is ostensibly generated through metasomatism of ambient peridotite by silicate melts derived from subducted oceanic crust or eclogites (Yaxley, 2000). This process of generating pyroxenites through interaction between eclogite-derived melts and ambient mantle was later shown to be possible by melting experiments, in which the pyroxenitic component reached the solidus at lower temperature than the surrounding peridotitic matrix (Mallik & Dasgupta, 2012, Figure 1.5). Later studies (e.g., Matzen *et al.*, 2013; Matzen *et al.*, 2017) have shown that these exceptional Ni, Mn and Ca contents of olivine can be replicated by increased melting pressure and temperature or early crystallisation of clinopyroxene. These studies thus suggest caution when using minor

elements alone as a proxy for lithological heterogeneity, highlighting the need for additional trace element observations to constrain whether pyroxenite is present, and to isolate the effects of melting and crystallisation parameters on olivine minor element concentrations.

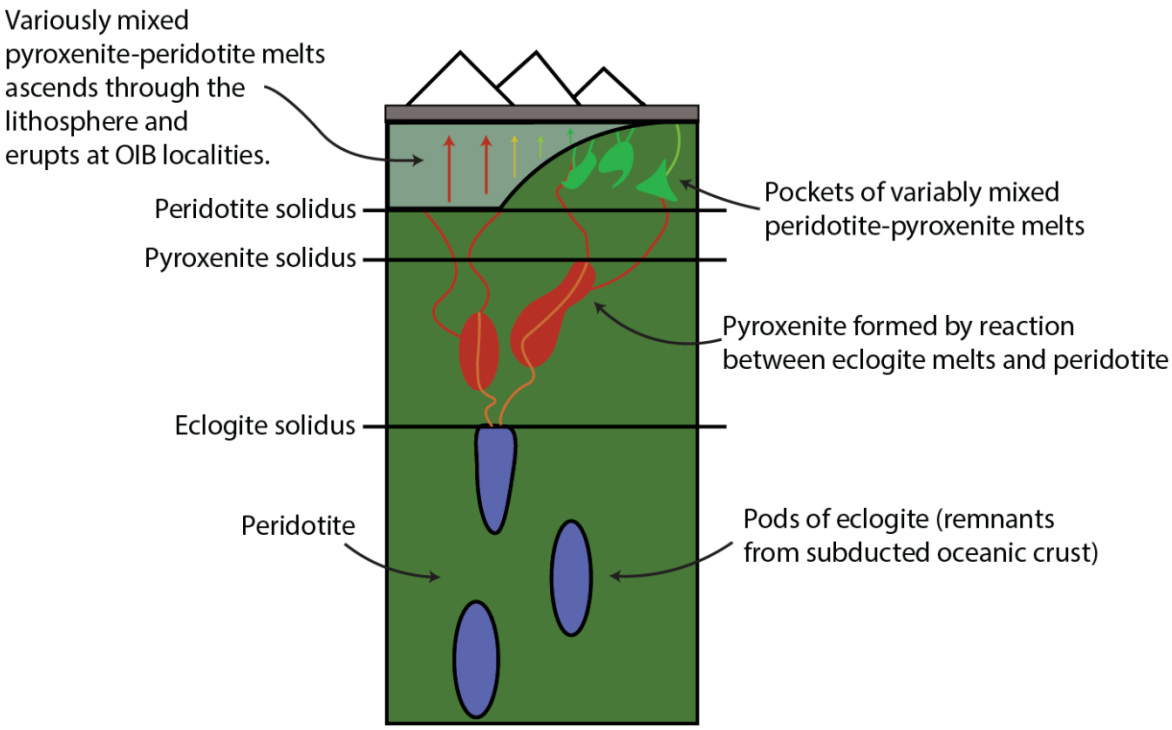

Figure 1.5 Cartoon displaying the process which converts peridotite to pyroxenite through metasomatism by eclogite (recycled oceanic crust)-derived melts. Melting of pyroxenite starts at greater depths due to the more fusible nature. After the solidus for peridotite is reached, the melts derived from pyroxenitic and peridotitic lithologies mix. At hot spots with thick lithospheres, the chemical fingerprint of pyroxenite is better preserved as less melt mixing occurs prior to eruption. The cartoon is not to scale and is heavily inspired by Mallik and Dasgupta (2012).

The aggregation of mantle-derived melts is likely to result in the signature from shallow-derived peridotite melts overwhelming that of more deeply-derived pyroxenite melts. Thus, the chemical fingerprint of secondary pyroxenitic components was suggested to be better preserved in locations where the mantle plume is overlain by a thick lithosphere (Sobolev *et al.*, 2007) or where short melting columns limits the degree of melt mixing between pyroxenite- and peridotite derived melts (e.g., Gibson *et al.*, 2000; Kokfelt *et al.*, 2006). Despite being overlain mostly by a thin lithosphere (<50 km; Bjarnason & Schmeling, 2009), the Icelandic plume has been shown to be lithologically heterogenous on the basis of mantle-derived variations in isotopes, major and minor elements in Iceland basalts (e.g., Kokfelt *et al.*, 2006; Shorttle & Maclennan, 2011). Moreover, the presence of enriched pyroxenitic components have indeed been shown to be best sampled in regions where the lithospheric thickness is greater, such as South Iceland and West Iceland. Iceland thus represents an ideal setting to study the effect that a lithologically heterogenous mantle, resulting from the recycling of oceanic crust, has on the minor and trace element contents and various isotopic ratios of magmatic olivine.

1.5 The use of Mg and Fe isotopes in olivine

The study of non-traditional stable isotopes of major elements (elements with an abundance >0.1 % mass of the silicate Earth) offers a new perspective to trace the relative melt contribution from enriched and depleted components, as these elements are relatively evenly distributed between the two reservoirs. Conversely, the isotopic ratios of trace elements in erupted basalts (elements found in the silicate Earth at ppm concentrations or below, e.g. Pb, Sr and Nd) tend to be dominated by the contribution from any enriched component, obscuring the chemical signature of the depleted component (e.g., Stracke *et al.*, 2019). Variations in the stable isotope ratios of Mg and Fe have proven to be an effective tool for evaluating the origin of mantle heterogeneity, whether it reflects recycling of subducted sediments, subduction-derived fluid-mantle reactions (e.g., Teng *et al.*, 2016) or a distinct difference in source mineral assemblages (e.g., Williams & Bizimis, 2014; Gleeson *et al.*, 2020; Konter *et al.*, 2016; Nebel *et al.*, 2019).

As Mg and Fe are major elements in olivine (ol), this phase seems a promising medium for the study of source-derived isotopic variations in Mg and Fe. However, Fe isotope fractionation during crystallisation of individual phases, such as olivine, is poorly constrained and is strongly controlled by the Fe-O bond strength, which is a complex product of Fe-O bond length, oxidation state and the coordination of Fe in a given medium (e.g., Polyakov & Mineev, 2000; Shahar *et al.*, 2008; Roskosz *et al.*, 2015). Moreover, despite the advantage provided by using olivine chemistry as a proxy for primary melt composition, the presence of olivine within a chemically different matrix, in this case a more evolved melt, has been shown to result in modifications of source-derived Mg and Fe isotopic ratios by diffusion (e.g., Sio *et al.*, 2018; Sio *et al.*, 2013; Teng *et al.*, 2011; Oeser *et al.*, 2015; Dauphas *et al.*, 2010). The diffusive flux, or exchange of atoms between two phases is controlled by the size, location and bonding environment of the atom within the original medium and the chemical gradient of the atomic species between the phases (the degree of disequilibrium). As the controls on diffusion of Mg and Fe are similar in olivine, their inter-exchange has often been used to evaluate transportation timescales for magmas through the crust (e.g., Costa & Chakraborty, 2008) and for identifying temporal changes in the plumbing system (e.g., Kahl *et al.*, 2011).

Diffusive re-equilibration of Mg and Fe in olivine accumulated in crustal mush reservoirs has been suggested as a mechanism for chemically homogenising the cores of Icelandic olivine crystals prior to eruption, thereby explaining the remarkably homogenous core Mg and Fe compositions characteristic of Icelandic olivine (Thomson & Maclennan, 2013; Hansen & Grönvold, 2000). However, the extent of diffusion and the difference between the various volcanic regions is still unknown. Moreover, the current Mg and Fe isotopic data for Icelandic rocks is very limited (Schuessler *et al.*, 2009; Pogge von Strandmann *et al.*, 2008; Weyer & Ionov, 2007), leaving a gap in our knowledge of how the presence of recycled crust and pyroxenite is reflected in the Mg and Fe isotopic characteristics of Icelandic basalts.

1.6 Introduction to the PhD project and a summary of findings

The overall aim of this PhD project was 1) to evaluate signatures and characteristics of chemical heterogeneity in the mantle beneath Iceland and, as a follow up, 2) to investigate processes affecting magmas in the Icelandic crust.

The results of the study were expected to provide better understanding of: (i) the use of olivine as a tool for studying mantle processes; (ii) the geochemical characteristics of chemically distinctive domains present in the Icelandic mantle; and (iii) magmatic processes occurring in Icelandic magma plumbing systems.

Based on this, three main scientific questions arise:

1. How do minor and trace elemental concentrations in olivine vary regionally and what do they reveal about the mantle beneath Iceland?

2. Oxygen isotope ratios of Icelandic basalts are notably distinct from MORB-sourced basalts. Is this caused by primary heterogeneities within the mantle or secondary processes occurring in the crust?

3. Do Mg and Fe isotopic ratios in magmatic olivine record source heterogeneities? And what can these isotope systems reveal about the Iceland mantle?

These questions are the base for three individual manuscripts (Chapters 2, 3 and 4), and were answered by studying the geochemical systematics of olivine from the most primitive Icelandic phyric lavas found in the neovolcanic rift and flank zones as well as older Quaternary and Tertiary crust (Figure 1.4). Questions 1) and 2) were addressed with the use of *in-situ* measurements of the same set of olivines by Electron MicroProbe Analyser (EMPA) at the University of Iceland, Laser Ablation Inductively Coupled Plasma Mass Spectrometry (LA-ICP-MS) at the University of Cambridge and Secondary Ion Mass Spectrometry (SIMS) at the NORDSIM facility in Stockholm, with additional laser fluorination (LF) oxygen isotope measurements of the same samples performed at the University of Oregon. Question 3) was addressed through combined *in-situ* EMPA and bulk digestion and analysis by Multi Collector-Inductively Coupled Plasma Mass Spectrometer (MC-ICP-MS) of new olivine crystals from the same samples used to answer Questions 1) and 2). The EMPA measurements were performed at the University of Iceland and the elemental separations and MC-ICP-MS measurements of Mg and Fe isotopes were done in two sessions at the University of Cambridge. Key for targeting certain sample separates and vital for the later findings was the presence of previously published $^{3}He/^{4}He$ data for the same sample separates (Harðardóttir *et al.*, 2018).

The first research question was evaluated by analysis of minor- and trace element variations in high-forsterite olivine and published as an article in *Earth and Planetary Science Letters*. Here we found that the mantle beneath Iceland is indeed lithologically heterogenous, which is reflected in the chemistry of high-forsterite olivine. Moreover, we find that the signal of a pyroxenitic component is strongest in olivine from South Iceland, which also displays some of the highest $^{3}He/^{4}He$ values measured in olivine from the Holocene. We identify the presence of four mantle components necessary to explain the trace elemental variations

observed in olivine macrocrysts found in Iceland. We conclude that the high $^{3}He/^{4}He$ values observed in all of Iceland (except for Snæfellsnes) mark the contribution from plume-derived melts and that the spatial distribution and sampling of the four mantle components is controlled by a northward tilted mantle plume. These observations are supported by previous geophysical and geochemical evidence of plume stem displacement for the Iceland and Hawaiian plumes, suggesting that plume geometry is a contributing factor in controlling how lithological heterogeneity is sampled by melting beneath ocean islands.

The second research question was evaluated by a combination of *in-situ* analysis and single, and bulk crystal (high-precision) determinations of $\delta^{18}O$ on the same set of olivine crystals and samples as targeted for the minor and trace element study. This manuscript is under evaluation with *Proceedings of the National Academy of Sciences*. Here, we found that low $\delta^{18}O$ values down to 4.2 ‰ measured in high-forsterite olivine are intrinsic to the Iceland plume. By considering samples that represent plume activity from the Miocene until today, we show that the coupled lowering in $\delta^{18}O$ and $^{3}He/^{4}He$ from the initiation of the Iceland plume until the present day is controlled by an increase in recycled oceanic lithosphere (*ROL*) entrained by the plume component. Moreover, we find, that the increase in *ROL* with time is tied to an increase in plume temperature, suggesting that the overall flux of the Iceland plume has increased over time. The increasing presence and incorporation of *ROL* along with an increase in the plume flux, is likely caused by the capability of high-$^{3}He/^{4}He$ plumes to entrain the densest lower mantle material, which can include dense *ROL*. We find that alignment of the Iceland plume and the North Atlantic rift around the same time likely enhanced melt production of the plume. Thus, we conclude that an increase in plume flux and tectonic reorganisation of the North Atlantic lead to the introduction of *ROL* into the Iceland plume and the formation of the Iceland plateau ~ 25 Ma.

The third research question was evaluated using combined *in-situ* minor elemental measurements and bulk measurements of Mg and Fe isotopes in new crystals from the same samples as targeted for the two previous manuscripts. This manuscript is currently in preparation but is planned for submission to *Geochimica et Cosmochimica Acta* or a similar journal. The aim of the manuscript is to evaluate the Mg and Fe isotopic variations found in high-forsterite olivine. We find that Mg isotopic ratios in Icelandic olivine mostly overlap with the field expected from melting of a mantle component without recycled carbonates present. Moreover, we find large variation in Fe isotopes which exceeds that predicted from melting of a single lithology. However, the lack of correlation between Mg and Fe isotope ratios and trace element ratios that record the presence of a lithological heterogeneity implies that the variation observed in Fe isotopes reflects secondary rather than primary processes. Indeed, we find that very low Fe isotope values can be explained by a coupled diffusion of Mg and Fe isotopes, enabling us to evaluate the control that crystal size and magma transport exert on the Fe isotopic composition of Icelandic olivines.

1.7 References

Ballmer, M. D., Houser, C., Hernlund, J. W., Wentzcovitch, R. M., & Hirose, K. (2017). Persistence of strong silica-enriched domains in the Earth's lower mantle. *Nature Geoscience, 10*(3), 236-240.

Bindeman, I., Gurenko, A., Sigmarsson, O., & Chaussidon, M. (2008). Oxygen isotope heterogeneity and disequilibria of olivine crystals in large volume Holocene basalts from Iceland: Evidence for magmatic digestion and erosion of Pleistocene hyaloclastites. *Geochimica et Cosmochimica Acta, 72*(17), 4397-4420.

Bjarnason, I. T., & Schmeling, H. (2009). The lithosphere and asthenosphere of the Iceland hotspot from surface waves. *Geophysical Journal International, 178*(1), 394-418.

Bouhifd, M. A., Jephcoat, A., Porcelli, D., Kelley, S., & Marty, B. (2020). Potential of Earth's core as a reservoir for noble gases: Case for helium and neon. *Geochemical Perspectives Letters*, 15-18.

Chacko, T., Cole, D. R., & Horita, J. (2001). Equilibrium oxygen, hydrogen and carbon isotope fractionation factors applicable to geologic systems. *Reviews in Mineralogy and Geochemistry, 43*(1), 1-81.

Chauvel, C., & Hémond, C. (2000). Melting of a complete section of recycled oceanic crust: trace element and Pb isotopic evidence from Iceland. *Geochemistry, Geophysics, Geosystems, 1*(2).

Costa, F., & Chakraborty, S. (2008). The effect of water on Si and O diffusion rates in olivine and implications for transport properties and processes in the upper mantle. *Physics of the Earth and Planetary Interiors, 166*(1-2), 11-29.

Dauphas, N., Teng, F.-Z., & Arndt, N. T. (2010). Magnesium and iron isotopes in 2.7 Ga Alexo komatiites: Mantle signatures, no evidence for Soret diffusion, and identification of diffusive transport in zoned olivine. *Geochimica et Cosmochimica Acta, 74*(11), 3274-3291.

Dziewonski, A. M. (1984). Mapping the lower mantle: determination of lateral heterogeneity in P velocity up to degree and order 6. *Journal of Geophysical Research: Solid Earth, 89*(B7), 5929-5952.

Eiler, J. (2001). Oxygen Isotope Variations of Basaltic Lavas and Upper Mantle Rocks. *Reviews in Mineralogy and Geochemistry, 43*.

Faure, G., & Hurley, P. M. (1963). The Isotopic Composition of Strontium in Oceanic and Continental Basalts: Application to the Origin of Igneous Rocks 1. *Journal of Petrology, 4*(1), 31-50.

Gast, P. W. (1960). Limitations on the composition of the upper mantle. *Journal of Geophysical Research (1896-1977), 65*(4), 1287-1297.

Gibson, S. A., Thompson, R. N., & Dickin, A. P. (2000). Ferropicrites: geochemical evidence for Fe-rich streaks in upwelling mantle plumes. *Earth and Planetary Science Letters, 174*(3), 355-374.

Gleeson, M. L. M., Gibson, S. A., & Williams, H. M. (2020). Novel insights from Fe-isotopes into the lithological heterogeneity of Ocean Island Basalts and plume-influenced MORBs. *Earth and Planetary Science Letters, 535*, 116114.

Gonnermann, H. M., & Mukhopadhyay, S. (2009). Preserving noble gases in a convecting mantle. *Nature, 459*(7246), 560.

Graham, D. W. (2002). Noble gas isotope geochemistry of mid-ocean ridge and ocean island basalts: Characterization of mantle source reservoirs. *Reviews in Mineralogy and Geochemistry, 47*(1), 247-317.

Halldórsson, S. A., Bali, E., Hartley, M. E., Neave, D. A., Peate, D. W., Guðfinnsson, G. H., Bindeman, I., Whitehouse, M. J., Riishuus, M. S., Pedersen, G. B. M., Jakobsson, S., Askew, R., Gallagher, C. R., Guðmundsdóttir, E. R., Gudnason, J., Moreland, W. M., Óskarsson, B. V., Nikkola, P., Reynolds, H. I., Schmith, J., & Thordarson, T. (2018). Petrology and geochemistry of the 2014–2015 Holuhraun eruption, central Iceland: compositional and mineralogical characteristics, temporal variability and magma storage. *Contributions to Mineralogy and Petrology, 173*(8), 64.

Hansen, H., & Grönvold, K. (2000). Plagioclase ultraphyric basalts in Iceland: the mush of the rift. *Journal of Volcanology and Geothermal Research, 98*(1–4), 1-32.

Harðardóttir, S. (2020). *Spatial distribution and geochemical characterization of Icelandic mantle end-members.* (Master's thesis), University of Iceland,

Harðardóttir, S., Halldórsson, S. A., & Hilton, D. R. (2018). Spatial distribution of helium isotopes in Icelandic geothermal fluids and volcanic materials with implications for location, upwelling and evolution of the Icelandic mantle plume. *Chemical Geology*.

Hart, S., Hauri, E., Oschmann, L., & Whitehead, J. (1992). Mantle plumes and entrainment: isotopic evidence. *Science, 256*(5056), 517-520.

Hart, S. R., Schilling, J. G., & Powell, J. L. (1973). Basalts from Iceland and Along the Reykjanes Ridge: Sr Isotope Geochemistry. *Nature Physical Science, 246*(155), 104-107.

Hattori, K., & Muehlenbachs, K. (1982). Oxygen isotope ratios of the Icelandic crust. *Journal of Geophysical Research: Solid Earth, 87*(B8), 6559-6565.

Herzberg, C., Cabral, R. A., Jackson, M. G., Vidito, C., Day, J. M. D., & Hauri, E. H. (2014). Phantom Archean crust in Mangaia hotspot lavas and the meaning of heterogeneous mantle. *Earth and Planetary Science Letters, 396*, 97-106.

Hilton, D., Thirlwall, M., Taylor, R., Murton, B., & Nichols, A. (2000). Controls on magmatic degassing along the Reykjanes Ridge with implications for the helium paradox. *Earth and Planetary Science Letters, 183*(1-2), 43-50.

Jackson, M. G., Hart, S. R., Koppers, A. A. P., Staudigel, H., Konter, J., Blusztajn, J., Kurz, M., & Russell, J. A. (2007). The return of subducted continental crust in Samoan lavas. *Nature, 448*(7154), 684-687.

Jackson, M. G., Konter, J. G., & Becker, T. W. (2017). Primordial helium entrained by the hottest mantle plumes. *Nature, 542*(7641), 340-343.

Jakobsson, S. P., Jónasson, K., & Sigurdsson, I. A. (2008). The three igneous rock series of Iceland. *Jökull, 58*, 117-138.

Kahl, M., Chakraborty, S., Costa, F., & Pompilio, M. (2011). Dynamic plumbing system beneath volcanoes revealed by kinetic modeling, and the connection to monitoring data: An example from Mt. Etna. *Earth and Planetary Science Letters, 308*(1–2), 11-22.

Kellogg, L. H., Hager, B. H., & van der Hilst, R. D. (1999). Compositional Stratification in the Deep Mantle. *Science, 283*(5409), 1881-1884.

Kokfelt, T. F., Hoernle, K., Hauff, F., & Fiebig, J. (2006). Combined Trace Element and Pb-Nd-Sr-O Isotope Evidence for Recycled Oceanic Crust (Upper and Lower) in the Iceland Mantle Plume. *Journal of Petrology, 47*(9), 1705-1749.

Konter, J. G., Pietruszka, A. J., Hanan, B. B., Finlayson, V. A., Craddock, P. R., Jackson, M. G., & Dauphas, N. (2016). Unusual δ^{56}Fe values in Samoan rejuvenated lavas generated in the mantle. *Earth and Planetary Science Letters, 450*, 221-232.

Maclennan, J. (2008). Concurrent mixing and cooling of melts under Iceland. *Journal of Petrology, 49*(11), 1931-1953.

Maclennan, J. (2019). Mafic tiers and transient mushes: evidence from Iceland. *Philosophical Transactions of the Royal Society A: Mathematical, Physical and Engineering Sciences, 377*(2139).

Macpherson, C., Hilton, D., Day, J., Lowry, D., & Gronvold, K. (2005). High-$^{3}He/^{4}He$, depleted mantle and low-$\delta^{18}O$, recycled oceanic lithosphere in the source of central Iceland magmatism. *Earth and Planetary Science Letters, 233*(3-4), 411-427.

Mallik, A., & Dasgupta, R. (2012). Reaction between MORB-eclogite derived melts and fertile peridotite and generation of ocean island basalts. *Earth and Planetary Science Letters, 329*, 97-108.

Matzen, A. K., Baker, M. B., Beckett, J. R., & Stolper, E. M. (2013). The Temperature and Pressure Dependence of Nickel Partitioning between Olivine and Silicate Melt. *Journal of Petrology, 54*(12), 2521-2545.

Matzen, A. K., Wood, B. J., Baker, M. B., & Stolper, E. M. (2017). The roles of pyroxenite and peridotite in the mantle sources of oceanic basalts. *Nature Geosci, advance online publication*.

McKenzie, D. P. (1966). The viscosity of the lower mantle. *Journal of Geophysical Research (1896-1977), 71*(16), 3995-4010.

Muehlenbachs, K., Anderson, A. T., & Sigvaldason, G. E. (1974). Low-^{18}O basalts from Iceland. *Geochimica et Cosmochimica Acta, 38*(4), 577-588.

Nebel, O., Sossi, P. A., Bénard, A., Arculus, R. J., Yaxley, G. M., Woodhead, J. D., Rhodri Davies, D., & Ruttor, S. (2019). Reconciling petrological and isotopic mixing mechanisms in the Pitcairn mantle plume using stable Fe isotopes. *Earth and Planetary Science Letters, 521*, 60-67.

O'Nions, R., Evensen, N., & Hamilton, P. (1979). Geochemical modeling of mantle differentiation and crustal growth. *Journal of Geophysical Research: Solid Earth, 84*(B11), 6091-6101.

Oeser, M., Dohmen, R., Horn, I., Schuth, S., & Weyer, S. (2015). Processes and time scales of magmatic evolution as revealed by Fe–Mg chemical and isotopic zoning in natural olivines. *Geochimica et Cosmochimica Acta, 154*, 130-150.

Peate, D. W., Breddam, K., Baker, J. A., Kurz, M. D., Barker, A. K., Prestvik, T., Grassineau, N., & Skovgaard, A. C. (2010). Compositional Characteristics and Spatial Distribution of Enriched Icelandic Mantle Components. *Journal of Petrology, 51*(7),

Pogge von Strandmann, P. A. E., Burton, K. W., James, R. H., van Calsteren, P., Gislason, S. R., & Sigfússon, B. (2008). The influence of weathering processes on riverine magnesium isotopes in a basaltic terrain. *Earth and Planetary Science Letters, 276*(1), 187-197.

Polyakov, V. B., & Mineev, S. D. (2000). The use of Mössbauer spectroscopy in stable isotope geochemistry. *Geochimica et Cosmochimica Acta, 64*(5), 849-865.

Rasmussen, M. B., Halldórsson, S. A., Gibson, S. A., & Guðfinnsson, G. H. (2020). Olivine chemistry reveals compositional source heterogeneities within a tilted mantle plume beneath Iceland. *Earth and Planetary Science Letters, 531*, 116008.

Roskosz, M., Sio, C. K. I., Dauphas, N., Bi, W., Tissot, F. L. H., Hu, M. Y., Zhao, J., & Alp, E. E. (2015). Spinel–olivine–pyroxene equilibrium iron isotopic fractionation and applications to natural peridotites. *Geochimica et Cosmochimica Acta, 169*, 184-199.

Roth, A. S. G., Liebske, C., Maden, C., Burton, K. W., Schönbächler, M., & Busemann, H. (2019). The primordial He budget of the Earth set by percolative core formation in planetesimals. *Geochemical Perspectives Letters, 9*, 26-31.

Schuessler, J. A., Schoenberg, R., & Sigmarsson, O. (2009). Iron and lithium isotope systematics of the Hekla volcano, Iceland — Evidence for Fe isotope fractionation during magma differentiation. *Chemical Geology, 258*(1-2), 78-91.

Shahar, A., Young, E. D., & Manning, C. E. (2008). Equilibrium high-temperature Fe isotope fractionation between fayalite and magnetite: An experimental calibration. *Earth and Planetary Science Letters, 268*(3), 330-338.

Shorttle, O., & Maclennan, J. (2011). Compositional trends of Icelandic basalts: Implications for short-length scale lithological heterogeneity in mantle plumes. *Geochemistry, Geophysics, Geosystems, 12*(11).

Sigmarsson, O., Maclennan, J., & Carpentier, M. (2008). Geochemistry of igneous rocks in Iceland: a review. *Jökull, 58*, 139-160.

Sigmundsson, F., Einarsson, P., Hjartardóttir, Á. R., Drouin, V., Jónsdóttir, K., Árnadóttir, T., Geirsson, H., Hreinsdóttir, S., Li, S., & Ófeigsson, B. G. (2020). Geodynamics of Iceland and the signatures of plate spreading. *Journal of Volcanology and Geothermal Research, 391*, 106436.

Sio, C. K., Roskosz, M., Dauphas, N., Bennett, N. R., Mock, T., & Shahar, A. (2018). The isotope effect for Mg-Fe interdiffusion in olivine and its dependence on crystal orientation, composition and temperature. *Geochimica et Cosmochimica Acta, 239*, 463-480.

Sio, C. K. I., Dauphas, N., Teng, F.-Z., Chaussidon, M., Helz, R. T., & Roskosz, M. (2013). Discerning crystal growth from diffusion profiles in zoned olivine by in situ Mg–Fe isotopic analyses. *Geochimica et Cosmochimica Acta, 123*, 302-321.

Sobolev, A. V., Hofmann, A. W., Kuzmin, D. V., Yaxley, G. M., Arndt, N. T., Chung, S. L., Danyushevsky, L. V., Elliott, T., Frey, F. A., Garcia, M. O., Gurenko, A. A., Kamenetsky, V. S., Kerr, A. C., Krivolutskaya, N. A., Matvienkov, V. V., Nikogosian, I. K., Rocholl, A., Sigurdsson, I. A., Sushchevskaya, N. M., & Teklay, M. (2007). The amount of recycled crust in sources of mantle-derived melts. *Science, 316*(5823), 412-417.

Sobolev, A. V., Hofmann, A. W., Sobolev, S. V., & Nikogosian, I. K. (2005). An olivine-free mantle source of Hawaiian shield basalts. *Nature, 434*(7033), 590-597.

Stracke, A. (2012). Earth's heterogeneous mantle: A product of convection-driven interaction between crust and mantle. *Chemical Geology, 330*, 274-299.

Stracke, A., Genske, F., Berndt, J., & Koornneef, J. M. (2019). Ubiquitous ultra-depleted domains in Earth's mantle. *Nature Geoscience, 12*(10), 851-855.

Stracke, A., Hofmann, A. W., & Hart, S. R. (2005). FOZO, HIMU, and the rest of the mantle zoo. *Geochemistry, Geophysics, Geosystems, 6*(5).

Sveinbjörnsdóttir, Á. E., Stefánsson, A., Heinemeier, J., Arnórsson, S., Eiríksdóttir, E. S., & Ólafsdóttir, R. (2020). Assessing the sources of inorganic carbon in surface-, soil- and non-thermal groundwater in iceland by $\delta^{13}C$ and ^{14}C. *Geochimica et Cosmochimica Acta*.

Tatsumoto, M. (1966). Isotopic composition of lead in volcanic rocks from Hawaii, Iwo Jima, and Japan. *Journal of Geophysical Research (1896-1977), 71*(6), 1721-1733.

Teng, F.-Z., Dauphas, N., Helz, R. T., Gao, S., & Huang, S. (2011). Diffusion-driven magnesium and iron isotope fractionation in Hawaiian olivine. *Earth and Planetary Science Letters, 308*(3-4), 317-324.

Teng, F.-Z., Hu, Y., & Chauvel, C. (2016). Magnesium isotope geochemistry in arc volcanism. *Proceedings of the National Academy of Sciences, 113*(26), 7082-7087.

Thirlwall, M. F., Gee, M. A. M., Lowry, D., Mattey, D. P., Murton, B. J., & Taylor, R. N. (2006). Low $\delta^{18}O$ in the Icelandic mantle and its origins: Evidence from Reykjanes Ridge and Icelandic lavas. *Geochimica et Cosmochimica Acta, 70*(4), 993-1019.

Thomson, A., & Maclennan, J. (2013). The distribution of olivine compositions in Icelandic basalts and picrites. *Journal of Petrology, 54*(4), 745-768.

Urey, H. C. (1947). The thermodynamic properties of isotopic substances. *Journal of the Chemical Society (Resumed)*(0), 562-581.

van Keken, P. E., Hauri, E. H., & Ballentine, C. J. (2002). Mantle mixing: the generation, preservation, and destruction of chemical heterogeneity. *Annual review of earth and planetary sciences, 30*(1), 493-525.

Wang, Z., & Eiler, J. M. (2008). Insights into the origin of low-$\delta^{18}O$ basaltic magmas in Hawaii revealed from in situ measurements of oxygen isotope compositions of olivines. *Earth and Planetary Science Letters, 269*(3-4), 377-387.

Weyer, S., & Ionov, D. A. (2007). Partial melting and melt percolation in the mantle: The message from Fe isotopes. *Earth and Planetary Science Letters, 259*(1-2), 119-133.

Williams, H. M., & Bizimis, M. (2014). Iron isotope tracing of mantle heterogeneity within the source regions of oceanic basalts. *Earth and Planetary Science Letters, 404*, 396-407.

Winpenny, B., & Maclennan, J. (2011). A partial record of mixing of mantle melts preserved in Icelandic phenocrysts. *Journal of Petrology, 52*(9), 1791-1812.

Workman, R. K., Eiler, J. M., Hart, S. R., & Jackson, M. G. (2008). Oxygen isotopes in Samoan lavas: Confirmation of continent recycling. *Geology, 36*(7), 551-554.

Yaxley, G. M. (2000). Experimental study of the phase and melting relations of homogeneous basalt+ peridotite mixtures and implications for the petrogenesis of flood basalts. *Contributions to Mineralogy and Petrology, 139*(3), 326-338.

Zindler, A., & Hart, S. (1986). Chemical geodynamics. *Annual review of earth and planetary sciences, 14*, 493-571.

2 Chapter 2

Olivine chemistry reveals compositional source heterogeneities within a tilted mantle plume beneath Iceland

M. B. Rasmussen, S. A. Halldórsson, S. A. Gibson, G. H. Guðfinnsson

Published in Earth and Planetary Science Letters

https://doi.org/10.1016/j.epsl.2019.116008

Keywords: olivine, trace elements, mantle heterogeneity, Iceland, helium isotopes

Abstract

High-Fo olivine (Fo=Mg/(Mg+Fe) mol%) is an ideal proxy for establishing the compositions of primary melts and their mantle sources. This has been exploited in establishing lithological variations in the mantle source regions of oceanic basalts, including in Iceland. However, previous studies on Icelandic olivine lack spatial and temporal coverage. We present high-precision *in-situ* major, minor and trace element analyses of Fo-rich olivine from a suite of 53 primitive basalts erupted in the neovolcanic rift and flank zones of Iceland, as well as in older regions of Quaternary and Tertiary crust. Most of these samples have previously been analysed for $^{3}He/^{4}He$, which ranges from 6.7 to 47.8 R_A, the largest span reported for any oceanic island. By combining trace elemental variability with $^{3}He/^{4}He$, we assess the extent of lithological variability in the Icelandic mantle plume. Trace-element ratios that are likely to preserve information about mantle source regions (e.g., Mn/Fe, Ni/(Mg/Fe), Ga/Sc, Zn/Fe and Mn/Zn) suggest a peridotitic mantle source in all rift-related volcanic regions, as well as in the off-rift flank zones of Öræfajökull and Snæfellsnes. However, a signal of a more pyroxenitic mantle lithology is clearly visible in olivine from the South Iceland Volcanic Zone, which represents the southward propagation of the Eastern Rift Zone, while olivine from Tertiary lavas suggests a mixed peridotite-pyroxenite source composition. We are able to identify four components present in the Icelandic mantle: a lithologically heterogeneous plume component with $^{3}He/^{4}He$ >MORB; a depleted MORB-like peridotite; an isotopically enriched MORB-like peridotite; and a peridotitic component with $^{3}He/^{4}He$ <MORB, sampled in the off-rift flank zone at Öræfajökull. The spatial distribution of these four components can be explained by a northward tilted mantle plume. This has previously been proposed by geophysical and geochemical studies of both Hawaii and Iceland suggesting that the plume geometry could be a contributing factor in controlling some of the spatial variation in source lithology beneath ocean islands.

2.1 Introduction

Early-formed, high-forsterite (Fo =Mg/(Mg+Fe) mol%) olivine in Ocean Island Basalts (OIBs) is an ideal proxy for primary melt and mantle source compositions. This is particularly true for slowly diffusing minor and trace elements, and isotopic ratios which are resilient to overprinting of primary chemical composition by crustal processes. Traditionally, studies of compositional variations in the mantle beneath oceanic islands have largely relied on the analysis of whole-rock samples, glasses and melt inclusions. Nevertheless, this material is often heavily modified by magmatic processes occurring in the Earth's crust such as fractional crystallisation and weathering on its surface. Meanwhile, the development of high-precision minor and trace elemental analysis of high-Fo olivine to determine mantle compositions, makes it possible to target regions where pristine glasses or whole-rock samples are unavailable, or where melt inclusions have been extensively modified following lava emplacement. An example of this approach is the use of minor elemental characteristics of such crystals as tools to unravel mantle-derived source heterogeneities by distinguishing between olivine-poor and olivine-rich mantle lithologies in the Earth's mantle (e.g., Sobolev *et al*., 2005; 2007; Herzberg *et al.*, 2016). However, this simplified model has been criticised in several studies and caution has been suggested when applying Ni and Mn as a proxy for mantle source lithology. This is because the mineral-melt partition coefficients of both of these elements are highly temperature and pressure-dependent (e.g., Matzen *et al*., 2013; 2017a; 2017b), and vulnerable to crustal processes, such as mixing, recharge events and early clinopyroxene crystallisation (Herzberg *et al*., 2014; 2016; Gleeson & Gibson, 2019; Hole, 2018). Nevertheless, careful consideration of other trace elements (e.g., Howarth & Harris, 2017; Le Roux *et al*., 2011) and lithospheric thickness (e.g., Matzen *et al*., 2017b) can aid in distinguishing between primary mantle source features and the effect of crustal processes. Another element that has been proven useful for distinguishing source lithological variations is Zn. Both Zn/Fe and Mn/Zn have been shown to be very sensitive to the melting of an olivine-free and garnet-rich source (pyroxenite) as this process fractionates the Zn, Fe and Mn (Le Roux *et al*., 2011; Howarth & Harris, 2017) while fractionation between these elements during melting of an ol-opx assemblage (peridotite) is minimal.

Iceland is an ideal location to test relationships between isotopic variability and olivine chemistry as there is an abundance of suitable olivine-phyric samples, as well as a wealth of studies focusing on radiogenic isotopes and trace elements in the same or similar locations. Three different geochemical and petrological igneous rock series are observed within individual rift and off-rift systems in Iceland: tholeiitic in the rift zones and transitional and alkalic in the off-rift zones (Jakobsson *et al*., 2008). Basalts from these rock series have specific isotopic characteristics that are thought to reflect geographically distinct heterogeneities within the mantle source regions beneath the island (e.g., Kokfelt *et al*., 2006; Peate *et al*., 2010; Harðardóttir *et al*., 2018; Shorttle *et al*., 2013). In their global study of olivine from both Mid Ocean Ridge Basalt (MORB) and several OIB localities, Sobolev *et al*. (2007) included 23 samples from 12 locations in the neovolcanic regions of Iceland to identify the presence of pyroxenite, representing the incorporation of recycled oceanic crust in the underlying mantle source region. They suggested that OIBs overlying thin lithosphere, such as Iceland, would be predominantly derived from a peridotitic source. This is because any deeper pyroxenitic signal would be overprinted by shallower peridotitic melts generated

by larger degrees of adiabatic decompression melting. The positive correlation between indicators of a pyroxenitic source lithology (e.g., low Mn/Fe_{ol}) and the long-lived $^{187}Os/^{188}Os$ radiogenic system (Sobolev *et al*., 2008), however, supports the presence of pyroxenite derived from recycled oceanic crust in the Icelandic mantle source. A reason for this inconsistency was proposed by Neave *et al*. (2018), who found that, despite the olivine chemistry from Reykjanes Peninsula suggesting a peridotitic source lithology, glass and whole-rock compositions required variability in the amount of clinopyroxene present in their sources, highlighting the need for coupled datatsets to cover the entire variability sampled by Icelandic magmas. Finally, independent studies on radiogenic isotope compositions of Icelandic lavas have shown that the enriched components in the Icelandic mantle show several signs of being related to the incorporation of old recycled components (e.g., Koornneef *et al*., 2012) stressing the need to characterise these components further.

Most previous studies of lithological heterogeneity in the Icelandic mantle suffer from a lack of regional and temporal coverage (e.g., Sobolev *et al*., 2007; Nikkola *et al*., 2019; Neave *et al*., 2018). In this study, we attempt to overcome these limitations by targeting high-Fo olivine from primitive basalts covering all neovolcanic rift and flank zones as well as regions of older Quaternary and Tertiary crust. By further coupling inferences from mineral chemistry with previously published analyses of $^{3}He/^{4}He$ in the same set of samples we can: (i) identify regions directly affected by the up-welling Icelandic plume; (ii) distinguish between the presence of recycled (low $^{3}He/^{4}He$) and primordial (high $^{3}He/^{4}He$) mantle domains; and (iii) establish how these different domains contribute to melt generation in the various volcanic regions in Iceland.

2.2 Sample selection and prior work

The studied sample suite consists of 53 samples (listed in data supplement for Chapter 2, T1) from primitive lavas that contain some of the most Fo-rich olivine sampled in neovolcanic (<1 Ma), Quaternary and Tertiary (1-15 Ma) Icelandic basalts (Figure 2.1a). Many of these samples have been included in previous investigations (Harðardóttir *et al*., 2018 and references therein) and we refer to these studies for other data pertaining to the sample suite. A primary motivation for focusing on olivine in this sample suite is that their $^{3}He/^{4}He$ values span the largest range reported for any oceanic island (from 6.7 to 47.8 R_A, where R_A=air $^{3}He/^{4}He$; see Harðardóttir *et al*. (2018) and Figure 2.1b). The highest $^{3}He/^{4}He$ were found in olivine fluid and melt inclusions from Tertiary lavas in the West Fjords (TER, up to 47.8 R_A) and in neovolcanic lavas from Central Iceland (ERZ, Eastern Rift Zone) with values up to 24.5 R_A. These high-He domains were interpreted as the location of previous and current plume centres (Harðardóttir *et al*., 2018). Critically for this study, He isotopic ratios of the targeted high-Fo olivine are unlikely to be affected by secondary processes and should therefore be representative of their mantle source (see section 5.3). For simplicity, the data presented in this study is classified according to the regions defined in Figure 2.1 where ERZ, WRZ (Western Rift Zone) and NRZ (Northern Rift Zone) all lie along the current rift axis. SIVZ (South Iceland Volcanic Zone) is a flank zone located at the southern tip of ERZ, which is regarded as a propagation of the main rift. ÖVZ (Öræfajökull Volcanic Zone) and SNS (Snæfellsnes) are both flank zones where transitional and alkalic magmas prevail. TER is olivine from Tertiary lavas, mostly from the West Fjords, while HRP (Hreppar formation) represents an isolated region with Plio-Pleistocene aged rocks (Kristjánsson *et al*., 1998), located between the WRZ and ERZ (Figure 2.1a).

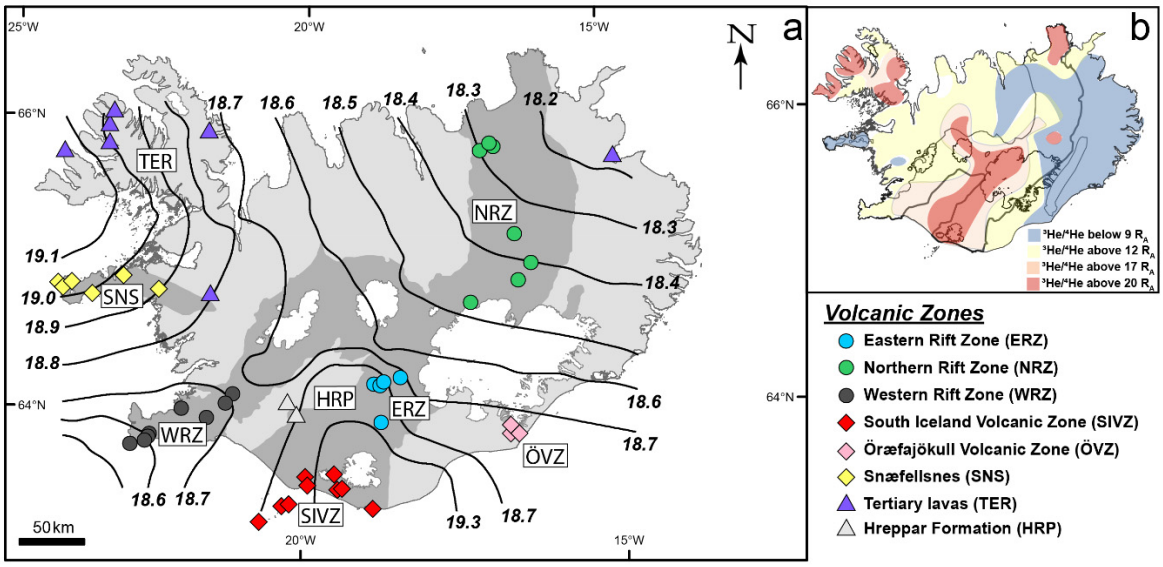

Figure 2.1 Localities of samples used in this study (a) and a summary of the results of helium interpolation maps from Harðardóttir et al. *(2018) in the upper right corner (b). The sample map has been overlain by $^{206}Pb/^{204}Pb$ contours (modified from Kokfelt* et al.*, 2006) and shows that the most radiogenic Pb isotopic compositions are present in both SNS and SIVZ. Abbreviations are as follows: ERZ: Eastern Rift Zone, NRZ: Northern Rift Zone, WRZ: Western Rift Zone, SIVZ: South Iceland Volcanic Zone, ÖVZ: Öræfajökull Volcanic Zone, SNS: Snæfellsnes, TER: Tertiary lavas, HRP: Hreppar Formation. The blue areas represent regions with $^{3}He/^{4}He$ <9 R_A and the red areas represent regions with $^{3}He/^{4}He$ >20 R_A.*

2.3 Analytical methods

2.3.1 Electron microprobe analyser (EMPA)

Epoxy mounts were prepared with 3-8 olivine grains per sample. The olivines were analysed for major and minor elements (Si, Mg, Fe, Ni, Mn and Ca) by EMPA using a JEOL JXA-8230 electron microprobe at the Institute of Earth Sciences, University of Iceland with the method and settings developed by Batanova *et al*. (2015) and described by Gómez-Ulla *et al*. (2017). A modification was made to the processing time for the EDS analyses of Si, Fe and Mg which reduced the deadtime by 56%, closer to the optimum range of 20-50%. San Carlos olivine, provided by the Smithsonian Institution (NMNH 111312-44), was used as a primary standard for analyses of Si and as a secondary standard for comparison with the reference values presented in Batanova *et al*. (2015). The relative standard deviation (RSD) for San Carlos olivine analyses was below 0.6% for major elements (Si, Mg and Fe) and below 1.2% for minor elements (Ni, Mn and Ca). Further information regarding the reproducibility of individual elements is given in section 5.1.

To avoid any effect of chemical zonation and possible heterogeneity, we analysed a minimum of three points at the core of each olivine. For comparison with published data, normalisation between our standard values and those of Sobolev *et al*. (2007) was performed

for Ni and Mn concentrations. A corresponding correction was added to our measured values, which are the values that will be used throughout this study. Both data sets are available in data supplement for Chapter 2, T2.

2.3.2 Laser ablation inductively coupled plasma mass spectrometry (LA-ICP-MS)

To directly relate the trace element concentrations to our EMPA measurements, the exact same spots were analysed by a ESI UP193UC laser system coupled to a Perkin Elmer Nexion 350D Inductively Coupled Plasma Mass Spectrometer (LA-ICP-MS) at the Department of Earth Sciences, University of Cambridge. These analyses were performed with a circular spot size of 100µm, a repetition rate of 20 Hz and laser power of 0.7 mJ (7 J/cm^2) throughout the whole study in order to optimise the signal, while avoiding obvious melt and mineral inclusions. NIST 612 was used for calibration and in-house San Carlos (BD4074OL) olivine was used as secondary standard while BIR-1G and NIST 614 were analysed as unknown standards. Relative Standard Deviation (RSD) for Al, Sc, V, Cr, Co and Zn in San Carlos olivine was well below 5% but Ga had a RSD of 22% (see section 5.1.2). However, the concentration of Ga in the San Carlos standard is below 0.05 ppm, close to the detection limit, while the average concentration measured in the samples was around 0.2 ppm with an average RSD of 6% (see data supplement for Chapter 2, T3). The accuracy for all elements measured in the standards is reported in section 5.1, Table 5.2-5.4. To ensure accurate and representative results three points were analysed by LA-ICP-MS in each grain. Following the measurements, the signals were evaluated and reduced using the GLITTER software package. After filtering the data for impurities in the signal, the three measurements were averaged to avoid heterogeneity resulting from the presence of minor inclusions. The error bars presented on the graphs are based on the largest error whether it be sample intra-variability (2SD) or analytical error (2SD). The exact 2SDs are found beneath each element in data supplement for Chapter 2, T2 and T3 and section 5, Table 5.1-5.2. If no error bar is present, the 2SD is smaller than the symbol.

2.4 Results

The Icelandic olivines analysed in our study range from $Fo_{79.9}$ to $Fo_{91.8}$ (Figure 2.2). We observed limited intra-grain variability but some intra-sample variation (see T1 and T2 in data supplement for Chapter 2). Importantly, variations in elemental concentrations of the olivines significantly exceed the analytical precision, given as 2SD (standard deviation) at any given Fo content (see data supplement for Chapter 2). Below follows an overview of the chemical variations recorded with regards to minor and trace elements in Icelandic olivine and a selection of elemental ratios.

2.4.1 Minor element variations (>0.1 weight%)

Olivine in primitive Icelandic basalts record a variation in Ni and Mn concentrations between 990-3060 ppm and 1010–2174 ppm, respectively, whereas Ca contents range from 1532 to 2774 ppm (Figure 2.2). This is in good agreement with the olivine dataset published by Nikkola *et al*. (2019). Olivine from the rift-related regions ERZ, NRZ, WRZ and the off-rift regions ÖVZ and SNS is generally characterised by lower Ni contents (as low as 1820 ppm

in SNS at Fo_{89}) and higher Mn and Ca contents (up to 1327 and 2746 ppm at Fo_{89}) than olivine from SIVZ and in the TER samples at the same Fo content (Figure 2.2). Notably, olivine from SIVZ records the highest Ni concentrations (up to 3024 ppm at Fo_{89}) and the correspondingly lowest Mn and Ca concentrations (down to 1069 and 1618 ppm at Fo_{89}) relative to the other volcanic regions at similar Fo contents. Olivine from NRZ display greater variation and covers most of the Icelandic range, while olivine from HRP, located to the west of ERZ, shows decoupled minor elements with a relative enrichment in Ni without a concomitant depletion in Ca and Mn.

2.4.2 Trace element variations (<0.1 weight%)

The measured trace element concentrations for Icelandic olivines are listed in Table T3 in data supplement for Chapter 2 and a selection of elements (Al, Sc, Zn, and Ga) are plotted against Fo content in Figure 2.3. Al concentrations vary from 516 ppm at Fo_{92} in NRZ to 139 ppm at Fo_{85} in ERZ, and 204 ppm at Fo_{80} in SIVZ (Figure 2.3a), completely overlapping previously published data. Sc (Figure 2.3b) shows a variation across Iceland from 3.4 to 7.5 ppm, seemingly independent of the change in Fo content and region. Zinc concentrations (Figure 2.3c) however, correlate negatively with Fo content and range between 66 and 164 ppm, mostly overlapping with previously published data. The highest concentrations of Zn are found in olivine from SIVZ. Ga concentrations (Figure 2.3d) range between 0.1 and 0.26 ppm and show no tangible correlation with the change in Fo content or regional affiliation.

2.4.3 Elemental ratios

100Mn/Fe ranges between 1.23 and 1.76 but does not correlate with Fo content (Figure 2.4a). The lowest 100Mn/Fe values are found in olivine from SIVZ and TER, while the highest are observed in olivine from the rift zones and SNS. A similar pattern is seen in Mn/Zn (Figure 2.4b), which ranges between 9 and 21, with the lowest ratios found in olivine from SIVZ and TER. The highest Ni* values (Ni/(Mg/Fe)1000) are found in olivine from SIVZ and TER (up to 1.20), while the lowest are found in olivine from the rift zones, SNS and ÖVZ (<0.5), as seen in Figure 2.4c. Ni* also appears unaffected by changes in Fo content (Figure 2.4c), although there might be a weak negative correlation between Ni* and Fo content in the case of ÖVZ. A similar systematic is observed for Ga/Sc (Figure 2.4d); with higher ratios found in samples from SIVZ and TER, while rift-related olivine, and olivine from SNS, typically exhibit lower ratios. However, no apparent correlation is visible between Ga/Sc and Fo content. The same distribution is observed for variations in Zn/Fe that overlap with previously published data for Iceland. The variation, however, is less distinct and therefore makes regional differences less clear (Figure 2.4e). Ca/Al as presented in Figure 2.4f does not vary significantly with Fo content and overlaps with previously published olivine data from Iceland.

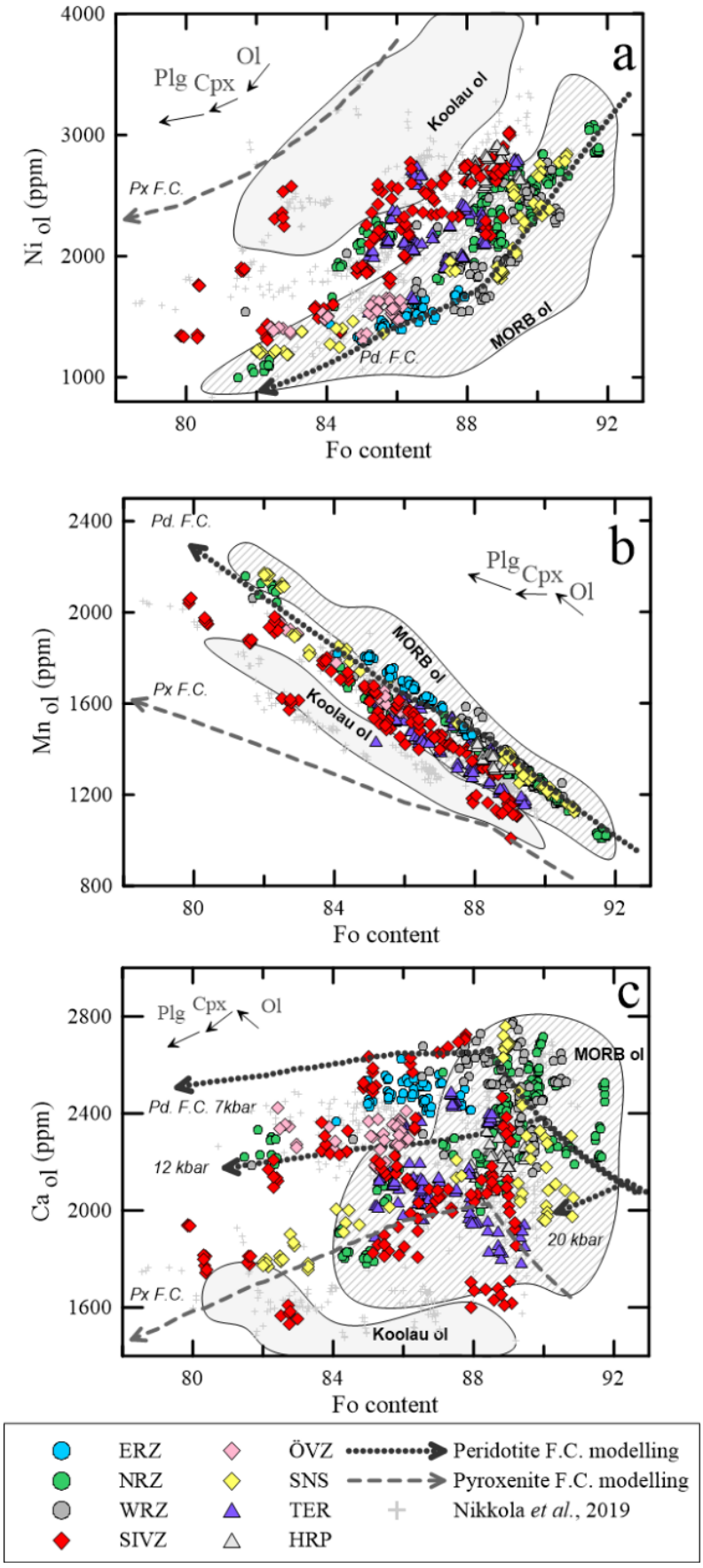

See figure caption on the next page

Figure 2.2 to the left a) Ni, b) Mn and c) Ca versus Fo content in Icelandic olivine. Figure on the previous page. Olivine from ERZ, NRZ, WRZ, ÖVZ and SNS is dominantly characterised by lower Ni content and higher Mn and Ca contents relative to olivine from the SIVZ and the TER samples at the same Fo content. The black and grey dotted lines represent the modelled fractional crystallisation (F.C.) path following melting from a purely peridotitic (Pd. F.C.) and pyroxenitic (Px. F.C.) lithology, respectively at 7 kbar. For the modelled F.C. path from a peridotitic melt, the initial crystallisation pressure was further increased to 12 and 20 kbar resulting in earlier crystallisation of clinopyroxene which in turn resulted in low-Ca olivine mimicking the effect of lithological variations. However, these crystallisation pressures exceeds the known crystallisation pressures for Icelandic magmas and high-pressure clinopyroxene crystallisation is therefore unlikely to be the main control on the variation in Ca. The grey and striped fields represent previously published data for Koolau (Hawaiian) and MORB olivine from Sobolev et al. *(2007) while the grey crosses represent high-precision analysis of Icelandic olivine from Nikkola* et al. *(2019). The error is smaller than the symbols.*

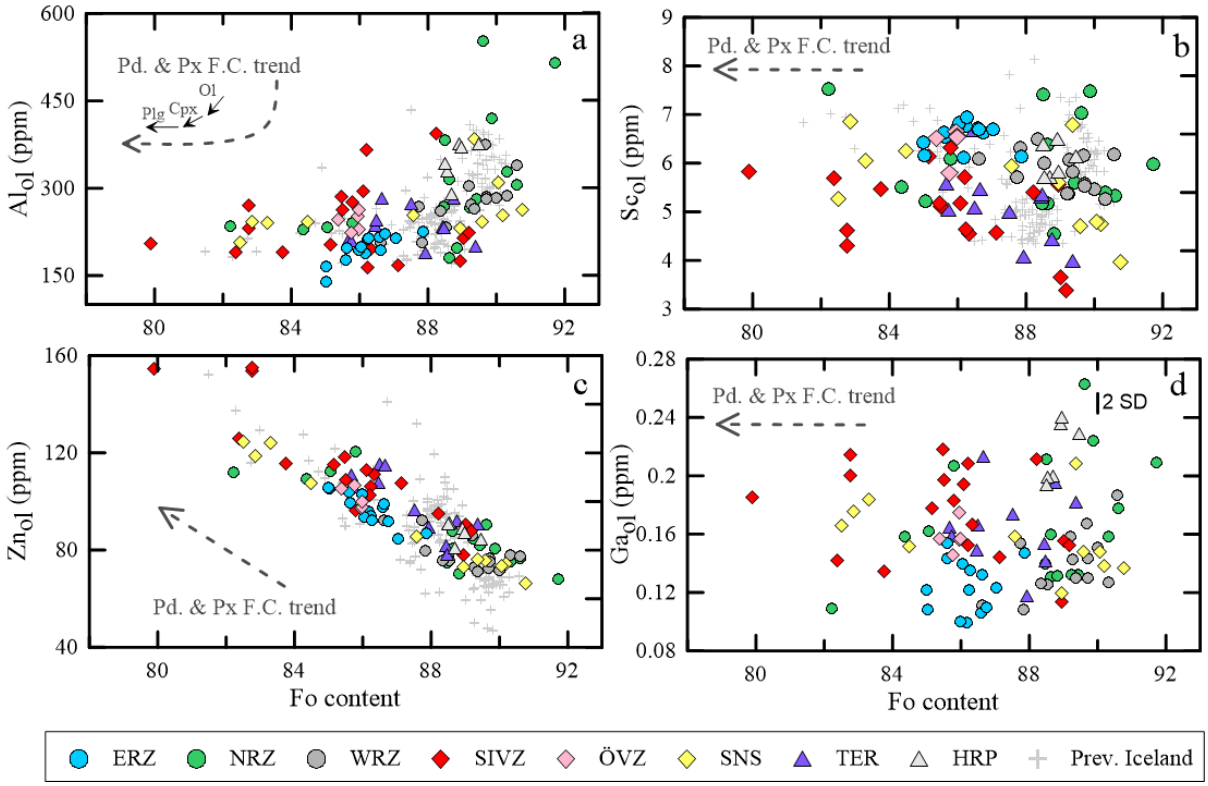

Figure 2.3 *Trace element concentrations versus Fo content in Icelandic olivine. a) The Al content appears to be spatially independent, suggesting that other features, such as source temperature, may play a role (see section 2.5.2). b) Sc content shows no clear correlation with Fo content but mostly overlaps with previous published data. c) The negative correlation between Zn content and Fo content suggests that Zn concentrations are highly dependent on Fo, like Mn. d) Ga content in olivine appears independent of Fo content. Despite the very low concentrations, we observe a big variation, exceeding the 2SD. The grey crosses represent high-precision analysis of Icelandic olivine from Neave* et al. *(2018) and Nikkola* et al. *(2019). If no error bar is marked, the error is smaller than the symbol.*

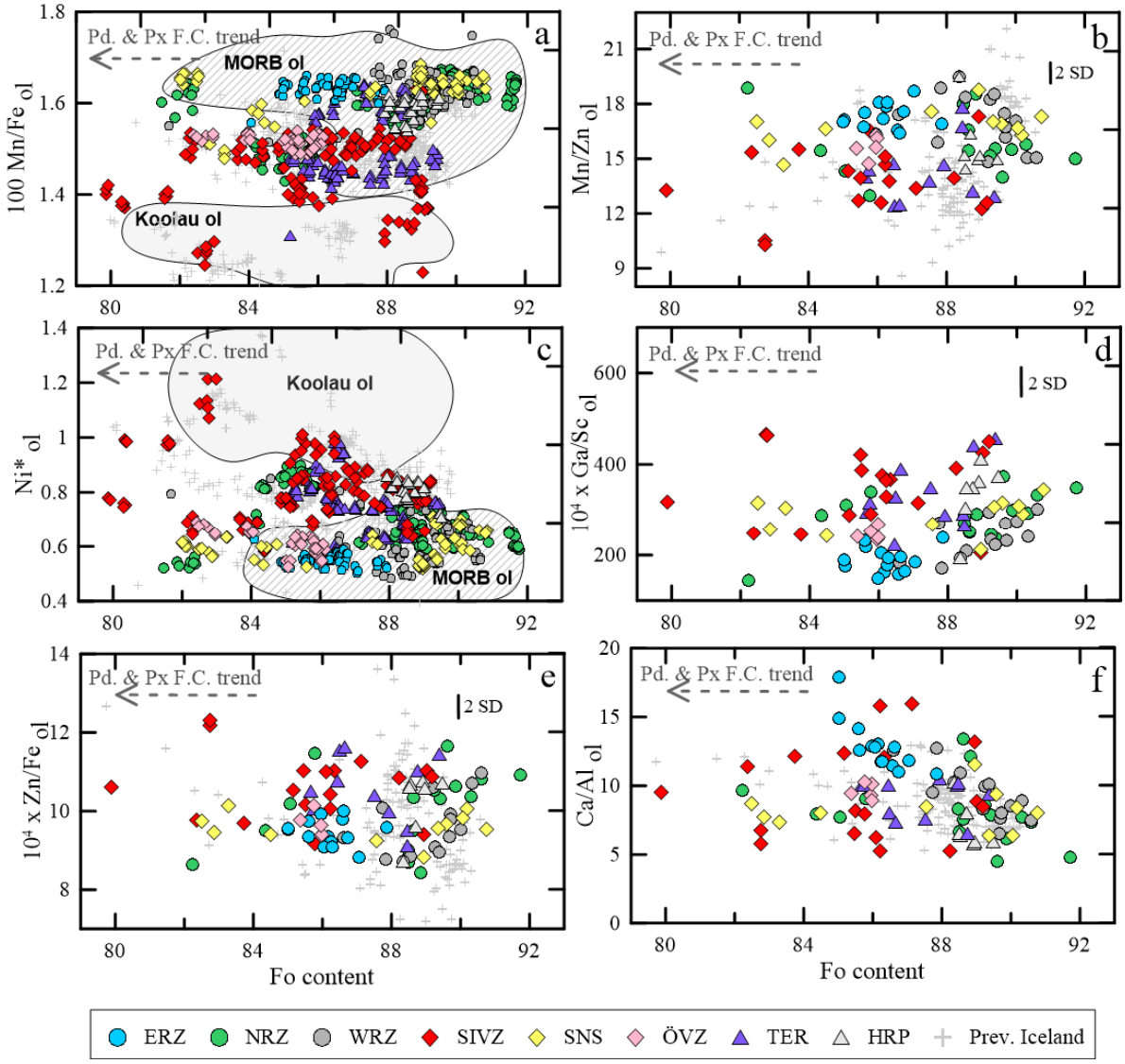

Figure 2.4 Elemental ratios versus Fo content in Icelandic olivine. Plot a)-f) shows chemical ratios that all show a lack of correlation with Fo content. This suggests that these ratios are controlled by source parameters, such as changes in the dominant source lithology. Notably, olivine from SIVZ and TER overlap with Koolau (Hawaiian) olivine in a) and c) suggesting various proportions of pyroxenitic derived melt. The rest of the Icelandic olivines plot in the MORB-generated field, suggesting a dominantly peridotitic source lithology. A similar image is seen in b) where low Mn/Zn is characteristic of a more pyroxenitic source lithology. d) Olivine from SIVZ and TER plot with relatively high Ga/Sc, mirroring the trends of the ratios adopted in a) to c). e) Likewise, Zn/Fe ratios show higher Zn/Fe (indicative of a more pyroxenite-garnet dominated source) in SIVZ and TER. f) Ca/Al appears to be largely unaffected by a lowering in Fo content. However, olivine from ERZ appears to show a negative trend, which might be caused by re-equilibration processes, as discussed in section 2.5.2. The MORB and Koolau fields in a) and c) are based on data from Sobolev et al. *(2007) and the grey crosses represent high-precision analysis of Icelandic olivine from Neave* et al. *(2018) and Nikkola* et al. *(2019). If no error bar is marked, the error is smaller than the symbol.*

2.5 Discussion

2.5.1 Chemical characteristics of Icelandic olivine; identifying modified mantle signatures

Magmatic crustal processes, such as fractional crystallisation, assimilation and diffusion-induced modifications, can conceal mantle-derived chemical heterogeneity. When evaluating the preservation and implications of source-derived signatures, we therefore attempt to circumvent the effects of these crustal processes. While Fe and Mg contents have been used extensively for evaluating crustal residence times based on rates of diffusion (e.g., Kahl *et al*., 2013), the minor and trace elements considered in this study generally undergo slower diffusion in olivine than Fe and Mg (Spandler & O'Neill, 2010). Therefore, the effects of fractional crystallisation, assimilation and diffusion superimposed on the olivine chemistry can be evaluated by considering variations in elemental concentrations with Fo content. Any correlations between these elemental concentrations and Fo content are likely indicative of such secondary processes.

First, we emphasize that the olivines analysed in this study display a significant range in minor and trace elemental concentrations at a given Fo content (Figure 2.2 and Figure 2.3), a feature which is difficult to explain with fractional crystallisation alone. To further test the effects of fractional crystallisation on olivine chemistry, we calculated crystal fractionation paths using a forward modelling approach with the Petrolog software (Danyushevsky & Plechov, 2011). Model parameters, including partition coefficient models, are presented in section 5.2. We considered a simple closed-system crystallisation with co-crystallisation of olivine, clinopyroxene and plagioclase at 7 kbar from melts derived from two end-member source compositions, pyroxenite and peridotite, based on compositions given in Sobolev *et al*. (2007) and Walter (1998), respectively. Model results for Ni, Mn, and Ca are superimposed on Figure 2.2 and the general crystallisation trends are marked in Figure 2.3 and Figure 2.4. It can be clearly seen that a simple fractional crystallisation model using a melt from a single lithology cannot explain the complete variation recorded in the chemistry of Icelandic olivine, as was also suggested by Shorttle & Maclennan (2011). The concentration of Ca does not correlate with Fo content (Figure 2.2c), suggesting that other aspects might be the controlling factor, such as source lithology, mantle temperature or high-pressure crystallisation of clinopyroxene (Sobolev *et al*., 2007; De Hoog *et al*., 2010; Hole, 2018). A melt that has undergone early high-pressure crystallisation of clinopyroxene can crystallise high-Fo olivine with lower Ca and higher Ni, falsely suggesting a more pyroxenite-rich melt-source (Hole, 2018). High-pressure clinopyroxene crystallisation might indeed explain the low Ca content in low-Fo olivine from SNS and NRZ (Figure 2.2c) and the correspondingly high Ni-olivine in NRZ but cannot explain the entire variation we observe in SIVZ. However, the pressures necessary to explain the low Ca and high Ni in SIVZ, NRZ and low Ca in SNS by high-pressure clinopyroxene crystallisation (>12kbar) greatly exceeds the expected crystallisation pressures for primitive Icelandic magmas (up to 10 kbar; e.g., Winpenny & Maclennan, 2011) suggesting either that: the melts crystallise olivine much deeper than previously thought, or that another process is responsible for the variable Ca content of Icelandic olivine. Ca and Ni have further been shown to be susceptible to crustal processes, such as melt mixing and mafic recharge events that lower and increase the concentrations, respectively (Herzberg *et al*., 2014; 2016; Gleeson & Gibson, 2019), and these processes might explain the decoupling of Ni enrichment and Mn and Ca depletion in the HRP olivine (Figure 2.2). However, as the high Ni and low Ca concentrations are

consistently coupled with low Mn in the remaining sample suite, this effect appears to be uncommon in Icelandic olivine. Finally, the lack of clear correlations of Mn/Fe, Mn/Zn, Ni*, Ga/Sc, Zn/Fe and Ca/Al with Fo content (Figure 2.4) suggests that any variations recorded by these ratios are primary features rather than secondary. As the overall regional trends are similar for Zn/Fe and Mn/Zn, but clearer in the latter case, we will use Mn/Zn as a measure of Zn variations unaffected by crustal processes in the following sections.

2.5.2 Implications of olivine minor and trace element variability for lithological heterogeneities within the Icelandic mantle

Based on olivine minor elemental data from Hawaii, Sobolev *et al*. (2005; 2007) suggested that Ni, Mn and Ca contents of high-Fo olivine may be used to distinguish between melts derived from a dominantly olivine-poor pyroxenitic or olivine-rich peridotitic mantle lithology. This interpretation was based upon findings by Yaxley & Green (1998) in which the formation of an olivine-free source lithology, or hybrid pyroxenite, was by a reaction between eclogite-derived silicate melts and peridotite, thereby entailing the incorporation of recycled oceanic crust. Mallik and Dasgupta (2012) later showed that melts derived from eclogite pods in an upwelling plume, can react with surrounding fertile peridotite at shallow pressures to generate pyroxenites. In contrast, Herzberg *et al*. (2014) found that variable extents of re-fertilisation of peridotite by pyroxenite-generated melts were the main control on the range of Mn/Fe in olivine from the Cook Islands. Alternatively, the re-fertilised plume component may generate melts from a mixed peridotite-pyroxenite component, as was proposed for SIVZ by Nikkola *et al*. (2019). While we cannot distinguish between these various models, common to them is the incorporation of recycled material in the source and this recycled signal being preserved in the compositional variability of primary olivine. Accordingly, we use the term "pyroxenitic" to express the presence of incorporated recycled material in the source of Icelandic olivines.

In this section, we aim to evaluate and discuss the trace elemental variation observed in Icelandic olivine considering the possible lithological heterogeneities present in the Icelandic mantle. Figure 2.2 shows the newly acquired Icelandic data set overlain with compositional fields for olivine from Koolau (Hawaii), representing a dominantly pyroxenitic source, and from MORB, representing a dominantly peridotitic source (Sobolev *et al*., 2007). We note that Icelandic olivine from SIVZ and TER and part of NRZ (Upptyppingar and Vaðalda) plot in the Koolau field, suggesting that there may be a significant contribution of pyroxenite-derived melt. However, as discussed in section 2.5.1, these NRZ samples are possibly affected by co-crystallisation of clinopyroxene and we will therefore not consider them further. The rest of Icelandic olivines plot within the field of MORB, suggesting peridotite-derived melts dominating these volcanic systems. A similar observation is made with regards to Mn/Fe and Ni* in Figure 2.4a and c. The co-variation of these ratios (r^2=0.55; p-value of <0.05), presented in Figure 2.5a, shows how high Ni* is largely coupled to high Mn/Fe in the Icelandic data set. Similar regional trends are observed on a plot of Ga/Sc versus Mn/Zn (Figure 2.5b), which are elemental ratios that have previously been proposed as useful means of distinguishing between peridotitic and pyroxenitic source lithologies (Howarth & Harris, 2017; Søager *et al*., 2015). Here we find a negative correlation (r^2=0.64; p-value of <0.05) between these ratios, where olivine from SIVZ have the highest Ga/Sc and lowest Mn/Zn, characteristic of olivine derived from a dominantly pyroxenitic mantle component and/or a high modal abundance of garnet in the source lithology. Olivines from the rift zones (ERZ, NRZ, WRZ), SNS, HRP and ÖVZ,

however, plot in the peridotite-derived melt field, while TER olivine creates a continuous link between the two fields.

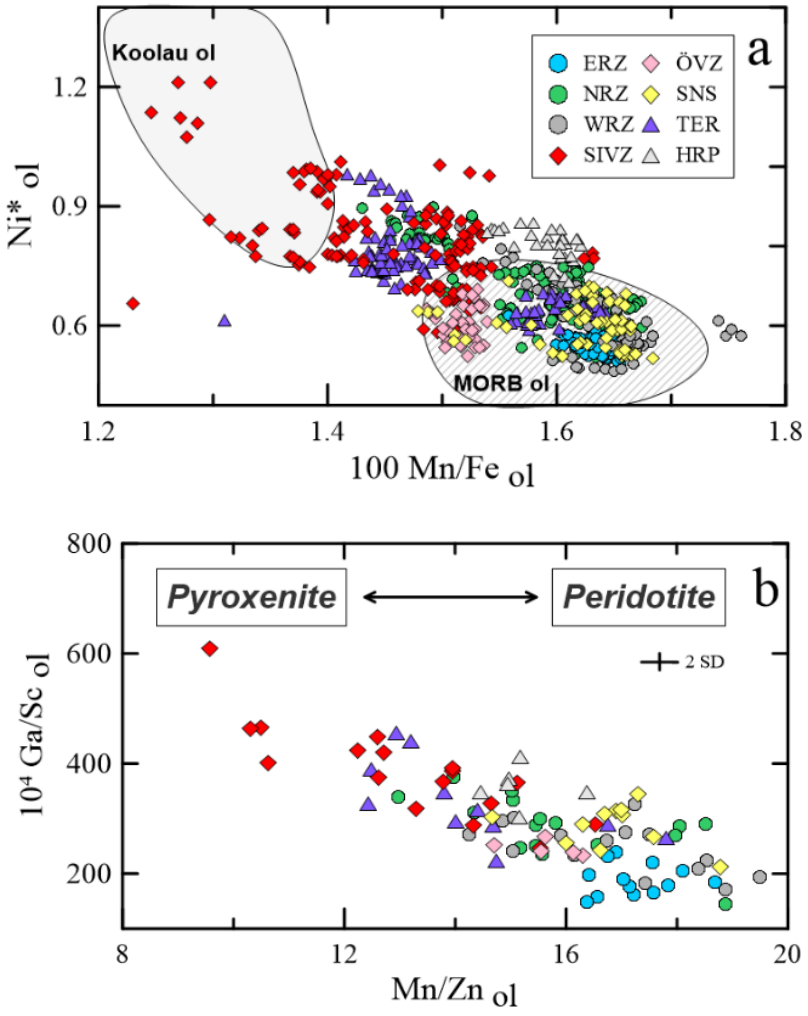

Figure 2.5 Trace elemental ratios reflecting lithological variations in the Iceland mantle. a) A negative correlation can be seen between Ni and Mn/Fe. Olivine from the rift-related zones, ÖVZ and SNS plot mostly within the MORB field as defined by Sobolev* et al. *(2007). Overlap of SIVZ and Koolau (Hawaiian) olivine compositions suggests that the source of SIVZ lavas have various proportions of pyroxenite within their source lithology. b) The negative correlation between Ga/Sc and Mn/Zn suggests that these ratios are related. Howarth & Harris (2017) recommend the use of Mn/Zn when distinguishing between peridotite and pyroxenite as the dominant source lithology, with an approximate boundary at Mn/Zn ratios of 14. Olivine from the rift-related zones, but also from ÖVZ and SNS fall within the field characteristic for the melting of a dominantly peridotitic source lithology. However, olivine from the SIVZ falls mostly within the pyroxenitic field and TER between the two fields. This strong correlation suggests that pyroxenite-derived olivine is depleted in Sc relative to peridotite-derived olivine, which could be controlled by the presence of garnet. If no error bar is marked, the error is smaller than the symbol.*

As demonstrated by several experimental studies (e.g., Pertermann & Hirschmann, 2003; Mallik & Dasgupta, 2012), the melting of a more fusible pyroxenite component would commence at higher pressure or greater depths during mantle ascent than a more refractory peridotitic component. Therefore, if pyroxenite is present in the Icelandic mantle, the strongest signals are expected in olivine from flank zones where the melting columns are shorter, and more likely to preserve this deep-derived pyroxenitic signal. Short and deeply truncated melting columns were indeed proposed to be the cause of preferred sampling of radiogenic, enriched components in SIVZ and SNS by Kokfelt *et al*. (2006) who suggested that this enriched nature was the result of the presence of a garnet pyroxenite. Somewhat surprisingly, this depth-of-sampling model is inconsistent with the chemistry of olivine from SNS which consistently indicates a purely peridotitic mantle lithology (e.g., low Mn/Fe and high Ni*, see Figure 2.5a). A possible explanation for this inconsistency was presented in Gómez-Ulla *et al*. (2017), as an effect of re-equilibration of the deep-sourced melts with dunite conduits in the lithosphere to generate a peridotitic "fingerprint". They argued that this process could be traced by Ca/Al in olivine with high Ca/Al indicative of lower crystallisation temperatures related to heat loss following the re-equilibration process. Using similar arguments, we find that, despite a notable difference in Mn/Fe, olivine from SNS and SIVZ have comparable Ca/Al (Figure 2.6), suggesting similar crystallisation temperatures and a relatively fast ascent (Gómez-Ulla *et al*., 2017). The chemistry of olivine from ERZ however, suggests crystallisation at relatively lower temperatures (Figure 2.6). In the latter case, this is consistent with the frequent occurrence of evolved tholeiitic basalts in the region (e.g., Kokfelt *et al*., 2006) indicative of an extensive plumbing system allowing for re-equilibration and melt evolution. Although we cannot exclude the possibility of different re-equilibration processes occurring in SNS (or other processes controlling the enrichment here, see also Shorttle and Maclennan, 2011), it seems unlikely that similar processes would be absent in the SIVZ. Another possibility for the decoupling of radiogenic enrichment and olivine chemistry is the presence of a clinopyroxene-rich but olivine-bearing component in the mantle (as shown for WRZ by Neave *et al*., 2018) or a re-fertilised peridotitic mantle component which could have been overprinted by recycled radiogenic signal as shown for the Cook Islands by Herzberg *et al*. (2014).

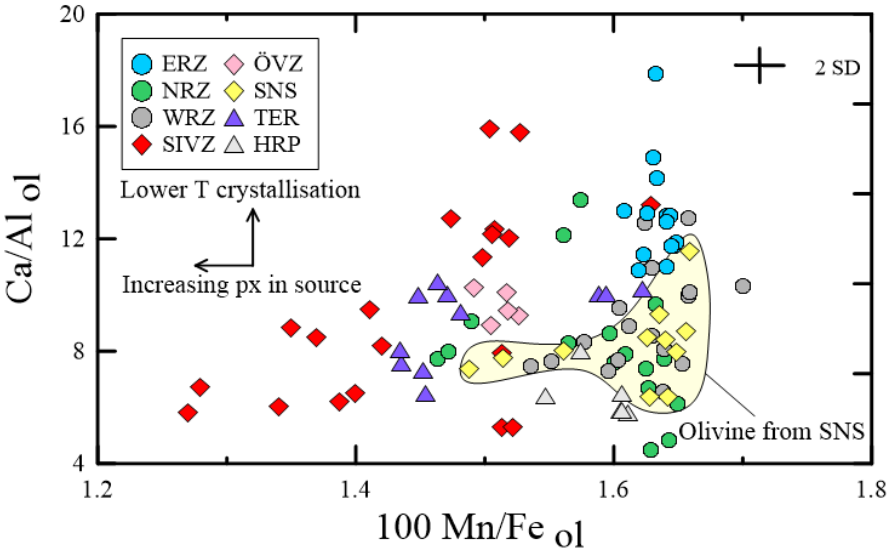

Figure 2.6 Ca/Al as a proxy for olivine crystallisation temperature versus Mn/Fe as a proxy for source lithological variations. A higher Ca/Al was proposed by Gómez-Ulla et al. *(2017) to represent lower crystallisation temperature caused by re-equilibration of the mantle melts with deep crustal dunitic conduits, increasing the Mn/Fe ratio. This effect is not observed in the chemistry of SNS olivine, suggesting that such a process is not important there. Rather, high Mn/Fe in olivine from SNS is produced by melting of a peridotitic source lithology.*

Variations in temperature and pressure have been shown to affect the partitioning of Ni and Mn into olivine, such that a change in melting depth could mimic a change in source lithology (e.g., Matzen *et al*., 2013; 2017a; 2017b). For evaluating this effect on our dataset, we used the method of Matzen *et al*. (2017b) that correlates the depth of melting, or the lithospheric thickness (depth to the Lithospheric-Asthenospheric Boundary, LAB), with NiO/MnO corrected to Fo_{89}, essentially considering olivine from melts from which only olivine is expected to crystallise. With this model, Matzen *et al*. (2017b) showed how peridotitic melts that are generated at high pressure (4-4.5 GPa, corresponding to a LAB of 120 km) crystallise olivine at low pressures with high Ni and low Mn concentrations or a $NiO_{89}/MnO_{89}>2.5$ resulting in a seemingly pyroxenitic source composition. We find that Icelandic olivines with Fo >88 display NiO_{89}/MnO_{89} between 1.3–2.6 (Figure 2.7), which overlaps with published data from Icelandic samples (Matzen *et al*., 2017b). Importantly, high NiO_{89}/MnO_{89} values (up to 2.6) are found exclusively in olivine from SIVZ. These values are comparable to olivine crystallised from Hawaiian basalts where the plume upwells beneath lithosphere with a thickness of about 90 km (Watson and McKenzie, 1991). However, the lithosphere underlying the actively rifting volcanic regions of Iceland is 45 km thick or less (Bjarnason and Schmeling, 2009; Jenkins *et al*., 2018). Although lithospheric thickness has not been measured directly beneath SIVZ, a pressure corresponding to a depth of 45 km was found to explain final melt equilibration depths for olivine in SIVZ (Nikkola *et al*., 2019). As a lithospheric thickness of 90 km would be necessary in order to explain NiO_{89}/MnO_{89} as high as 2.6 (see Figure 2.7), this highlights the importance of lithological controls on the chemistry of olivine from the SIVZ.

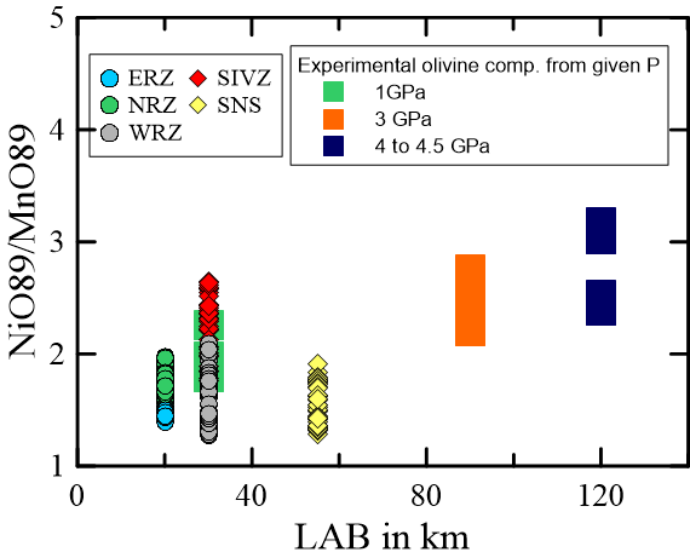

Figure 2.7 A plot showing NiO_{89}/MnO_{89} of Icelandic olivine following the approach of Matzen et al. *(2017b), versus Lithospheric-Asthenospheric-Boundary (LAB) depths (Bjarnason and Schmeling, 2009). Final melting at depths greater than 90 km (and pressures of 3 GPa) would be necessary to explain the variations observed in SIVZ, an unlikely scenario for the neovolcanic zones of Iceland. The LAB beneath SIVZ is based on data from the WRZ, but we note that the lithosphere is likely thicker under the former. In the case of SNS we have adopted depth estimates available for the Northwest Fjords, noting that these likely represent maximum values for the LAB under SNS.*

2.5.3 Helium isotopic implications for the origin of lithological heterogeneity

Unique to our study is the extensive $^3He/^4He$ database compiled and published by Harðardóttir *et al*. (2018) for the same set of samples. As ^3He is a primordial isotope, $^3He/^4He$ values >MORB of 8 R_A (e.g., Graham, 2002) are generally associated with the tapping of a primordial or incompletely degassed reservoir. In the case of Iceland, a region of high $^3He/^4He$ (up to 25 R_A) present in much of central and South Iceland, is indicative of active plume upwelling (Harðardóttir *et al*., 2018). Further, the $^3He/^4He$ of the sample suite targeted for this study are unaffected by crustal processes, such as crustal and air contamination accompanying the degassing of He (see section 5.3). Therefore, we plot sample-averaged Mn/Fe and Ga/Sc as proxies for lithological variations alongside $^3He/^4He$ in Figure 2.8. Here, we observe three trends, two of which show a correlation between He isotopes and the proxies of mantle source lithology (Figure 2.8) and are present in rift zone samples, but also in samples from SIVZ and TER. The third trend, which involves constant $^3He/^4He$, is evident in samples from SNS, ÖVZ and low-$^3He/^4He$ samples (MORB-like) from the NRZ. Importantly, the observed correlations suggest that an increase in a plume-derived component, as traced by $^3He/^4He$ >MORB, is accompanied by a greater pyroxenitic contribution beneath some segments of the rift zones, as well as SIVZ and TER. A similar correlation was previously identified in both recent volcanic products and in the early Icelandic plume, suggesting that this is a long-term characteristic of the plume (e.g., Brandon *et al*., 2007; Debaille *et al*., 2009; Starkey *et al*., 2009). Notably, SIVZ, which represents the southward propagation of ERZ, displays some of the highest $^3He/^4He$ found in the

neovolcanic zones (up to 21.6 R_A). Olivines from this region also have the lowest Mn/Fe of all samples studied, suggesting a dominantly plume-related pyroxenitic contribution.

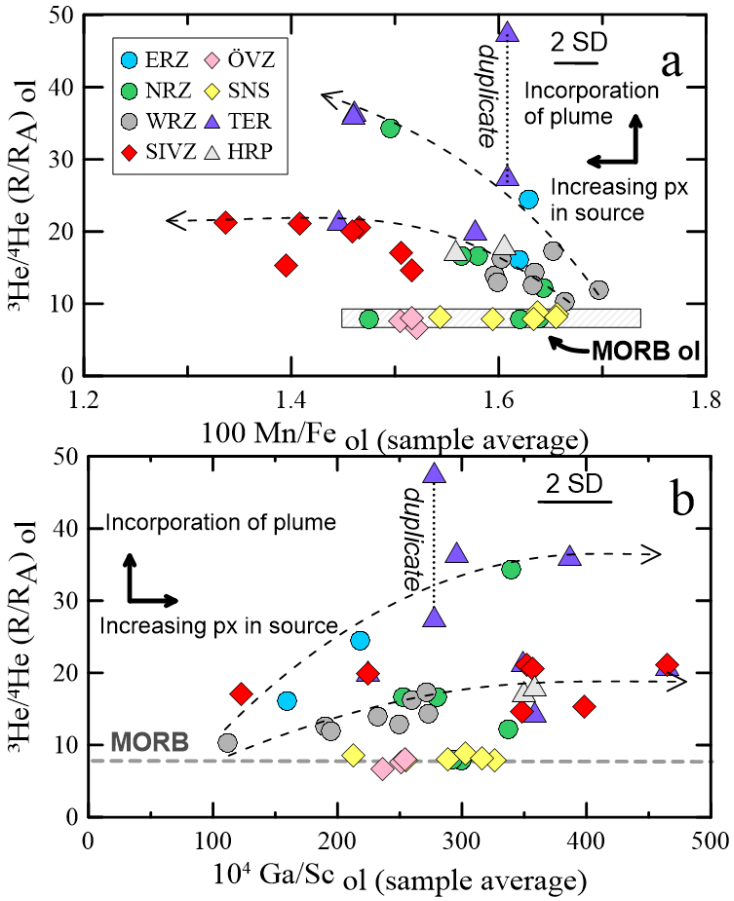

Figure 2.8 Helium isotopic ratios measured in the same set of olivines versus sample-averaged a) Mn/Fe and b) Ga/Sc. Three groups plot along various mixing lines; one with values close to those observed in MORB (general MORB $^3He/^4He$ values of 8 R_A ± 1 and olivine data from Sobolev et al. *(2007)); the second trending towards very low Mn/Fe and high Ga/Sc ratios (suggesting a greater incorporation of pyroxenite) and helium ratios of around 20 R_A; and the third trending towards intermediate Mn/Fe and Ga/Sc and very high $^3He/^4He$ of up to ~40 R_A. The third trend is especially defined by the TER samples, while the second trend is mostly defined by young Icelandic volcanics. Ga/Sc ratios for MORB olivine are unavailable but the horizontal line has helium isotopic ratio of 8 R_A ± 1. The two TER points connected with a dotted line represent a duplicate of a single sample (see Harðardóttir* et al.*, 2018).*

This positive correlation between the proportion of pyroxenitic melt (representing a recycled enriched component) and high $^3He/^4He$ appears incongruous as a recycled component would be expected to have low $^3He/^4He$ due to the increase in radiogenic ^4He with time and expected loss of ^3He during subduction. Interestingly, melt inclusions in olivine from early Icelandic plume volcanics (Starkey *et al.*, 2012) suggest the presence of high $^3He/^4He$ in both enriched and depleted mantle components in the Icelandic plume. The lack of $^3He/^4He$ data from olivine from ERZ creates difficulties when attempting a similar interpretation.

However, based on the exceptionally high average $^{3}He/^{4}He$ recorded in clinopyroxene, volcanic glasses, geothermal fluids and two olivine samples of 18-25 R_A in this region (Harðardóttir *et al*., 2018), we can assume that a high $^{3}He/^{4}He$ component is likely to dominate here. Further, olivine from ERZ suggests a purely peridotitic source and is readily explained by extensive melting at shallow levels, which would overwhelm any deep-sourced pyroxenitic signature (Sobolev *et al*., 2007). This suggests that an extended melting column, as is likely to be present beneath central Iceland, causes overprinting of the deeply-sourced more fusible components. The opposite is likely the case for SIVZ where a shorter melting column would preferentially tap the pyroxenitic component, as was proposed by Kokfelt *et al*. (2006). As evident from the early Icelandic plume, this implies that high $^{3}He/^{4}He$ is characteristic for both the enriched (more pyroxenite-rich) and depleted (more peridotitic) mantle components. The distribution of high $^{3}He/^{4}He$ irrespective of lithological variations, could easily be explained by rapid loss of He from the peridotite following incipient melting and segregation of volatile-rich melts. In this case, low absolute abundances of ^{3}He in the pyroxenite would be overprinted by peridotite-derived, high [^{3}He] and $^{3}He/^{4}He$ which exclusively resided in the peridotitic component.

2.5.4 A model for the modern Icelandic plume

Based on a model proposed for the Hawaiian plume, Hofmann *et al*. (2011) suggested that the displacement of high $^{3}He/^{4}He$ domains in Iceland could be explained by northward tilting of the Icelandic plume (with the plume stem extending to the south). The displacement at depth was proposed to occur beneath the Reykjanes Ridge at least 100 km south from the inferred centre of the Icelandic plume, and to be caused by plate-driven upper mantle flow (see also Shen *et al*., 2002). Later, by detailed mapping of the helium isotope distribution in Iceland, Harðardóttir *et al*. (2018) demonstrated how the distribution of the high $^{3}He/^{4}He$ signal along ERZ and into SIVZ could be explained by a northward tilted Icelandic plume stem, as inferred from mantle anisotropy, global mantle circulation models and receiver function seismology (e.g., Shen *et al*., 2002). In accordance with this model and on the basis of recent studies of the Hawaiian plume (e.g., Abouchami *et al*., 2005; Jones *et al*., 2017), we propose that the preferred tapping of melts from the various mantle lithologies identified in this study can be realised by a northward tilting plume sampling a heterogenous basal layer of the lower mantle. Notably, this model can satisfactorily explain the olivine chemistry we observe and the distribution of $^{3}He/^{4}He$ across Iceland (Figure 2.1b).

In the case of a tilted Icelandic plume, tapping of high $^{3}He/^{4}He$ melts generated deep in the plume stem would result in the preferential sampling of the more fusible pyroxenite-rich component, as evident in olivine from SIVZ (Figure 2.9). This would be a region of relatively low degrees of melting, which would lessen the dilution from the shallow, preferentially peridotite melting. In contrast to this, the centre of the plume would tap a mixture of deeply-derived pyroxenite-rich melts and shallower peridotite melts (Figure 2.9). The centre of the plume stem and the active rift zones are regions of high degrees of melting that would dilute any pyroxenite-derived melts sampled at depth, as the chemistry of rift-related olivine shows. The varying but mostly MORB-like $^{3}He/^{4}He$ in olivine from NRZ suggest that the contribution from the high $^{3}He/^{4}He$ plume component decreases towards the north and that another MORB-like peridotitic component must be sampled here. Similar arguments apply when evaluating the >MORB $^{3}He/^{4}He$ captured in olivine from the WRZ. Here, a mixture of a peridotite-dominated high $^{3}He/^{4}He$ plume component and a slightly enriched MORB-like component could explain the chemical variations observed.

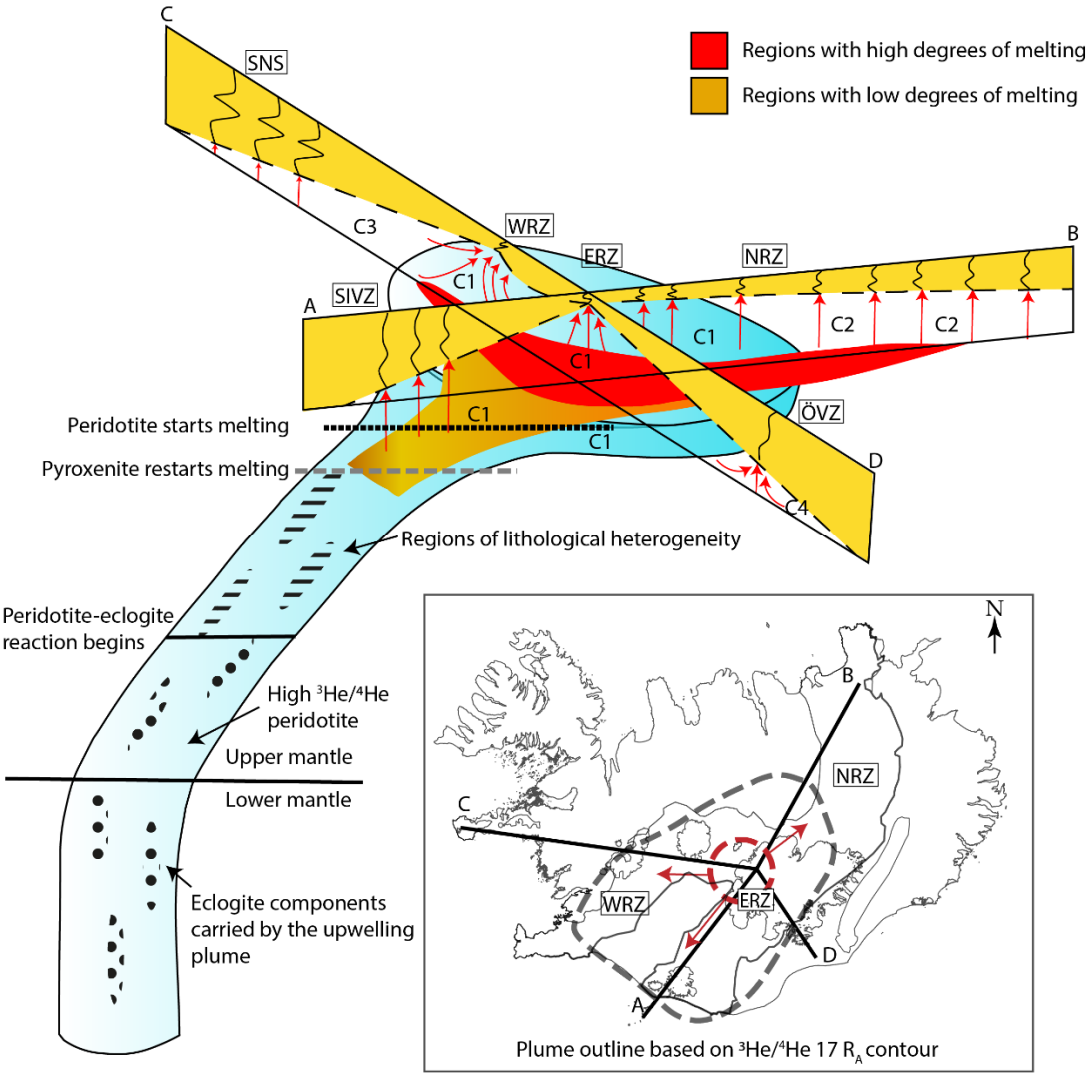

Figure 2.9 Conceptual model of a tilted Icelandic mantle plume based on trace-element patterns presented in this study and previously published $^{3}He/^{4}He$ isotopic variations (Harðardóttir et al.*, 2018 and references therein). Four components can be used to explain the chemical patterns captured in Icelandic olivines. The characteristics of the components C1-4 are summarised in section 2.6. The red field marks a region of high-degree melting (which extends up to the base of the lithosphere), while the orange field marks regions of low-degree melts. The blue field marks the presence and interaction of plume-derived melts (>MORB $^{3}He/^{4}He$). The eclogite (dotted fields) is carried within the plume and reacts with the surrounding peridotite somewhere in the upper mantle, generating lithological heterogeneities, such as pyroxene-enriched and olivine-depleted (pyroxenite) lithologies. The more fusible pyroxenite component (dashed fields) starts melting deeper in the plume column and tapping of melts from this low degree melt region (orange field) will result in pyroxenite-dominated melt compositions and olivine with low Mn/Fe and high Ga/Sc. The tilting results in low-degree melts with high $^{3}He/^{4}He$, similar to those sampled at the plume head under ERZ. Due to the high degrees of melting in the rift zones, any trace of pyroxenite-derived melts will be overprinted by the peridotitic signatures. The red circle and arrows on the inset map of Iceland represent the proposed location of the plume head based on Harðardóttir* et al. *(2018) and the dispersion of the high $^{3}He/^{4}He$ component. This is a modified version of a model for a tilted Hawaiian plume from Jones* et al. *(2017).*

As previously noted, the source beneath SNS has been proposed to show signs of the incorporation of a recycled component. SNS lavas, which are characterised by more radiogenic Pb compositions relative to rift related lavas (Figure 2.1a), appear to primarily represent sampling of deep, low-degree melts (Kokfelt *et al*., 2006; Peate *et al*., 2010). However, the enrichment in radiogenic Pb (Figure 2.1a) does not correlate with any lithologically controlled elemental ratios discussed here, suggesting that the enrichment is not caused by the incorporation of recycled oceanic crust. Moreover, no signs of porous flow reactions, such as those observed in the chemistry of olivine from the Canary Islands (Gómez-Ulla *et al*., 2017), were identified in olivine from SNS, which could otherwise explain the high Mn/Fe. In light of the MORB-like $^{3}He/^{4}He$ that prevail in this region (Harðardóttir *et al*., 2018), it seems probable that the mantle beneath SNS is unaffected by any plume activity and that the radiogenic compositions found here are decoupled from the plume source and related to other processes, such as re-fertilisation rather than the direct incorporation of a recycled component at depth (see Shorttle and Maclennan, 2011). Importantly, the lack of plume-derived components – as traced with $^{3}He/^{4}He$ – and lack of any signs of pyroxenitic signatures in the SNS, suggests that the Icelandic plume is the main carrier of these lithological heterogeneities.

Finally, we note that $^{3}He/^{4}He$ similar to, and lower than MORB, coupled with peridotite source-like Mn/Fe are found in olivine from ÖVZ (Figure 2.8a). The low $^{3}He/^{4}He$ is unique for this region and likely relate to the anomalous Pb and Sr isotopic patterns observed here (Peate *et al*., 2010; Manning and Thirlwall, 2014), indicative of the incorporation of recycled sediments in the mantle source (e.g., Halldórsson *et al*., 2016) or the melting of a sliver of continental lithosphere entrained in the Icelandic mantle (e.g., Torsvik *et al*., 2015). In this case, however, lowering of $^{3}He/^{4}He$ by ~ 1 R_A and the olivine chemical characteristics cannot be used to distinguish between these processes.

2.5.5 Implications for the origin and preservation of a high $^{3}He/^{4}He$ mantle domain in the Icelandic plume

The exceptionally high $^{3}He/^{4}He$ measured in olivine from Tertiary Icelandic basalts (up to 47.8 R_A) with intermediate Mn/Fe compositions suggest that the lithological heterogeneity of the Icelandic plume is not a recent phenomenon. These observations agree with the findings of Starkey *et al*. (2012) and suggestions made by Yaxley (2000). Higher $^{3}He/^{4}He$ (up ~50 R_A) found in olivine both from Tertiary Icelandic basalts, Greenland and Baffin Island (the proto-Icelandic plume) relative to recent Icelandic volcanics (up to 34 R_A; see Harðardóttir *et al*., 2018) further suggest that the Icelandic plume has tapped a mantle reservoir evolving with time. Combined high $^{3}He/^{4}He$ and signs of the incorporation of a recycled crustal component in the same mantle domain could indicate that a recycled component has been continuously added into the Icelandic plume's melt-source region during the Cenozoic (Mundl-Petermeier *et al*., 2019).

This observation also raises the question as to how high $^{3}He/^{4}He$ are preserved while recycled components are incorporated. This process has been discussed in several papers (e.g., Brandon *et al*., 2007; Tolstikhin and Hofmann, 2005; Starkey *et al*., 2009), but the common conclusion of them all is, that the initial reservoir, primordial or not (see Tolstikhin and Hofmann, 2005), must have been greatly enriched in He. In a recent study, Roth *et al*. (2019) suggest that sufficient He was incorporated into the core during core-mantle differentiation to consistently resupply the lower mantle with primordial helium, thus

characterised by high $^{3}He/^{4}He$. Either way, based on the lowering of $^{3}He/^{4}He$ characteristic for the Icelandic plume, the upwelling lower mantle reservoir is either degassing with time and/or continuously incorporating greater amounts of recycled components. This model is supported by thermometry which shows an overall cooling of the Icelandic plume with time (e.g., Herzberg and Gazel, 2009). A similar conclusion was drawn for the Galapagos plume and attributed to slower ascent rates following incorporation of recycled crust (Trela *et al*., 2015). Previous studies suggested that the incorporation of a minimum of 5% recycled oceanic crust and excess mantle potential temperatures of ~1480 °C were required to explain published geophysical and geochemical observations in Iceland (Shorttle *et al*. (2014); Matthews *et al*., 2016). These estimates and the high buoyancy of the Icelandic plume (Jackson *et al*., 2017) make the current transport and incorporation of a minimum of 5% oceanic crust and possibly up to 40% (Shorttle and Maclennan, 2011) a likely scenario.

2.6 Conclusions

High-Fo olivine crystals found in large suites of primitive basalts collected from across Iceland show significant variations in minor and trace elements (Ni, Mn, Ca, Al, Sc, Zn and Ga). Olivine from the South Iceland Volcanic Zone cannot be explained by differences in the melting pressure but requires various contributions from a pyroxenitic or re-fertilised peridotitic mantle. We see no evidence for the incorporation of a recycled oceanic crust in the form of pyroxenite in Snæfellsnes, despite indications from radiogenic isotopic enrichment. Helium isotopes previously measured on the same set of samples confirm the trends observed in the trace element patterns and suggest that the Icelandic plume, as traced by high $^{3}He/^{4}He$ isotopes, is lithologically heterogenous. We propose the presence of four components in the Icelandic mantle that are sampled to various degrees across the neovolcanic zones:

(i) A lithologically heterogenous component ("C1" on Figure 2.9) with high-$^{3}He/^{4}He$ values. Melts derived from this component crystallises olivine with variable Mn/Fe and Ga/Sc indicating the presence of both peridotitic and more pyroxenitic lithologies. The sampling of pyroxenitic dominated melts appears to be proportionally greatest in South Iceland (SIVZ), where the melting column is shorter and there is less dilution by shallow peridotite-derived melts whereas peridotite-sourced melts are dominating central Iceland (ERZ) where large degrees of low-pressure melting is dominant.

(ii) Peridotite with MORB-like $^{3}He/^{4}He$ forms melts that crystallise olivine with high Mn/Fe and low Ga/Sc. This component ("C2" on Figure 2.9) is more prevalent in the northern part of the Northern Rift Zone (NRZ).

(iii) Peridotite with MORB-like $^{3}He/^{4}He$ ("C3" on Figure 2.9) and high $^{206}Pb/^{204}Pb$ generates melts that crystallise olivine with high Mn/Fe and low Ga/Sc sampled mainly in Snæfellsnes (SNS). This component is possibly slightly re-fertilised based on the high $^{206}Pb/^{204}Pb$ but shows no signs of being enriched through recycled crust interaction.

(iv) Peridotite with $^{3}He/^{4}He$ slightly below MORB and EM1-type radiogenic isotopic compositions sampled only at Öræfajökull (ÖVZ). This component ("C4" on Figure 2.9) appears otherwise to be similar to "C2" sampled in NRZ.

The spatially controlled sampling of these four components can be explained by a northward tilt of the Icelandic plume stem (Figure 2.9), as previously inferred from geophysical evidence (e.g., Shen *et al*., 2002). We show that olivines from Tertiary Icelandic basalts with exceptionally high $^{3}He/^{4}He$ (up to 47.8 R_A; Harðardóttir *et al*., 2018) have Mn/Fe compositions that are intermediate between those crystallised from peridotite and pyroxenite sourced melts and suggest that the lithological heterogeneity of the Icelandic plume is long-lived.

2.7 Acknowledgements

This work was funded by the Nordic Volcanological Center. SAH further acknowledges support from the Icelandic Research Fund (Grant #196139-051) and the University of Iceland Research Fund. We are grateful to Jason Day for assistance with LA-ICP-MS analyses and data evaluation, and Charlotte Jackson, Eemu Ranta and Rósa Ólafsdóttir for help with data treatment and drafting of figures. Karl Grönvold, Ingvar Atli Sigurðsson, Paavo Nikkola and Kristján Geirsson are thanked for supplying some of the samples and Thomas F. Kokfelt, Paul Martin Holm for good discussions. Special thanks to Sunna Harðardóttir for all her work on the Iceland helium data. We are very grateful for the comments and suggestions provided by our reviewers David Neave and Claude Herzberg who have made this a better manuscript and for the editorial handling by Rajdeep Dasgupta. Finally, we would like to express our gratitude to David Hilton for his help and guidance in the initial stages of this project and his indispensable contributions to the scientific community.

2.8 References

Abouchami, W., Hofmann, A. W., Galer, S. J. G., Frey, F. A., Eisele, J., & Feigenson, M. (2005). Lead isotopes reveal bilateral asymmetry and vertical continuity in the Hawaiian mantle plume. *Nature, 434*, 851.

Batanova, V. G., Sobolev, A. V., & Kuzmin, D. V. (2015). Trace element analysis of olivine: High precision analytical method for JEOL JXA-8230 electron probe microanalyser. *Chemical Geology, 419*, 149-157.

Bjarnason, I. T., & Schmeling, H. (2009). The lithosphere and asthenosphere of the Iceland hotspot from surface waves. *Geophysical Journal International, 178*(1), 394-418.

Brandon, A. D., Graham, D. W., Waight, T., & Gautason, B. (2007). ^{186}Os and ^{187}Os enrichments and high-$^{3}He/^{4}He$ sources in the Earth's mantle: evidence from Icelandic picrites. *Geochimica et Cosmochimica Acta, 71*(18), 4570-4591.

Danyushevsky, L. V., & Plechov, P. (2011). Petrolog3: Integrated software for modeling crystallization processes. *Geochemistry, Geophysics, Geosystems, 12*(7).

De Hoog, J. C. M., Gall, L., & Cornell, D. H. (2010). Trace-element geochemistry of mantle olivine and application to mantle petrogenesis and geothermobarometry. *Chemical Geology, 270*(1-4), 196-215.

Debaille, V., Trønnes, R. G., Brandon, A. D., Waight, T. E., Graham, D. W., & Lee, C.-T. A. (2009). Primitive off-rift basalts from Iceland and Jan Mayen: Os-isotopic evidence for a mantle source containing enriched subcontinental lithosphere. *Geochimica et Cosmochimica Acta, 73*(11), 3423-3449.

Gleeson, M. L. M., & Gibson, S. A. (2019). Crustal controls on apparent mantle pyroxenite signals in ocean-island basalts. *Geology, 47*(4), 321-324.

Gómez-Ulla, A., Sigmarsson, O., & Gudfinnsson, G. H. (2017). Trace element systematics of olivine from historical eruptions of Lanzarote, Canary Islands: Constraints on mantle source and melting mode. *Chemical Geology, 449*, 99-111.

Graham, D. W. (2002). Noble gas isotope geochemistry of mid-ocean ridge and ocean island basalts: Characterization of mantle source reservoirs. *Reviews in Mineralogy and Geochemistry, 47*(1), 247-317.

Halldórsson, S. A., Barnes, J. D., Stefánsson, A., Hilton, D. R., Hauri, E. H., & Marshall, E. W. (2016). Subducted lithosphere controls halogen enrichments in the Iceland mantle plume source. *Geology, 44*(8), 679-682.

Harðardóttir, S., Halldórsson, S. A., & Hilton, D. R. (2018). Spatial distribution of helium isotopes in Icelandic geothermal fluids and volcanic materials with implications for location, upwelling and evolution of the Icelandic mantle plume. *Chemical Geology, 480*, 12-27.

Herzberg, C., & Gazel, E. (2009). Petrological evidence for secular cooling in mantle plumes. *Nature*, *458*(7238), 619.

Herzberg, C., Cabral, R. A., Jackson, M. G., Vidito, C., Day, J. M. D., & Hauri, E. H. (2014). Phantom Archean crust in Mangaia hotspot lavas and the meaning of heterogeneous mantle. *Earth and Planetary Science Letters*, *396*, 97-106.

Herzberg, C., Vidito, C., & Starkey, N. A. (2016). Nickel–cobalt contents of olivine record origins of mantle peridotite and related rocks. *American Mineralogist, 101*(9), 1952-1966.

Hofmann, A. W., Farnetani, C. G., Spiegelman, M., & Class, C. (2011). Displaced helium and carbon in the Hawaiian plume. *Earth and Planetary Science Letters*, *312*(1-2), 226-236.

Hole, M. J. (2018). Mineralogical and geochemical evidence for polybaric fractional crystallization of continental flood basalts and implications for identification of peridotite and pyroxenite source lithologies. *Earth-Science Reviews, 176,* 51-67.

Howarth, G. H., & Harris, C. (2017). Discriminating between pyroxenite and peridotite sources for continental flood basalts (CFB) in southern Africa using olivine chemistry. *Earth and Planetary Science Letters, 475*, 143-151.

Jackson, M. G., Konter, J. G., & Becker, T. W. (2017). Primordial helium entrained by the hottest mantle plumes. *Nature*, *542*(7641), 340.

Jakobsson, S. P., Jónasson, K., & Sigurdsson, I. A. (2008). The three igneous rock series of Iceland. *Jökull, 58*, 117-138.

Jenkins, J., Maclennan, J., Green, R. G., Cottaar, S., Deuss, A. F., & White, R. S. (2018). Crustal formation on a spreading ridge above a mantle plume: receiver function imaging of the Icelandic crust. *Journal of Geophysical Research: Solid Earth*, *123*(6), 5190-5208.

Jones, T. D., Davies, D. R., Campbell, I. H., Iaffaldano, G., Yaxley, G., Kramer, S. C., & Wilson, C. R. (2017). The concurrent emergence and causes of double volcanic hotspot tracks on the Pacific plate. *Nature, 545*, 472.

Kahl, M., Chakraborty, S., Costa, F., Pompilio, M., Liuzzo, M., & Viccaro, M. (2013). Compositionally zoned crystals and real-time degassing data reveal changes in magma transfer dynamics during the 2006 summit eruptive episodes of Mt. Etna. *Bulletin of Volcanology*, *75*(2), 692.

Kokfelt, T. F., Hoernle, K., Hauff, F., & Fiebig, J. (2006). Combined trace element and Pb-Nd-Sr-O isotope evidence for recycled oceanic crust (Upper and Lower) in the Iceland Mantle Plume. *Journal of Petrology, 47*(9), 1705-1749.

Koornneef, J. M., Stracke, A., Bourdon, B., Meier, M., Jochum, K., Stoll, B., & Grönvold, K. (2012). Melting of a two-component source beneath Iceland. *Journal of Petrology, 53*(1), 127-157.

Kristjánsson, L., Duncan, R. A., & Guðmundsson, Á. (1998). Stratigraphy, palaeomagnetism and age of volcanics in the upper regions of þjórsárdalur valley, central southern Iceland. *Boreas, 27(1),* 1-13.

Le Roux, V., Dasgupta, R., & Lee, C. T. (2011). Mineralogical heterogeneities in the Earth's mantle: constraints from Mn, Co, Ni and Zn partitioning during partial melting. *Earth and Planetary Science Letters*, *307*(3-4), 395-408.

Mallik, A., & Dasgupta, R. (2012). Reaction between MORB-eclogite derived melts and fertile peridotite and generation of ocean island basalts. *Earth and Planetary Science Letters*, *329*, 97-108.

Manning, C. J., & Thirlwall, M. F. (2014). Isotopic evidence for interaction between Öræfajökull mantle and the Eastern Rift Zone, Iceland. *Contributions to Mineralogy and Petrology*, *167*(1), 959.

Matthews, S., Shorttle, O., & Maclennan, J. (2016). The temperature of the Icelandic mantle from olivine-spinel aluminum exchange thermometry. *Geochemistry, Geophysics, Geosystems, 17*(11), 4725-4752.

Matzen, A. K., Baker, M. B., Beckett, J. R., & Stolper, E. M. (2013). The temperature and pressure dependence of nickel partitioning between olivine and silicate melt. *Journal of Petrology, 54*(12), 2521-2545.

Matzen, A. K., Baker, M. B., Beckett, J. R., Wood, B. J., & Stolper, E. M. (2017a). The effect of liquid composition on the partitioning of Ni between olivine and silicate melt. *Contributions to Mineralogy and Petrology*, *172*(1), 3.

Matzen, A. K., Wood, B. J., Baker, M. B., & Stolper, E. M. (2017b). The roles of pyroxenite and peridotite in the mantle sources of oceanic basalts. *Nature Geoscience 10, 530-535*.

Mundl-Petermeier, A., Walker, R. J., Jackson, M. G., Blichert-Toft, J., Kurz, M. D., & Halldórsson, S. A. (2019). Temporal evolution of primordial tungsten-182 and $^{3}He/^{4}He$ signatures in the Iceland mantle plume. *Chemical Geology*, *525*, 245-259.

Neave, D. A., Shorttle, O., Oeser, M., Weyer, S., & Kobayashi, K. (2018). Mantle-derived trace element variability in olivines and their melt inclusions. *Earth and Planetary Science Letters, 483*, 90-104.

Nikkola, P., Guðfinnsson, G. H., Bali, E., Rämö, O. T., Fusswinkel, T., & Thordarson, T. (2019). Signature of deep mantle melting in South Iceland olivine. *Contributions to Mineralogy and Petrology*, *174*(5), 43.

Peate, D. W., Breddam, K., Baker, J. A., Kurz, M. D., Barker, A. K., Prestvik, T., Grassineau, N., & Skovgaard, A. C. (2010). Compositional characteristics and spatial distribution of enriched Icelandic mantle components. *Journal of Petrology, 51*(7), 1447-1475.

Pertermann, M., & Hirschmann, M. M. (2003). Partial melting experiments on a MORB-like pyroxenite between 2 and 3 GPa: Constraints on the presence of pyroxenite in basalt source regions from solidus location and melting rate. *Journal of Geophysical Research: Solid Earth, 108*(B2).

Roth, A. S. G., Liebske, C., Maden, C., Burton, K. W., Schönbächler, M., & Busemann, H. (2019). The primordial He budget of the Earth set by percolative core formation in planetesimals. *Geochemical Perspectives Letters, 9*, 26-31.

Shen, Y., Solomon, S. C., Bjarnason, I. T., Nolet, G., Morgan, W. J., Allen, R. M, Vogfjörd, K., Jakobsdóttir, S., Stefánsson, R., Julian, B. R., Foulger, G. R. (2002). Seismic evidence for a tilted mantle plume and north–south mantle flow beneath Iceland. *Earth and Planetary Science Letters*, *197*(3-4), 261-272.

Shorttle, O., & Maclennan, J. (2011). Compositional trends of Icelandic basalts: Implications for short–length scale lithological heterogeneity in mantle plumes. *Geochemistry, Geophysics, Geosystems, 12*(11).

Shorttle, O., Maclennan, J., & Piotrowski, A. M. (2013). Geochemical provincialism in the Iceland plume. *Geochimica et Cosmochimica Acta*, *122*, 363-397.

Shorttle, O., Maclennan, J., & Lambart, S. (2014). Quantifying lithological variability in the mantle. *Earth and Planetary Science Letters, 395*, 24-40.

Sobolev, A. V., Hofmann, A. W., Brugmann, G., Batanova, V. G., & Kuzmin, D. V. (2008). A quantitative link between recycling and osmium isotopes. *Science, 321*(5888), 536.

Sobolev, A. V., Hofmann, A. W., Kuzmin, D. V., Yaxley, G. M., Arndt, N. T., Chung, S. L., Danyushevsky, L. V., Elliott, T., Frey, F. A., Garcia, M. O., Gurenko, A. A., Kamenetsky, V. S., Kerr, A. C., Krivolutskaya, N. A., Matvienkov, V. V., Nikogosian, I. K., Rocholl, A., Sigurdsson, I. A., Sushchevskaya, N. M., & Teklay, M. (2007). The amount of recycled crust in sources of mantle-derived melts. *Science, 316*(5823), 412-417.

Sobolev, A. V., Hofmann, A. W., Sobolev, S. V., & Nikogosian, I. K. (2005). An olivine-free mantle source of Hawaiian shield basalts. *Nature, 434*(7033), 590-597.

Spandler, C., & O'Neill, H. S. C. (2010). Diffusion and partition coefficients of minor and trace elements in San Carlos olivine at 1,300 C with some geochemical implications. *Contributions to Mineralogy and Petrology*, *159*(6), 791-818.

Starkey, N. A., Fitton, J. G., Stuart, F. M., & Larsen, L. M. (2012). Melt inclusions in olivines from early Iceland plume picrites support high $^{3}He/^{4}He$ in both enriched and depleted mantle. *Chemical Geology, 306*, 54-62.

Starkey, N. A., Stuart, F. M., Ellam, R. M., Fitton, J. G., Basu, S., & Larsen, L. M. (2009). Helium isotopes in early Iceland plume picrites: Constraints on the composition of high 3 He/4 He mantle. *Earth and Planetary Science Letters, 277*(1), 91-100.

Søager, N., Portnyagin, M., Hoernle, K., Holm, P. M., Hauff, F., & Garbe-Schönberg, D. (2015). Olivine major and trace element compositions in Southern Payenia Basalts, Argentina: Evidence for pyroxenite–peridotite melt mixing in a back-arc setting. *Journal of Petrology, 56*(8), 1495-1518.

Tolstikhin, I., & Hofmann, A. W. (2005). Early crust on top of the Earth's core. *Physics of the Earth and Planetary Interiors*, *148*(2-4), 109-130.

Torsvik, T. H., Amundsen, H. E., Trønnes, R. G., Doubrovine, P. V., Gaina, C., Kusznir, N. J., Steinberger, B., Corfu, F., Ashwal, L. D., & Griffin, W. L. (2015). Continental crust beneath southeast Iceland. *Proceedings of the National Academy of Sciences*, 201423099.

Trela, J., Vidito, C., Gazel, E., Herzberg, C., Class, C., Whalen, W., Jicha, B., Bizimis, M., & Alvarado, G. E. (2015). Recycled crust in the Galápagos Plume source at 70 Ma: Implications for plume evolution. *Earth and Planetary Science Letters*, *425*, 268-277.

Yaxley, G. M. (2000). Experimental study of the phase and melting relations of homogeneous basalt+ peridotite mixtures and implications for the petrogenesis of flood basalts. *Contributions to Mineralogy and Petrology, 139*(3), 326-338.

Yaxley, G. M., & Green, D. H. (1998). Reactions between eclogite and peridotite: mantle refertilisation by subduction of oceanic crust. *Schweiz. Mineral. Petrogr. Mitt, 78*(2), 243-255.

Walter, J. M. (1998). Melting of Garnet Peridotite and the Origin of Komatiite and Depleted Lithosphere. *Journal of Petrology*, *39*(1), 29-60

Watson, S., & McKenzie, D. A. N. (1991). Melt generation by plumes: a study of Hawaiian volcanism. *Journal of Petrology, 32*(3), 501-537.

Winpenny, B., & Maclennan, J. (2011). A partial record of mixing of mantle melts preserved in Icelandic phenocrysts. *Journal of Petrology*, *52*(9), 1791-1812.

3 Chapter 3

Formation of the Iceland Plateau by enhanced plume flux and entrainment of deeply stored domains

Maja B. Rasmussen, Sæmundur A. Halldórsson, Matthew G. Jackson, Ilya N. Bindeman, Martin J. Whitehouse

Submitted to Proceedings of the National Academy of Sciences (PNAS)

Keywords: Oxygen isotopes, Helium isotopes, olivine, Iceland Plateau, mantle heterogeneity

Abstract

Icelandic basalts have exceptionally low $\delta^{18}O$ values compared to other ocean island localities. While often ascribed to the assimilation of low-$\delta^{18}O$ crust, a low-$\delta^{18}O$ mantle beneath Iceland has also been suggested. To discern crustal from mantle-derived signals, we obtained high-quality *in-situ* and bulk crystal $\delta^{18}O$ measurements on olivine crystals covering 16 Ma of activity at the Iceland hotspot. We integrate $\delta^{18}O_{olivine}$ and $^{3}He/^{4}He_{olivine}$ and demonstrate that low-$\delta^{18}O$ components (down to $\delta^{18}O_{olivine}$ = 4.2 ‰) are a trait of the modern Iceland plume and that low-$\delta^{18}O$ and low-$^{3}He/^{4}He$ components have become more apparent in the hotspot products since 60 Ma. Olivine trace elemental characteristics suggests, that this low-$\delta^{18}O$ component is best sampled in melts that reflect contributions from pyroxenitic mantle lithologies, likely related to the recycling of oceanic lithosphere. We suggest that an increase in plume flux, as traced by increasing plume temperatures and plume buoyancy after 35 Ma, led to enhanced entrainment of lower mantle material carrying recycled low-$\delta^{18}O$ oceanic lithosphere. This material has become more apparent with time as is reflected in source-derived low-$\delta^{18}O$ and high $^{3}He/^{4}He$ values in olivine from the modern Iceland plume. We further suggest that the coincidence of the Iceland plume head and the North Atlantic Rift at ~25 Ma, assisted and further promoted enhanced plume-melting. Thus, the combination of changes in mantle upwelling and tectonic reorganisation of the North Atlantic lead to the introduction of recycled oceanic lithosphere into the Iceland plume and the formation of the Iceland Plateau ~25 Ma.

3.1 Introduction

Oxygen is the most abundant element in the silicate Earth, and its isotopes are widely used as fingerprints of relative mantle and crustal contributions in melts. Deviations from the canonical upper mantle $\delta^{18}O$ (where $\delta^{18}O$ is defined as the relative difference between sample and standard $^{18}O/^{16}O$ ratios in ‰) are widespread in ocean island basalts and have been associated with chemical heterogeneities in the source region (Workman *et al.*, 2008, Day & Hilton, 2011). Iceland is the largest subaerial expression of an oceanic ridge segment, which is due to the juxtaposition of a high-buoyancy, deep-seated mantle plume beneath the North Atlantic Rift. Basalts from the individual rift and off-rift systems constituting the volcanically active regions in Iceland, usually referred to as the neovolcanic volcanic zones, have unique geochemical and isotopic characteristics (Harðardóttir *et al.*, 2018, Kokfelt *et al.*, 2006). Moreover, $\delta^{18}O$ values of Icelandic basalts are notably low compared to the depleted MORB mantle (DMM) which has otherwise homogenous $\delta^{18}O_{ol}$ (5.2 ± 0.3 ‰, [Eiler, 2001]). Two prevailing hypotheses have been considered to account for this: shallow assimilation of low-$\delta^{18}O$ crust, or heterogeneity within the mantle source, possibly inherited from low-$\delta^{18}O$ oceanic crust recycled from ancient subduction zones (Muehlenbachs *et al.*, 1974).

In this study we attempt to determine if low-$\delta^{18}O$ values are present in the mantle beneath Iceland by combining $^{3}He/^{4}He$ and $\delta^{18}O$ in olivine (ol) with compositional analyses of the same olivine populations. To circumvent material likely to be affected by interaction with low-$\delta^{18}O$ crust, we target high-forsterite (Fo = Mg/(Mg+Fe) mol%) olivines, which represent one of the first phases to precipitate from a mantle-derived melt prior to significant crustal assimilation. Despite evidence of overprinting of mantle-derived $\delta^{18}O_{ol}$ values in large volume tholeiitic basalts (Bindeman *et al.*, 2008), previous studies have suggested the presence of a low-$\delta^{18}O$ component in the sub-Iceland mantle (Kokfelt *et al.*, 2006, Macpherson *et al.*, 2005, Thirlwall *et al.*, 2006, Winpenny & Maclennan, 2014). Unfortunately, most of these studies are based on bulk olivine analyses (Kokfelt *et al.*, 2006, Macpherson *et al.*, 2005, Thirlwall *et al.*, 2006) which does not resolve intra-crystal variations as was previously shown to skew results towards crustal modified $\delta^{18}O$ values rather than primary mantle-derived values (Bindeman *et al.*, 2008). Thus, merely bulk analyses create difficulties when distinguishing between primary source-derived and secondary process-derived $\delta^{18}O$ values.

We present *in-situ* Secondary Ion Mass Spectrometry (SIMS, high spatial resolution) and single- and bulk crystal laser fluorination (LF, high-precision) $\delta^{18}O$ analysis of high-forsterite olivines (Fo_{80-91}) from the neovolcanic rift- and flank zones in Iceland as well as older Tertiary units (Figure 3.1). SIMS measurements were obtained at the NordSIMS facility while single and bulk analyses were acquired by LF at the University of Oregon. The samples analysed by SIMS were previously analysed for their elemental systematics (Rasmussen *et al.*, 2020) and most samples have previously been analysed for their $^{3}He/^{4}He$ values (where R_A represents atmospheric $^{3}He/^{4}He$ value [Harðardóttir *et al.*, 2018]). High $^{3}He/^{4}He$ values have been shown to trace the melt contribution from ancient domains hosted within the upwelling mantle plume beneath Iceland (Harðardóttir *et al.*, 2018). Thus, the extensive dataset collected on the same set of crystals presents a unique opportunity to identify primary versus secondary controls on the origin of the low-$\delta^{18}O$ signature predominating most Icelandic basalts.

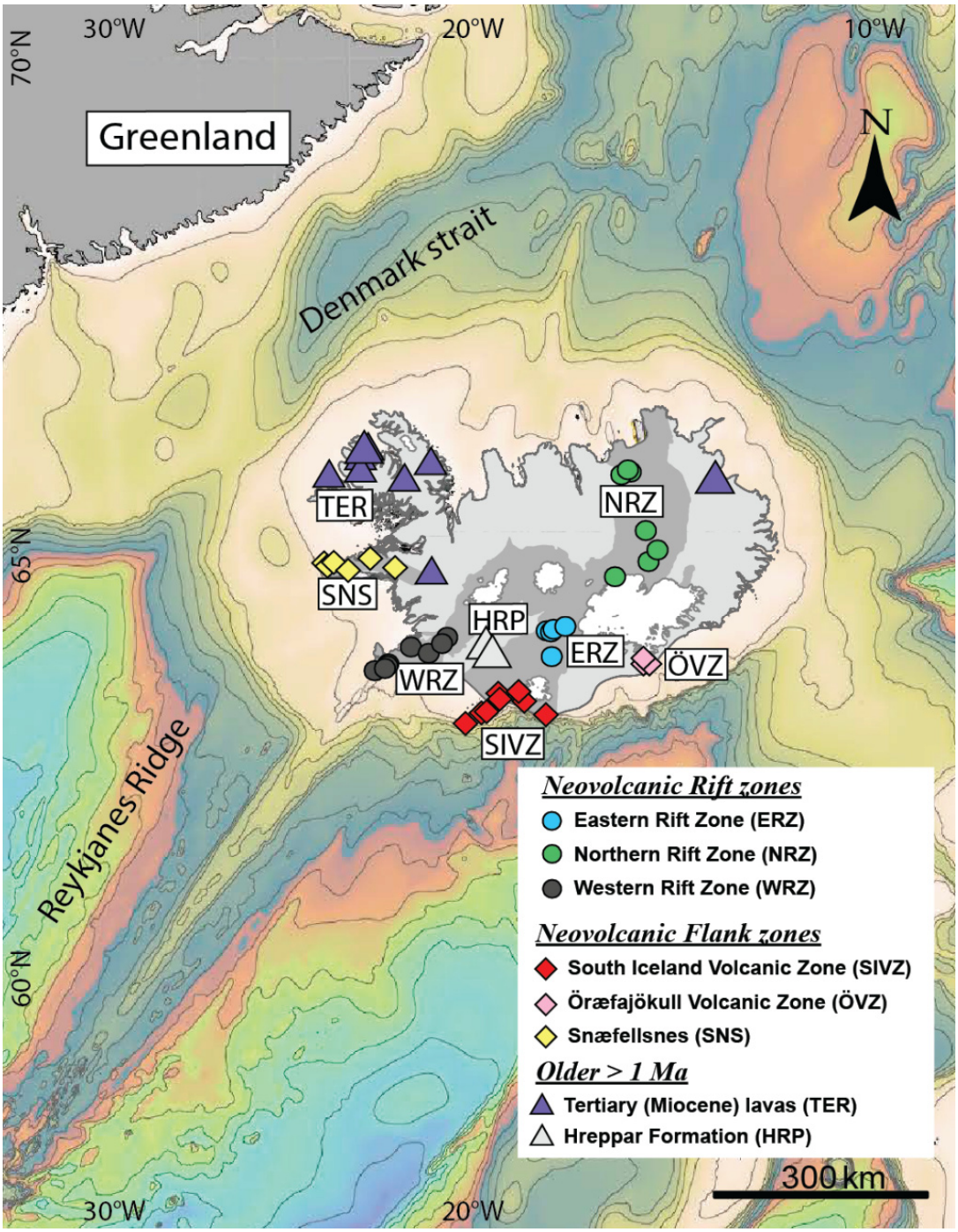

Figure 3.1 Projection of sample localities and volcanic zones on a GEBCO-bathymetric map displaying the extent of the Iceland Plateau and the V-shaped ridges along the Reykjanes Ridge. Sample locations and zone abbreviations are identical to the divisions used in Rasmussen, et al. (2020) and used throughout this study (data supplement for Chapter 3, T1). ERZ (Eastern Rift Zone), WRZ (Western Rift Zone) and NRZ (Northern Rift Zone) compromise the current rift axes. SIVZ (South Iceland Volcanic Zone) is a flank zone propagating from the southern tip of ERZ, while SNS (Snæfellsnes) and ÖVZ (Öræfajökull Volcanic Zone) are flank zones with alkalic to transitional magma products. TER covers Tertiary lavas, mostly from the West Fjords, while HRP (Hreppar formation) represents an isolated region with Plio-Pleistocene aged rocks, located between the WRZ and ERZ. The bathymetric map is generated using GMT software (Wessel & Smith, 1991).

3.1.1 Results

The SIMS results reveal limited intra-crystal variability (Figure 6.2) but collectively display a variation in $\delta^{18}O_{ol}$ of ~ 3 ‰ across Iceland (Figure 3.2, data supplement for Chapter 3, T2). Overall, the rift-related samples extend to lower $\delta^{18}O_{ol}$ than the flank-related samples (Figure 3.2a). Olivine from the older formations (Miocene Tertiary lavas [TER] and Plio-Pleistocene Hreppar Formation [HRP]) cover almost the same range (5.6 - 3.3 ‰) as the younger (<1 Ma) neovolcanic samples (6.1 - 2.8 ‰). Similarly, the LF-derived $\delta^{18}O_{ol}$ record a comparable range in the TER samples (5.3 - 3.7 ‰) and the neovolcanic samples (5.3 - 3.9 ‰, section 6.1.4). Thus, LF and SIMS-derived data are in good agreement, recording $\delta^{18}O_{ol}$ values mostly below expected DMM values (5.2 ± 0.3 ‰, Figure 3.2a), consistent with a low-$\delta^{18}O_{ol}$ anomaly previously observed in Icelandic basalts (Bindeman *et al.*, 2008; Macpherson *et al.*, 2005; Thirlwall *et al.*, 2006; Winpenny & Maclennan, 2014).

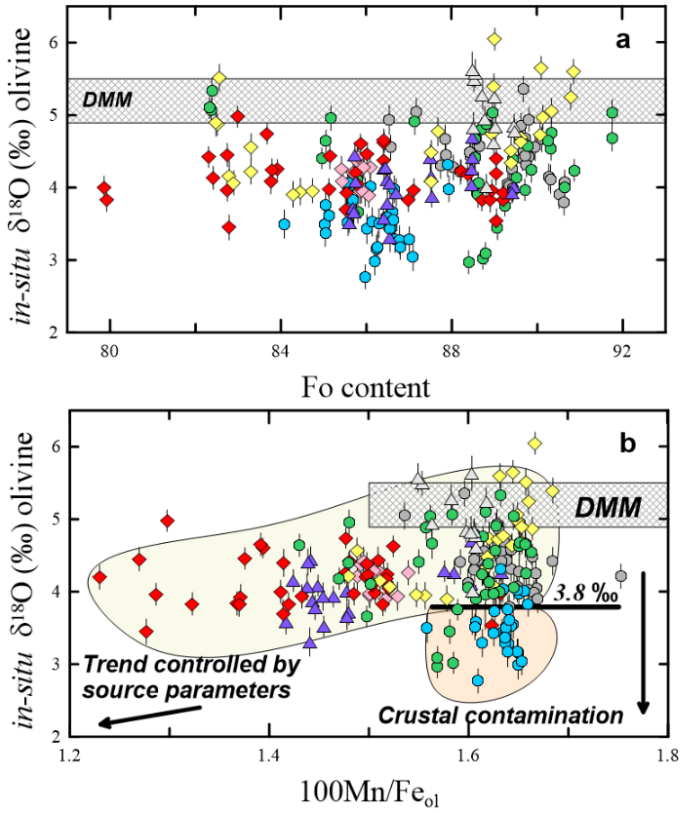

Figure 3.2 $\delta^{18}O$ systematics of Icelandic olivine. a-b, Rift zone olivine extent to lower $\delta^{18}O_{ol}$ than the flank zone olivines. a) No clear correlation between Fo content and $\delta^{18}O_{ol}$ suggests that the in-situ $\delta^{18}O$ values we observe are primary. b) 100Mn/Fe and $\delta^{18}O_{ol}$ on the same spots. As Mn/Fe are unaffected by crustal processes (Rasmussen et al., 2020; Gleeson & Gibson, 2019; Sobolev et al., 2007), any correlation between Mn/Fe and $\delta^{18}O_{ol}$ suggests a source-control on the $\delta^{18}O_{ol}$ (yellow field). However, the variations in $\delta^{18}O_{ol}$ along a constant 100Mn/Fe (orange field) suggests that some crustal assimilation also plays a role. This is observed especially in olivine from ERZ but also part of NRZ. To minimise $\delta^{18}O_{ol}$ values that may reflect crustal assimilation rather than source-derived $\delta^{18}O$ values, any measurements of $\delta^{18}O_{ol}$ below 3.8 ‰ (the lowest source-derived $\delta^{18}O_{ol}$ with Fo>90) at

constant 100Mn/Fe$_{ol}$ ~ 1.6 is excluded from any source-derived discussion (see text for details). The crossed field represent the δ^{18}O of mantle-derived olivine from Eiler (2001). The errors associated with each data point correspond to the instrumental error (1SD) and the symbols are the same as in Figure 3.1.

3.2 Discussion

3.2.1 Resolving primary versus secondary δ^{18}O values in Icelandic high-forsterite olivine

Both partial mantle melting and fractional crystallisation of mafic minerals would result in a mild (~ 0.1 - 0.2 ‰) increase in δ^{18}O (Eiler, 2001), so we can eliminate such processes to explain the low-δ^{18}O values we observe. Iceland's location at high latitudes results in exceptionally low-δ^{18}O meteoric water (down to -14 ‰ [Sveinbjörnsdóttir *et al.*, 2020]). The interaction of such waters with the Icelandic crust has been shown to result in subsurface hydrothermally altered basalts and hydrated subglacial basalts (hyaloclastites) with δ^{18}O$_{bulk}$ values down to -10.5 ‰ (Hattori & Muehlenbachs, 1982). However, the bulk Icelandic crust is usually assigned an overall δ^{18}O composition between 0 - 2 ‰ (e.g., Bindeman *et al.*, 2008, Macpherson *et al.*, 2005, Gautason & Muehlenbachs, 1998, Eiler *et al.*, 2000, Bindeman *et al.*, 2012). This range of crustal δ^{18}O values is supported by direct sampling of the crust, such as drill cores from Reyðarfjördur (Eastern Iceland) and Reykjavik (Southwest Iceland) that were characterised by δ^{18}O values of 2 ‰ at depths down to 3 km (Hattori & Muehlenbachs, 1982).

Two scenarios are often considered when evaluating assimilation of low-δ^{18}O crust: 1) assimilation of rhyolitic melts, resulting from remelting of altered and largely basaltic basic crust and 2) bulk or partial digestion of mafic low-δ^{18}O crust. For primitive basalts scenario 2 is often invoked to explain low-δ^{18}O as scenario 1 would result in a significant shift in major and trace element chemistry which has proved difficult to detect in Icelandic basalts (Breddam, 2002, Hartley *et al.*, 2013). A simple way of evaluating the effects of this interaction on our dataset involves considering possible correlations between δ^{18}O$_{ol}$ and indicators of evolving melt compositions, such as olivine Fo content. However, no clear correlation is evident between Fo content and *in-situ* δ^{18}O$_{ol}$ (Figure 3.2a), which differs from previous SIMS-based δ^{18}O$_{ol}$ studies on large volume basalts from Iceland's Eastern Rift Zone (ERZ [Bindeman *et al.*, 2008], see supplement Figure 6.5).

Following isostatic subsidence, caldera collapses and burial within rifts, low-δ^{18}O material can be present at depths of up to 11 km and may interact with upwelling mantle-derived magmas (Hattori & Muehlenbachs, 1982). Therefore, assimilation of low δ^{18}O hydrated basaltic crust, leading to a lowering of mantle-derived melt δ^{18}O values, will occur in the upper 11 km of the Icelandic crust (Hartley *et al.*, 2013). The majority of the Icelandic olivine crystals targeted here have high-forsterite values (Fo>85), and can thus be assigned crystallisation in the lower- to middle crust (>10 km; e.g., Neave & Putirka, 2017). These parts of the crust are likely dominated by intrusive materials characterised by canonical mantle-like δ^{18}O values (e.g., Hartley *et al.*, 2013). As a result, any melt-crust interactions taking place there would therefore not lead to a lowering of the δ^{18}O$_{melt}$ values. An exemption to this argument is olivine from ERZ. Here, basaltic melts have been shown to be prone to assimilation processes as recorded in a number of moderate to large-volume evolved

tholeiitic basalts (e.g., Bindeman *et al.*, 2008; Halldórsson *et al.*, 2018). Indeed, barometry of melts from ERZ has highlighted the importance of shallow to mid-crustal (<8 km) magma reservoirs in this region where magmas stall, crystallise and homogenise prior to eruption (e.g., Caracciolo *et al.*, 2020; Halldórsson *et al.*, 2018). Incomplete shallow storage homogenisation and diffusion processes, may result in development of chemically zoned olivine with large ranges of $\delta^{18}O$ values (e.g., Bindeman *et al.*, 2008), suggesting overprinting by low and crustally-inherited $\delta^{18}O$ values. Several moderate to large-volume basaltic lavas associated with the ERZ, including Laki and Holuhraun (Halldórsson *et al.*, 2018, Bindeman *et al.*, 2008), bear witness to mid- to lower-crustal assimilation processes, and thus olivine from ERZ will be evaluated with caution before assigning a mantle source origin for their low $\delta^{18}O$ characteristics. We highlight, however, that bulk assimilation of hyaloclastites is unlikely to account for low $\delta^{18}O_{ol}$ observed in older formations outside the neovolcanic zones (TER and HRP) as such low $\delta^{18}O$ material was not present in significant amounts before 3 Ma Carley *et al.*, 2020.

A low-$\delta^{18}O$ component has previously been ascribed to geochemically-enriched and fusible mantle components, possibly representing recycled material residing in the Icelandic plume (Macpherson *et al.*, 2005, Thirlwall *et al.*, 2006, Winpenny & Maclennan, 2014, Shorttle & Maclennan, 2011). Extensive minor- and trace-elemental variability, thought to reflect lithological heterogeneity carried by the Icelandic plume, is characteristic of the olivine crystals targeted here (Rasmussen *et al.*, 2020). The sampling of this heterogeneity was argued to be controlled by various proportions of melt derived from olivine-rich peridotite and olivine-poor pyroxenite (Rasmussen *et al.*, 2020), the latter resulting from incorporation of recycled oceanic crust. Trace elemental ratios that are not expected to change following crustal processes, such as $(Mn/Fe)_{ol}$ (Mn/Fe hereafter), was found to be a particularly useful tracer of such lithological variability (Sobolev *et al.*, 2007) and has previously been successful in tracing the presence of secondary pyroxenite in the Icelandic plume (Rasmussen *et al.*, 2020).

To evaluate the $\delta^{18}O$ composition of this pyroxenitic component, we plot $\delta^{18}O_{ol}$ versus Mn/Fe (Figure 3.2b). First, we note that most olivines with 100Mn/Fe<1.5 — indicative of a more pyroxenitic source lithology (e.g., Sobolev *et al.*, 2007, Rasmussen *et al.*, 2020, Gleeson & Gibson, 2019) — have $\delta^{18}O_{ol}$ below DMM. Second, we identify two general trends: one where Mn/Fe correlates positively with $\delta^{18}O_{ol}$, and another where Mn/Fe stays constant despite large variations in $\delta^{18}O_{ol}$. In high-forsterite olivine, Mn/Fe traces mantle source rather than crustal processes (Sobolev *et al.*, 2007, Gleeson & Gibson, 2019), so any correlation between this ratio and $\delta^{18}O_{ol}$ must be source-controlled and cannot be an effect of crustal contamination or other magmatic processes (Rasmussen *et al.*, 2020). Variations in $\delta^{18}O_{ol}$ that are not reflected in Mn/Fe variability are therefore more likely signal possible crustal assimilation. This can explain why some rift-related olivines (from ERZ) span a $\delta^{18}O$ range of over 2 ‰ while their Mn/Fe remains near-constant.

As ERZ-derived magmas have been shown to be especially susceptible to assimilation processes as discussed above, all ERZ olivine measurements will be excluded from further evaluation of source-derived Iceland plume components. Olivine from the Western Rift Zone (WRZ) cluster around a $\delta^{18}O_{ol}$ value of 4.3 ‰ (similar to findings by Thirlwall *et al.* 2006) at 100Mn/Fe around 1.6, while Northern Rift Zone (NRZ) olivine reveal highly heterogeneous $\delta^{18}O$ and 100Mn/Fe values (Figure 3.2b). Thus, it appears harder to distinguish whether crustal assimilation or source heterogeneity is the major control on the low $\delta^{18}O$ sampled in the WRZ and NRZ. However, olivine from WRZ with Fo content up

to Fo_{90-91} display $\delta^{18}O_{ol}$ values down to 3.8 ± 0.2 ‰ at 100Mn/Fe around 1.6 (Figure 3.2). Such high Fo contents likely reflect crystallisation of magmatic olivine buffered by peridotite-olivine (e.g., Albarede, 1992) and therefore crystallised within the mantle and thus, this $\delta^{18}O$ value reflects a lower limit for source-derived $\delta^{18}O$ values identified here. Indeed, a previous SIMS-based study, targeting primitive plagioclase crystals from NRZ, identified mantle-derived $\delta^{18}O_{ol}$ values down to 3.8 ‰ (Winpenny & Maclennan, 2014). In line with these observations and to reduce the role of crustal assimilation on our dataset, we exclude olivine with $\delta^{18}O$ below 3.8 ‰ at near-constant 100Mn/Fe values ~ 1.6 from further evaluation of source-derived $\delta^{18}O$ values (Figure 3.2b). We note that the majority of ERZ olivine are filtered out following this approach, further strengthening its use in identifying olivine crystals likely affected by crustal assimilation.

However, we emphasize that, for most olivines derived from Öræfajökull Volcanic Zone (ÖVZ), South Iceland Volcanic Zone (SIVZ), TER and part of the Northern Rift Zone (NRZ), Western Rift Zone (WRZ) and Snæfellsnes (SNS), a reduction of $\delta^{18}O_{ol}$ is clearly associated with lower Mn/Fe (with a p-value of << 0.05, Figure 3.2b). This approach confirms that a low-$\delta^{18}O$ (down to ~ 3.5 ‰ in SIVZ) can be associated with a greater contribution from pyroxenite-derived (and thereby recycled crust-derived) melting in the sub-Iceland mantle, similar to findings from other ocean islands (Day & Hilton, 2011). Previous findings support the conclusion of a low-$\delta^{18}O$ component associated with enriched components within the Iceland plume (e.g., Macpherson *et al.*, 2005; Winpenny & Maclennan, 2014), and a similarly low-$\delta^{18}O$ source component was even recognised in submarine basalts from Reykjanes Ridge that cannot have interacted with low $\delta^{18}O$ meteoric water (Thirlwall *et al.*, 2006).

3.2.2 A low-$\delta^{18}O$ Iceland plume: constraints from $^3He/^4He$

The samples studied here have previously been characterised for $^3He/^4He$ (Harðardóttir *et al.*, 2018, Jackson *et al.*, 2020). By focusing exclusively on samples that have not experienced post-eruptive radiogenic ^4He ingrowth (see section 6.3), then $^3He/^4He$ >8 R_A (i.e. values higher than DMM) provides unambiguous evidence for primordial components carried within the Icelandic plume (Harðardóttir *et al.*, 2018), and allows us to evaluate the extent to which the upwelling plume component controls the distribution of low-$\delta^{18}O$ in the Icelandic mantle (Figure 3.3).

Icelandic olivine crystals with $^3He/^4He$ >20 R_A have $\delta^{18}O_{ol}$ <5.2 ± 0.3 ‰ (i.e., the range of values characteristic for DMM), whereas olivine with $^3He/^4He$ <20 R_A reveal a larger range in $\delta^{18}O_{ol}$ (4.0 to 5.4 ‰, Figure 3.3) that partly overlaps with DMM. Olivine $\delta^{18}O$ values from western Iceland (WRZ, SNS and HRP) and previously published LF data from Reykjanes Ridge (Thirlwall *et al.*, 2006), all with $^3He/^4He$ <20 R_A, overlap partially with DMM (Figure 3.3c). Moreover, the WRZ and Reykjanes Ridge samples form clear trajectories from DMM-like $\delta^{18}O_{ol}$ values and $^3He/^4He_{ol}$ from 8-18 R_A towards a component characterised by lower $\delta^{18}O$ and $^3He/^4He$ (orange dashed arrow, Figure 3.3c). The $\delta^{18}O_{ol}$ for the TER sample with the highest $^3He/^4He$ of 42.9 R_A (Figure 3.3b) is 4.6 ± 0.1 ‰ (1SD) and we argue that this value best represents the pristine $^3He/^4He$-$\delta^{18}O$ composition of the *Miocene* plume. Olivine from the Vaðalda shield volcano carries the highest $^3He/^4He$ in the neovolcanic zone (34.3 R_A) and has corresponding $\delta^{18}O_{ol}$ of 4.2 ± 0.3 ‰, which is slightly lower than the *Miocene* plume. Based on the presence of the highest high $^3He/^4He_{ol}$ values in Vaðalda and in line

with prior studies (Hilton *et al.*, 2000), we argue that the He-O isotopic characteristic of Vaðalda best represent the *Modern* plume component.

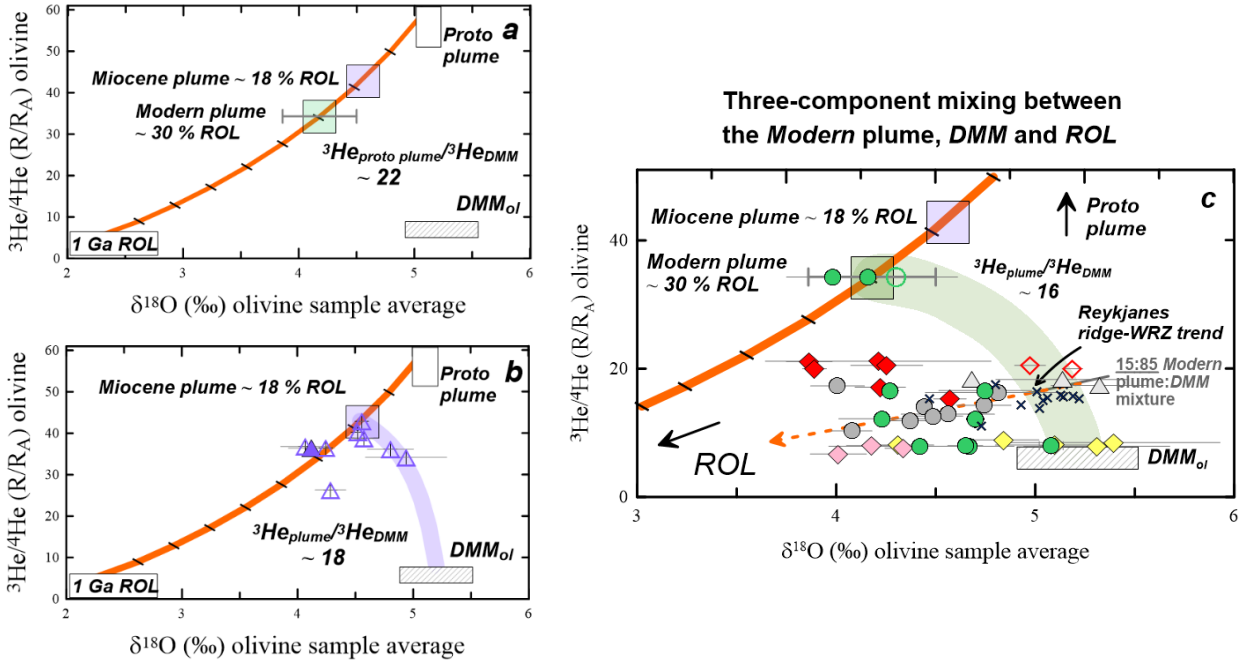

Figure 3.3 $\delta^{18}O$ (SIMS and LF)-$^3He/^4He$ systematics of Icelandic olivine. a) Mixing between the proto *Iceland plume ($\delta^{18}O$ = 5.1 ‰ $^3He/^4He$ = 60 RA) and a 1 Ga recycled oceanic lithosphere (*ROL, $\delta^{18}O$ ~ 2 ‰, $^3He/^4He$ = 0.01-6 R_A, *orange line) can replicate the* Miocene ($\delta^{18}O$ = 4.6 ± 0.1 ‰ $^3He/^4He$ = 42.9 R_A) *and* Modern ($\delta^{18}O$ = 4.2 ± 0.3 ‰, $^3He/^4He$ = 34.3 R_A) *plume components - reflecting the highest $^3He/^4He$ sampled by Tertiary and neovolcanic Iceland olivine - when the* proto *plume component has ^3He concentrations 22 times those of DMM. To explain the pattern presented by the Tertiary (b), Plio-Pleistocene and neovolcanic (c) dataset, a third component must be invoked, which is most likely DMM ($\delta^{18}O_{ol}$ = 4.9-5.5 ‰ $^3He/^4He$ 7-9 R_A), also reflected in SNS olivine. Mixing between the* Miocene *(b, purple line) or the* Modern *plume (c, green line) and* DMM *creates an envelope of compositions that can further mix with* ROL *in the upper mantle. An example of this is seen in the data from WRZ, HRP and previously published data from Reykjanes ridge (c, Thirlwall et al., 2006; Hilton et al., 2000) where a* Modern *plume:*DMM *mixture of 15:85 creates an endmember for further mixing with* ROL *(highlighted by the orange arrow). The exact composition of the various endmembers used for the mixing is available in the data supplement for Chapter 3, T6. The SIMS data are represented by filled symbols while the LF data are represented by unfilled symbols. The crosses represent literature LF data from Reykjanes Ridge from Thirlwall et al. (2006) and Hilton, et al. (2000) and additional data on the same samples (Th29, NAL 688, NAL 611 and THJOR-1) are included from (Macpherson et al., 2005; Thirlwall et al., 2006; Eiler et al., 2000). The symbols are the same as in Figure 3.1.*

3.2.3 Entrainment of deeply stored oceanic lithosphere into the Iceland plume source

The 60 Ma Baffin Island picrites associated with onset of hotspot volcanism above the *proto*-Iceland plume are characterised by the highest $^{3}He/^{4}He$ measured in any ocean island (up to 50 R_A [Starkey *et al.*, 2009]) and likely sourced from a reservoir with $^{3}He/^{4}He$ values up to 60 R_A (Mundl-Petermeier *et al.*, 2019). Apart from $^{3}He/^{4}He$, Baffin lavas are characterised by DMM-like isotopic compositions and average $\delta^{18}O_{ol}$ of 5.1 ‰ (5.03 - 5.21 ‰, [Willhite *et al.*, 2019]). When comparing the *proto*, *Miocene* and *Modern* Iceland plume, a coupled lowering of $\delta^{18}O_{ol}$ (from 5.1 to 4.2 ‰) and $^{3}He/^{4}He_{ol}$ (from 60 to 34 R_A) is therefore evident suggesting that a component with lower $\delta^{18}O$ and $^{3}He/^{4}He$ has been introduced over time.

A likely candidate for this low $\delta^{18}O$ and low $^{3}He/^{4}He$ component is recycled oceanic lithosphere (*ROL*, [Day & Hilton, 2011, Macpherson *et al.*, 2005]). Indeed, incorporation of *ROL* has frequently been proposed to explain the geochemical shift to higher $^{87}Sr/^{86}Sr$, $^{206}Pb/^{204}Pb$ and $^{187}Os/^{188}Os$ for the *Modern* versus the *proto* plume component (Kokfelt *et al.*, 2006, Hartley *et al.*, 2013, Dale *et al.*, 2009, Brandon *et al.*, 2007) and can explain the presence of secondary pyroxenite in the Iceland plume as shown by trace element variations in olivine (Rasmussen *et al.*, 2020). Here, *ROL* is characterised by $\delta^{18}O$ of ~ 2 ‰ and $^{3}He/^{4}He$ between 0.01-6 R_A, where the exact $^{3}He/^{4}He$ values and He concentrations depend on the age of *ROL* (data supplement, T6; Macpherson *et al.*, 2005, Gréau *et al.*, 2011, Brandon *et al.*, 2007). Because the concentration of O is essentially identical in the various mantle components, this variable is irrelevant for our mixing models.

We can replicate the *Miocene* and *Modern* Iceland plume compositions by the use of a simple two-component mixing model between a 1 Ga basalt (representing *ROL*, Brandon *et al.*, 2007) and a *proto* plume source with $\delta^{18}O$ of 5.1 ‰ and $^{3}He/^{4}He$ of 60 R_A (Figure 3.3a). Here, we find that the various hybrid plume compositions (*Miocene* and *Modern* plume, each corresponding to a certain mixture of the *proto* plume and *ROL*) are best simulated when the *proto* plume has ~ 22 times the ^{3}He content of DMM (DMM = 4.4 10^{-11} cc $^{3}He/g$, Porcelli & Ballentine, 2002) or $^{3}He_{proto\ plume}/^{3}He_{DMM} \sim 22$ (data supplement T6). This mixing model results in $^{3}He_{plume}/^{3}He_{DMM}$ enrichment for the *Miocene* and *Modern* plume of 18 and 16, respectively, which corresponds well with values proposed by Gonnermann and Mukhopadhyay (2007) for global plume sources and values proposed by Hilton *et al.* (2000) for the Iceland plume source. The models show that the *Miocene* plume can be replicated when we incorporate 18 % *ROL* in a *proto* plume while 30 % *ROL* is necessary to replicate the *Modern* plume (Figure 3.3a). The chosen age of the recycled component used for this model (1 Ga) is based on lower estimated model ages from Os and Pb isotopes (Brandon *et al.*, 2007, Kokfelt *et al.*, 2006). However, other estimates suggest a much younger Phanerozoic age for the recycled component in the Iceland plume (e.g., Thirlwall *et al.*, 2004; Halldórsson *et al.*, 2016). Yet, we note that changing the age of the recycled crust accordingly between 1 Ga and 250 Ma results in insignificant changes in the relative *ROL* amounts (by 1 % for the *Miocene* and 2 % for the *Modern* plume). However, this change requires that the $^{3}He_{proto\ plume}/^{3}He_{DMM}$ – controlling the curve of the proto-DMM mixing line representing the enrichment of ^{3}He in the *proto plume* relative to DMM – changes to ~ 5 (for 250 Ma *ROL*) or to ~ 11 (for 500 Ma *ROL*) in order for the mixing lines (orange, green and purple lines in Figure 3.3) to describe the data. We note that these values are all still within previous estimates (e.g., Hilton *et al.*, 2000).

Mixing between a hybrid Iceland plume and a *DMM* component has previously been shown to explain variations in He-N-Pb isotopic systematics of Icelandic and Reykjanes Ridge basalts (Halldórsson *et al.*, 2016, Hilton *et al.*, 2000). Additionally, *DMM* is directly recorded in our He-O isotope dataset by olivine from SNS (Figure 3.3c) – a region previously suggested to lack plume-derived melt inputs altogether (e.g., Rasmussen *et al.*, 2020) – supporting its role in the Iceland mantle. Indeed, our mixing model, as described above, easily replicates $\delta^{18}O$-$^{3}He/^{4}He$ trends in both *Miocene* (Figure 3.3b) and *Modern* datasets (Figure 3.3c) through mixing of the model hybrid plume compositions and *DMM*, which further supports a role for a *DMM* component in Icelandic neovolcanic lavas.

The mixing line between *Modern* plume and *DMM* (green line, Figure 3.3c) represents an endmember envelope for further mixing with *ROL* carried within the Icelandic plume. One such indication of this process is visible in data from HRP, WRZ and already published data from Reykjanes ridge (Hilton *et al.*, 2000, Thirlwall *et al.*, 2006). Here, olivine from Reykjanes ridge, coincides with a *Modern* plume:*DMM* mixture of approximately 15:85. The WRZ-Reykjanes ridge data trend (Figure 3.3c, highlighted by an orange dashed arrow) can thus be explained by mixing between this Reykjanes ridge endmember and *ROL*. Evidence of mixing between components plotting along the *Modern* plume-*DMM* mixing line (green line, Figure 3.3c) and *ROL* suggests that the incorporation of *ROL* occurs in the upper mantle too. Consequently, the incorporation of *ROL* happens deeply in the plume, as reflected by pure *proto* plume-*ROL* mixing – resulting in the pure *Modern* and *Miocene* plume compositions – and at more shallow levels in the upper mantle where *DMM* is introduced, as reflected by contemporary three-component mixing between the *Modern* plume, *DMM* and *ROL*.

Thus, we can conclude, that the He and O isotopic evolution of the Iceland plume can be replicated by mixing between three main mantle endmembers: *proto* plume, *DMM* and *ROL*. Moreover, the He-O patterns presented in Figure 3.3c are consistent with previous findings arguing for the notion that central (Vaðalda) and south Iceland (SIVZ) represents regions with the highest degree of plume-fed melts, characterised by low $\delta^{18}O$ and high $^{3}He/^{4}He$ values, while melts from NRZ and WRZ reveal an affinity towards more DMM-like $\delta^{18}O$ and $^{3}He/^{4}He$ values, and SNS shows a lack of plume contribution altogether (Rasmussen *et al.*, 2020).

3.2.4 Implications for temporal variations in activity of the Iceland plume

Initiation and manifestation of the Iceland plume occurred about 60 Ma, which led to continental break-up (at ~ 55 Ma) and initiation of North Atlantic basin formation (Figure 3.4, [Holbrook *et al.*, 2001]). In the Late Eocene (~ 35 Ma) plume activity rapidly decreased, causing relative thinning of the oceanic lithosphere, ocean floor subsidence, and ocean cooling (Holbrook *et al.*, 2001, Abelson *et al.*, 2008, Parnell-Turner *et al.*, 2014). Plume activity increased again around 25 Ma as evident from enhanced magma production related to the formation of the Iceland Plateau (Figure 3.4, [Holbrook *et al.*, 2001; Abelson *et al.*, 2008]). The Iceland Plateau (IP) has long been a puzzling topographic feature in the North Atlantic with its near-circular outline and propagating V-shaped ridges extending to the South (Figure 3.1, [Ito, 2001]) and the cause of its formation is still unknown. Here, we propose that the increase in plume activity leading to the formation of the IP was a result of

an increase in plume temperature, plume buoyancy and flux, and the contemporary alignment of the North Atlantic Ridge and the Iceland plume head around the same time.

High $^{3}He/^{4}He$ plumes, such as the Iceland plume, are associated with hotter mantle temperatures (Jackson *et al.*, 2017), suggesting that primordial high-$^{3}He/^{4}He$ domains must be deep and dense such that only the most buoyant plumes — which must be the hottest — entrain them (Jackson *et al.*, 2017). Previous studies have concluded that the temperature of the Iceland plume increased following a temperature low around 35 Ma (Spice *et al.*, 2016). As a result, this temperature increase must be accompanied by an increase in plume buoyancy and/or plume flux. While the *proto*-Iceland plume shows no evidence of *ROL*, the formation of the IP — resulting from enhanced plume-related melt production — coincides with the appearance of *ROL* in the Iceland plume. The increase in plume flux and the contemporary appearance of *ROL* suggests, that the increase in plume activity at ~ 25 Ma must be associated with enhanced entrainment of previously deeply stored, dense high $^{3}He/^{4}He$ domains and *ROL* (Figure 3.4). This dense lower mantle is likely characterised by high $^{3}He/^{4}He$ and DMM-like $\delta^{18}O$, as is a general trait of other high $^{3}He/^{4}He$ mantle plumes (Day & Hilton, 2011; Starkey *et al.*, 2016), while concurrent incorporation of *ROL* – and addition of ^{4}He – serves to counter the increase in $^{3}He/^{4}He_{plume}$ otherwise expected from enhanced entrainment of dense lower mantle material. Coupled lowering of $\delta^{18}O$ and $^{3}He/^{4}He$ in the *Miocene* and *Modern* plume, relative to the *proto* Iceland plume, can therefore effectively be attributed the degree of incorporation of *ROL* in the plume stem as has also been observed for other hot spots such as the Canary Islands and Hawaii (Day & Hilton, 2011, Lassiter & Hauri, 1998).

Alignment of the North Atlantic rift and the Iceland plume head occurred between 30-25 Ma (Howell *et al.*, 2014), around the same time of the formation of the IP. The coincidence of these two events suggests that the tectonic change, from a setting in which the Iceland plume was overlain by a thick continental crust to a thin oceanic crust, have assisted and promoted melting in the Iceland plume. Upon emplacement of the IP, plume activity became concentrated beneath the active rift systems (Figure 3.4) which further promoted melting by additional tectonic-aided upwelling. As was the case for the *proto*-Iceland plume, many large igneous provinces erupt through a thick continental crust, which results in chemical fingerprints reflecting both mantle and crustal signatures (Willhite *et al.*, 2019, Carlson *et al.*, 1981). Because of plate reorganization in the North Atlantic, the Iceland hot spot activity transitioned to an oceanic setting by 30-25 Ma (Howell *et al.*, 2014), facilitating identification of changes driven by mantle-derived upwellings. In this respect, the Iceland Plateau represents a unique surficial expression recording a temporally evolving mantle plume source. This temporal evolution is reflected in $\delta^{18}O_{ol}$-$^{3}He/^{4}He_{ol}$ space which highlights the usefulness of combining these systems when evaluating chemical traits of an evolving plume.

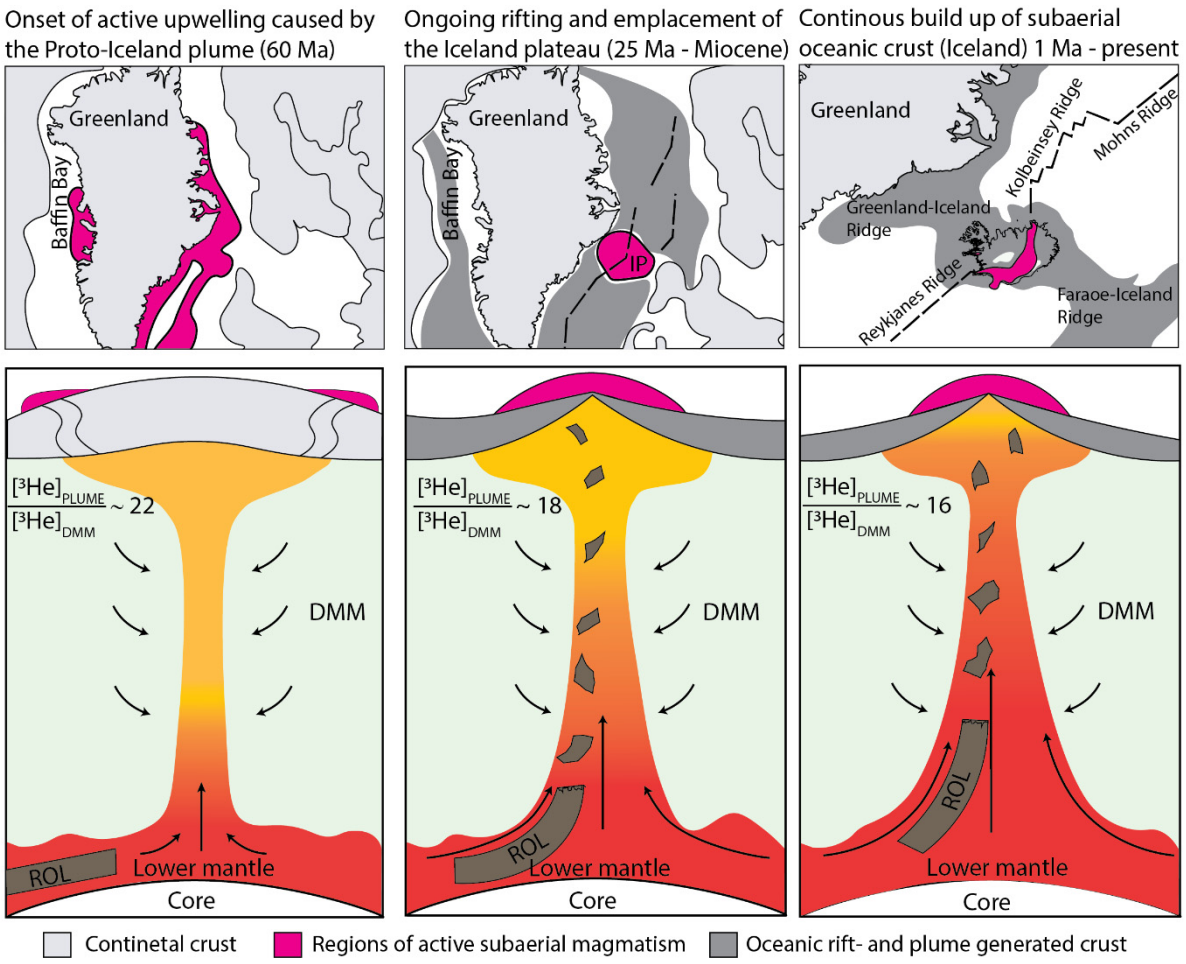

Figure 3.4 Conceptual model of the opening of the North Atlantic and the evolution of the Iceland plume. At 60 Ma, manifestation of the Iceland plume is recorded in magmatism along the borders of Greenland. At this time, the proto *plume is enriched in ^{3}He relative to DMM ($^{3}He_{PLUME}/^{3}He_{DMM}$) by a factor of 22. Enhanced melt production leading to the formation of the Iceland Plateau (IP) at 25 Ma coincides with an increase in plume temperature, plume flux and the appearance of recycled oceanic lithosphere (*ROL*) as traced by He-O isotopic systematics. The appearance of* ROL *along with an increase in plume flux suggests, that the increased plume flux led to enhanced entrainment of dense high ^{3}He/^{4}He domains and* ROL*. Moreover, tectonic changes in the North Atlantic between 30-25 Ma led to the alignment between the Iceland plume head and the ongoing North Atlantic rift, which likely promoted enhanced melting in the Iceland plume. Thus, the formation of the IP around 25 Ma is a result of temporal changes in the Iceland plume and plate reorganisation of the North Atlantic. Today, the plume-related magmatism (in pink) is centered beneath Iceland which has further promoted plume-related melting. The incorporation of* ROL*, and thereby addition of ^{4}He to the Iceland plume, over time is reflected in a lowering of the $^{3}He_{PLUME}/^{3}He_{DMM}$ from 22 in the* proto *plume to 16 in the* Modern *plume.*

3.3 Acknowledgement

The authors would like to thank Barbara Kleine for help with retrieving the SIMS data and Guðmundur Guðfinnsson, Lori Willhite, Rebekka Rúnarsdóttir and Kerstin Lindén for assistance with microprobe analysis and sample prep. Thanks to Eemu Ranta, Edward Marshall, Sally Gibson, Thomas Kokfelt and Paul Martin Holm for helpful discussions and Bryndís Brandsdóttir for help with the acquisition of a map for Figure 3.1.

This work was funded by the Nordic Volcanological Center. MBR and SAH further acknowledges support from the Icelandic Research Fund (Grant #196084-051 and #196139-051).

3.4 Materials and methods

In-situ $\delta^{18}O$ values of olivine (51 individual samples and 211 analyses), covering the entirety of the exposed modern Iceland (Holocene-Miocene), were acquired by Secondary Ion Mass Spectrometry (SIMS) at the NordSIM laboratory (detailed analytical details can be found in section 6.1.2). *In-situ* major, minor and trace element chemistry of the same spots was previously published by (Rasmussen *et al*., 2020) and we refer to this work for the analytical techniques adopted and uncertainties related to these measurements. We highlight, that laser ablation work was performed after the SIMS measurements. Moreover, $^{3}He/^{4}He$ isotopic analyses of the same samples were summarised by (Harðardóttir *et al.*, 2018) and similarly we refer to this work for reference to $^{3}He/^{4}He$ measurements.

For samples that revealed more than one chemical population with regards to their major and minor elemental composition, two analyses were performed on a minimum of two crystals while apparent homogenous samples (with regards to both major and minor elements) were analysed with three measurements at a minimum of one chemically representative crystal (section 6.1.2). We supplement these analyses with bulk and single crystal oxygen isotopic laser fluorination (LF) analysis of a subset of samples for northwest (Vestfirðir), central and south Iceland acquired at University of Oregon (20 samples and 53 analyses). Detailed analytical details can be found in section 6.1.3.

3.5 References

Abelson, M., Agnon, A., & Almogi-Labin, A. (2008). Indications for control of the Iceland plume on the Eocene–Oligocene "greenhouse–icehouse" climate transition. *Earth and Planetary Science Letters, 265*(1-2), 33-48.

Albarede, F. (1992). How deep do common basaltic magmas form and differentiate? *Journal of Geophysical Research: Solid Earth, 97*(B7), 10997-11009. doi:https://doi.org/10.1029/91JB02927

Bindeman, I., Gurenko, A., Carley, T., Miller, C., Martin, E., & Sigmarsson, O. (2012). Silicic magma petrogenesis in Iceland by remelting of hydrothermally altered crust based on oxygen isotope diversity and disequilibria between zircon and magma with implications for MORB. *Terra Nova, 24*(3), 227-232. doi:10.1111/j.1365-3121.2012.01058.x

Bindeman, I., Gurenko, A., Sigmarsson, O., & Chaussidon, M. (2008). Oxygen isotope heterogeneity and disequilibria of olivine crystals in large volume Holocene basalts from Iceland: Evidence for magmatic digestion and erosion of Pleistocene hyaloclastites. *Geochimica et Cosmochimica Acta, 72*(17), 4397-4420. doi:10.1016/j.gca.2008.06.010

Brandon, A. D., Graham, D. W., Waight, T., & Gautason, B. (2007). ^{186}Os and ^{187}Os enrichments and high-^{3}He/^{4}He sources in the Earth's mantle: evidence from Icelandic picrites. *Geochimica et Cosmochimica Acta, 71*(18), 4570-4591.

Breddam, K. (2002). Kistufell: primitive melt from the Iceland mantle plume. *Journal of Petrology, 43*(2), 345-373.

Caracciolo, A., Bali, E., Guðfinnsson, G. H., Kahl, M., Halldórsson, S. A., Hartley, M. E., & Gunnarsson, H. (2020). Temporal evolution of magma and crystal mush storage conditions in the Bárðarbunga-Veiðivötn volcanic system, Iceland. *Lithos, 352-353*, 105234. doi:https://doi.org/10.1016/j.lithos.2019.105234

Carley, T. L., Miller, C. F., Fisher, C. M., Hanchar, J. M., Vervoort, J. D., Schmitt, A. K., Economos, R. C., Jordan, B. T., Padilla, A. J., & Banik, T. J. (2020). Petrogenesis of Silicic Magmas in Iceland through Space and Time: The Isotopic Record Preserved in Zircon and Whole Rocks. *The Journal of Geology, 128*(1), 1-28. doi:10.1086/706261

Carlson, R. W., Lugmair, G. W., & Macdougall, J. D. (1981). Crustal influence in the generation of continental flood basalts. *Nature, 289*(5794), 160-162. doi:10.1038/289160a0

Dale, C., Pearson, D., Starkey, N., Stuart, F., Ellam, R., Larsen, L., Fitton, J., & Macpherson, C. (2009). Osmium isotopes in Baffin Island and West Greenland picrites: Implications for the ^{187}Os/^{188}Os composition of the convecting mantle and the nature of high 3He/4He mantle. *Earth and Planetary Science Letters, 278*(3-4), 267-277.

Day, J. M., & Hilton, D. R. (2011). Origin of ^{3}He/^{4}He ratios in HIMU-type basalts constrained from Canary Island lavas. *Earth and Planetary Science Letters, 305*(1-2), 226-234.

Eiler, J. (2001). Oxygen Isotope Variations of Basaltic Lavas and Upper Mantle Rocks. *Reviews in Mineralogy and Geochemistry, 43*.

Eiler, J., Grönvold, K., & Kitchen, N. (2000). Oxygen isotope evidence for the origin of chemical variations in lavas from Theistareykir volcano in Iceland's northern volcanic zone. *Earth and Planetary Science Letters, 184*(1), 269-286.

Gautason, B., & Muehlenbachs, K. (1998). Oxygen isotopic fluxes associated with high-temperature processes in the rift zones of Iceland. *Chemical Geology, 145*(3-4), 275-286.

Gleeson, M. L. M., & Gibson, S. A. (2019). Crustal controls on apparent mantle pyroxenite signals in ocean-island basalts. *Geology, 47*(4), 321-324. doi:10.1130/g45759.1

Gonnermann, H. M., & Mukhopadhyay, S. (2007). Non-equilibrium degassing and a primordial source for helium in ocean-island volcanism. *Nature, 449*(7165), 1037.

Gréau, Y., Huang, J.-X., Griffin, W. L., Renac, C., Alard, O., & O'Reilly, S. Y. (2011). Type I eclogites from Roberts Victor kimberlites: Products of extensive mantle metasomatism. *Geochimica et Cosmochimica Acta, 75*(22), 6927-6954. doi:10.1016/j.gca.2011.08.035

Halldórsson, S. A., Bali, E., Hartley, M. E., Neave, D. A., Peate, D. W., Guðfinnsson, G. H., Bindeman, I., Whitehouse, M. J., Riishuus, M. S., Pedersen, G. B. M., Jakobsson, S., Askew, R., Gallagher, C. R., Guðmundsdóttir, E. R., Gudnason, J., Moreland, W. M., Óskarsson, B. V., Nikkola, P., Reynolds, H. I., Schmith, J., & Thordarson, T. (2018). Petrology and geochemistry of the 2014–2015 Holuhraun eruption, central Iceland: compositional and mineralogical characteristics, temporal variability and magma storage. *Contributions to Mineralogy and Petrology, 173*(8), 64. doi:10.1007/s00410-018-1487-9

Halldórsson, S. A., Hilton, D. R., Barry, P. H., Füri, E., & Grönvold, K. (2016). Recycling of crustal material by the Iceland mantle plume: New evidence from nitrogen elemental and isotope systematics of subglacial basalts. *Geochimica et Cosmochimica Acta, 176*, 206-226.

Harðardóttir, S., Halldórsson, S. A., & Hilton, D. R. (2018). Spatial distribution of helium isotopes in Icelandic geothermal fluids and volcanic materials with implications for location, upwelling and evolution of the Icelandic mantle plume. *Chemical Geology*. doi:https://doi.org/10.1016/j.chemgeo.2017.05.012

Hartley, M. E., Thordarson, T., Fitton, J. G., & Eimf. (2013). Oxygen isotopes in melt inclusions and glasses from the Askja volcanic system, North Iceland. *Geochimica et Cosmochimica Acta, 123*, 55-73. doi:10.1016/j.gca.2013.09.008

Hattori, K., & Muehlenbachs, K. (1982). Oxygen isotope ratios of the Icelandic crust. *Journal of Geophysical Research: Solid Earth, 87*(B8), 6559-6565. doi:doi:10.1029/JB087iB08p06559

Hilton, D. R., Grönvold, K., Macpherson, C. G., & Castillo, P. R. (1999). Extreme $^{3}He/^{4}He$ ratios in northwest Iceland: constraining the common component in mantle plumes. *Earth and Planetary Science Letters, 173*(1-2), 53-60. doi:10.1016/s0012-821x(99)00215-0

Hilton, D. R., Thirlwall, M. F., Taylor, R. N., Murton, B. J., & Nichols, A. (2000). Controls on magmatic degassing along the Reykjanes Ridge with implications for the helium paradox. *Earth and Planetary Science Letters, 183*(1-2), 43-50.

Holbrook, W. S., Larsen, H., Korenaga, J., Dahl-Jensen, T., Reid, I. D., Kelemen, P., Hopper, J., Kent, G., Lizarralde, D., & Bernstein, S. (2001). Mantle thermal structure and active upwelling during continental breakup in the North Atlantic. *Earth and Planetary Science Letters, 190*(3-4), 251-266.

Howell, S. M., Ito, G., Breivik, A. J., Rai, A., Mjelde, R., Hanan, B., Sayit, K., & Vogt, P. (2014). The origin of the asymmetry in the Iceland hotspot along the Mid-Atlantic Ridge from continental breakup to present-day. *Earth and Planetary Science Letters, 392*, 143-153. doi:https://doi.org/10.1016/j.epsl.2014.02.020

Ito, G. (2001). Reykjanes' V'-shaped ridges originating from a pulsing and dehydrating mantle plume. *Nature, 411*(6838), 681-684.

Jackson, M. G., Blichert-Toft, J., Halldórsson, S. A., Mundl-Petermeier, A., Bizimis, M., Kurz, M. D., Price, A. A., Harðardóttir, S., Willhite, L. N., Breddam, K., Becker, T. W., & Fischer, R. A. (2020). Ancient helium and tungsten isotopic signatures preserved in mantle domains least modified by crustal recycling. *Proceedings of the National Academy of Sciences*, 202009663. doi:10.1073/pnas.2009663117

Jackson, M. G., Konter, J. G., & Becker, T. W. (2017). Primordial helium entrained by the hottest mantle plumes. *Nature, 542*(7641), 340-343. doi:10.1038/nature21023

Kokfelt, T. F., Hoernle, K., Hauff, F., & Fiebig, J. (2006). Combined Trace Element and Pb-Nd-Sr-O Isotope Evidence for Recycled Oceanic Crust (Upper and Lower) in the Iceland Mantle Plume. *Journal of Petrology, 47*(9), 1705-1749. doi:10.1093/petrology/egl025

Lassiter, J., & Hauri, E. (1998). Osmium-isotope variations in Hawaiian lavas: evidence for recycled oceanic lithosphere in the Hawaiian plume. *Earth and Planetary Science Letters, 164*(3-4), 483-496.

Macpherson, C., Hilton, D., Day, J., Lowry, D., & Gronvold, K. (2005). High-$^{3}He/^{4}He$, depleted mantle and low-$\delta^{18}O$, recycled oceanic lithosphere in the source of central Iceland magmatism. *Earth and Planetary Science Letters, 233*(3-4), 411-427. doi:10.1016/j.epsl.2005.02.037

Muehlenbachs, K., Anderson, A. T., & Sigvaldason, G. E. (1974). Low-O^{18} basalts from Iceland. *Geochimica et Cosmochimica Acta, 38*(4), 577-588.

Mundl-Petermeier, A., Walker, R., Jackson, M., Blichert-Toft, J., Kurz, M., & Halldórsson, S. A. (2019). Temporal evolution of primordial tungsten-182 and $^{3}He/^{4}He$ signatures in the Iceland mantle plume. *Chemical Geology, 525*, 245-259.

Neave, D. A., & Putirka, K. D. (2017). A new clinopyroxene-liquid barometer, and implications for magma storage pressures under Icelandic rift zones. *American Mineralogist, 102*(4), 777-794. doi:10.2138/am-2017-5968

Parnell-Turner, R., White, N., Henstock, T., Murton, B., Maclennan, J., & Jones, S. M. (2014). A continuous 55-million-year record of transient mantle plume activity beneath Iceland. *Nature Geoscience, 7*(12), 914-919. doi:10.1038/ngeo2281

Porcelli, D., & Ballentine, C. J. (2002). Models for distribution of terrestrial noble gases and evolution of the atmosphere. *Reviews in Mineralogy and Geochemistry, 47*(1), 411-480.

Rasmussen, M. B., Halldórsson, S. A., Gibson, S. A., & Guðfinnsson, G. H. (2020). Olivine chemistry reveals compositional source heterogeneities within a tilted mantle plume beneath Iceland. *Earth and Planetary Science Letters, 531*, 116008. doi:https://doi.org/10.1016/j.epsl.2019.116008

Shorttle, O., & Maclennan, J. (2011). Compositional trends of Icelandic basalts: Implications for short-length scale lithological heterogeneity in mantle plumes. *Geochemistry, Geophysics, Geosystems, 12*(11). doi:10.1029/2011gc003748

Sobolev, A. V., Hofmann, A. W., Kuzmin, D. V., Yaxley, G. M., Arndt, N. T., Chung, S. L., Danyushevsky, L. V., Elliott, T., Frey, F. A., Garcia, M. O., Gurenko, A. A., Kamenetsky, V. S., Kerr, A. C., Krivolutskaya, N. A., Matvienkov, V. V., Nikogosian, I. K., Rocholl, A., Sigurdsson, I. A., Sushchevskaya, N. M., & Teklay, M. (2007). The amount of recycled crust in sources of mantle-derived melts. *Science, 316*(5823), 412-417. doi:10.1126/science. 1138113

Spice, H. E., Fitton, J. G., & Kirstein, L. A. (2016). Temperature fluctuation of the Iceland mantle plume through time. *Geochemistry, Geophysics, Geosystems, 17*(2), 243-254.

Starkey, N. A., Jackson, C. R. M., Greenwood, R. C., Parman, S., Franchi, I. A., Jackson, M., Fitton, J. G., Stuart, F. M., Kurz, M., & Larsen, L. M. (2016). Triple oxygen isotopic composition of the high-^{3}He/^{4}He mantle. *Geochimica et Cosmochimica Acta, 176*, 227-238. doi:10.1016/j.gca.2015.12.027

Starkey, N. A., Stuart, F. M., Ellam, R. M., Fitton, J. G., Basu, S., & Larsen, L. M. (2009). Helium isotopes in early Iceland plume picrites: Constraints on the composition of high ^{3}He/^{4}He mantle. *Earth and Planetary Science Letters, 277*(1), 91-100.

Sveinbjörnsdóttir, Á. E., Stefánsson, A., Heinemeier, J., Arnórsson, S., Eiríksdóttir, E. S., & Ólafsdóttir, R. (2020). Assessing the sources of inorganic carbon in surface-, soil- and non-thermal groundwater in Iceland by δ^{13}C and ^{14}C. *Geochimica et Cosmochimica Acta*.

Thirlwall, M. F., Gee, M. A. M., Lowry, D., Mattey, D. P., Murton, B. J., & Taylor, R. N. (2006). Low δ^{18}O in the Icelandic mantle and its origins: Evidence from Reykjanes Ridge and Icelandic lavas. *Geochimica et Cosmochimica Acta, 70*(4), 993-1019. doi:10.1016/j.gca.2005.09.008

Thirlwall, M. F., Gee, M. A. M., Taylor, R. N., & Murton, B. J. (2004). Mantle components in Iceland and adjacent ridges investigated using double-spike Pb isotope ratios. *Geochimica et Cosmochimica Acta, 68*(2), 361-386. doi:10.1016/s0016-7037(03)00424-1

Wessel, P., & Smith, W. H. F. (1991). Free software helps map and display data. *Eos, Transactions American Geophysical Union, 72*(41), 441-446. doi:10.1029/90eo00319

Willhite, L. N., Jackson, M. G., Blichert-Toft, J., Bindeman, I., Kurz, M. D., Halldórsson, S. A., Harðardóttir, S., Gazel, E., Price, A. A., & Byerly, B. L. (2019). Hot and Heterogenous High-^{3}He/^{4}He Components: New Constraints From Proto-Iceland Plume Lavas From Baffin Island. *Geochemistry, Geophysics, Geosystems, 20*(12), 5939-5967. doi:10.1029/2019gc008654

Winpenny, B., & Maclennan, J. (2014). Short Length Scale Oxygen Isotope Heterogeneity in the Icelandic Mantle: Evidence from Plagioclase Compositional Zones. *Journal of Petrology, 55*(12), 2537-2566. doi:10.1093/petrology/egu066

Workman, R. K., Eiler, J. M., Hart, S. R., & Jackson, M. G. (2008). Oxygen isotopes in Samoan lavas: Confirmation of continent recycling. *Geology, 36*(7), 551-554.

4 Chapter 4

Evaluation of source and magmatic process-derived Mg and Fe isotope characteristics of Icelandic olivine crystals

Maja B. Rasmussen, Helen M. Williams, Edward T. Tipper, Callum D. J. Reekie, Sæmundur A. Halldórsson

To be submitted to Geochimica et Cosmochimica Acta.

Abstract

Geochemical variations in ocean island basalts have primarily been credited to the tapping of enriched components in the convecting mantle, possibly associated with recycled crust. Within the framework of such high-temperature igneous systems interaction between recycled crust and ambient mantle or a change in source lithology is expected to cause subtle variations in stable isotopic systems, such as Mg and Fe. Olivine, in which Mg and Fe are major constituents, is usually among the first minerals to precipitate from a mantle-derived melt making it an ideal proxy for primary melt and source composition.

Here we present a study of Mg and Fe isotopes in a set of well-characterised high-forsterite (> Fo_{80}) olivine crystals from 22 locations in the active neovolcanic zones and Quaternary and Tertiary lavas of Iceland. We couple single crystal (n=15) and bulk measurements (n=13) and show that while most $\delta^{26}Mg_{ol}$ values are unresolvable from values characteristic for mid ocean ridge basalts (MORBs; $\delta^{26}Mg$ between -0.31 and -0.19 ‰), $\delta^{56}Fe_{ol}$ values vary significantly, between -0.31 and +0.14 ‰, and are clearly resolvable from the canonical MORB range ($\delta^{56}Fe$ between +0.04 and +0.14 ‰) and previous published values for Iceland ($\delta^{56}Fe$ +0.025 to +0.18 ‰).

We find that while some of the observed variation in $\delta^{56}Fe_{ol}$ values can be explained by fractional crystallisation from MORB-like melts, the lowest $\delta^{56}Fe_{ol}$ values likely result from diffusive exchange of Mg and Fe between carrier melt and olivine. By evaluating possible correlations between $\delta^{56}Fe_{ol}$ and known chemical tracers of enriched mantle and recycled crustal components we find that $\delta^{56}Fe_{ol}$ values are decoupled from the presence of enriched mantle components. As a result, the large $\delta^{56}Fe_{ol}$ variation we observe – irrespective of olivine composition – is likely a result of binary diffusion of Mg and Fe, which act to overprint any source-derived $\delta^{56}Fe$ variability. The degree of diffusion is likely controlled by the residence time of the olivine in a more evolved melt and the preservation of diffusion patterns in the olivine crystals enable future studies to model and evaluate magma transport times for the units studied here.

4.1 Introduction

The chemistry of ocean island basalts (OIBs) differs from mid-ocean ridge basalts (MORBs) in ways that have been associated with the tapping of enriched mantle reservoirs, core-mantle interactions and the possible incorporation of recycled crustal material at depth (e.g., Zindler *et al.*, 1982; Hofmann & White, 1982; Hofmann, 1997; Soderman *et al.*, 2020; Lesher *et al.*, 2020). However, the nature and preservation of these enriched reservoirs is poorly constrained, and little is known about how recycled components are incorporated into upwelling mantle plumes. Despite this, trace elemental and isotopic variations in OIBs has provided a tool for distinguishing various chemical mantle endmembers and identifying the origin of the chemical anomaly associated with each endmember (e.g., Zindler & Hart, 1986) One such example is the evidence for the recycling of upper crustal material in OIBs derived from EMII-type mantle components (e.g., Zindler & Hart, 1986) provided by incompatible elemental radiogenic and stable isotopes, such as Sr and Cl (e.g., Zindler & Hart, 1986; Halldórsson *et al.*, 2016).

Another mechanism for integrating and preserving chemical traits of recycled material is through metasomatism of peridotite in the convecting mantle by recycled oceanic crust-derived melts (Yaxley & Green, 1998). This process was proposed to create lithological heterogeneity by generating olivine-free mantle assemblages or secondary pyroxenites (Sobolev *et al.*, 2005). Olivines crystallised from such pyroxenite-derived magmas were proposed to contain high Ni and low Mn and Ca contents relative to those crystallised from pure peridotite-derived melts, as the change in mineral assemblage was proposed to affect the overall partitioning of these elements in the mantle (Sobolev *et al.*, 2007; Sobolev *et al.*, 2005. This mechanism of recycling oceanic crust was later supported through experimental findings where it was found that the pyroxenitic component reached its solidus at lower temperatures and higher pressures than the surrounding peridotitic matrix (Mallik & Dasgupta, 2012). Due to melt mixing in the mantle, the signature of these pyroxenitic components was suggested to be better preserved where thick lithospheres resided above upwelling mantle plumes, such as Hawaii and other intraplate hot spots (Sobolev *et al.*, 2007), or where short melting columns limited the degree of mixing between pyroxenite- and peridotite derived melts (e.g., Kokfelt *et al.*, 2006).

The preservation and sampling of recycled oceanic crust can thus be traced through the multi-phase study of both glass and olivine chemistry. Olivine (ol) is among the first minerals to precipitate from a mantle-derived melt and considered stable over a large pressure range. Moreover, high-forsterite olivine crystals and melt inclusions imbedded in these olivines often exhibit noticeable chemical disequilibrium with their carrier melts (e.g., Wieser *et al.*, 2019). These olivines have been shown to record larger degrees of source-derived heterogeneity as melts are often a result of extensive magmatic processes occurring in the crust and the lithosphere, such as melt mixing, fractional crystallisation and assimilation (e.g., Maclennan, 2008; Wieser *et al.*, 2019; Bindeman *et al.*, 2008; Rudge *et al.*, 2013). This is indeed a common trait of Icelandic basalts and picrites (Thomson & Maclennan, 2013) where high-forsterite olivine is more likely to preserve the diverse and primitive signal from the mantle-derived melts. Thus, olivine is a valuable phase for the study of mantle source-derived heterogeneity, especially in outcrops where fresh glasses are unavailable.

The study of non-traditional stable isotopes of major elements offers a new perspective to trace melt contributions from enriched and depleted components, as these elements are evenly distributed between the two reservoirs, whereas the isotopic composition of elements which are incompatible in mantle mineral assemblages (e.g., Pb, Sr and Nd) tend to mostly reflect contribution from the enriched component (Stracke *et al.*, 2019). Moreover, stable isotopes of major elements, such as Mg and Fe, have been effective in identifying the recycling of subducted crust whether it reflects the incorporation of (i) carbonates, i.e. recycling of upper crust (e.g., Wang *et al.*, 2018; Liu *et al.*, 2017; Teng *et al.*, 2016), or (ii) the presence of pyroxenitic mantle assemblages (e.g., Williams & Bizimis, 2014; Gleeson *et al.*, 2020; Konter *et al.*, 2016; Nebel *et al.*, 2019), i.e. recycling of lower crust and lithospheric mantle. Moreover, recent evidence has suggested that variations in Fe isotopes can reflect core-mantle interaction, thus constraining the origin of possible isotopic variations (e.g. Lesher *et al.*, 2020; Soderman *et al.*, 2020). The combined study of Mg and Fe isotopes thereby represents a possibility for evaluating the preservation and recycling of an entire section of oceanic crust and possible core-contribution.

As Mg and Fe are major elements in olivine, this phase seems a promising medium for the study of source-derived isotopic variations in Mg and Fe space. However, Fe isotope fractionation during crystallisation of individual phases such as olivine is poorly constrained and is strongly controlled by the Fe-O bond strength which is a complex product of Fe-O bond length, oxidation state and the coordination of Fe in a given medium (e.g., Polyakov & Mineev, 2000; Shahar *et al.*, 2008; Roskosz *et al.*, 2015). Moreover, previous studies have highlighted the importance of considering effects from fractional crystallisation processes (e.g., Peters *et al.*, 2019) and post-crystallisation magmatic processes, such as diffusion, on the final Fe and Mg isotopes measured in olivine (e.g., Sio *et al.*, 2018; Sio *et al.*, 2013; Teng *et al.*, 2011; Oeser *et al.*, 2015; Dauphas *et al.*, 2010).

Despite being mostly overlain by a thin lithosphere (< 50 km; Bjarnason & Schmeling, 2009), variations in isotopic and trace element compositions characterising eruptive products from the various volcanic regions show that the Icelandic plume is characterised by a spatially heterogenous mantle (Rasmussen *et al.*, 2020; Rasmussen *et al.*, *submitted*; Harðardóttir *et al.*, 2018; Peate *et al.*, 2010; Kokfelt *et al.*, 2006). This heterogeneity is likely a result of entrainment of crustal material in the Iceland plume, possibly as secondary pyroxenite as described above (e.g., Kokfelt *et al.*, 2006; Neave *et al.*, 2018; Rasmussen *et al.*, *submitted*; Rasmussen *et al.*, 2020). The Iceland plume is moreover characterised by the highest $^{3}He/^{4}He$ values sampled by modern plumes, suggesting that the plume is sourced from the lower mantle. Iceland thus represents an ideal setting to study the effect that a lithological heterogenous plume has on the chemistry of magmatic olivine and whether the stable isotopic signatures of Mg and Fe can be related to the deep domains from which the Iceland plume originates.

We will attempt to separate the effect of magmatic processes such as fractional crystallisation and diffusion from source-inherited Mg and Fe isotopic values by studying previously well-characterised high-forsterite olivine. Trace element and oxygen isotopic values ($\delta^{18}O_{ol}$), that cannot be generated by crustal processes such as fractional crystallisation and assimilation, for these samples have already predicted the presence of recycled material in the shape of secondary pyroxenite (Rasmussen *et al.*, 2020; Rasmussen *et al.*, *submitted*). To further constrain the effects from post-crystallisation diffusion of Fe isotopes through olivine, we analysed Mg isotopes on the same aliquot, as the combined isotopic systematics has shown to be especially effective for evaluating the effect of

diffusion in olivine (e.g., Dauphas *et al.*, 2010; Teng *et al.*, 2011). Finally, as the $\delta^{26}Mg$ and $\delta^{56}Fe$ datasets for magmatic rocks in Iceland are currently very limited (Schuessler *et al.*, 2009; Pogge von Strandmann *et al.*, 2008; Weyer & Ionov, 2007) we hope to explore possible regional variations and evaluate the processes controlling these variations such as magma transport timescales and/or mantle heterogeneity.

4.2 Samples and prior work

The studied sample suite consists of 22 olivine separates (listed in the data supplement for Chapter 4, T1) from primitive lavas covering the active (neovolcanic <1 Ma) rift and flank zones along with older Quaternary and Tertiary (1-16 Ma) units (Figure 4.1).

The samples analysed in this study have previously been analysed for their minor- and trace element systematics and $\delta^{18}O_{ol}$ and $^{3}He/^{4}He_{ol}$ values (Rasmussen *et al.*, 2020; Harðardóttir *et al.*, 2018; Rasmussen *et al., submitted*) and show the largest $^{3}He/^{4}He$ range reported for any oceanic island (from 6.7 to 47.8 R_A, where R_A=air $^{3}He/^{4}He$). In summary, the previous studies found that minor (e.g., Ni, Ca and Mn) and trace (e.g., Zn, Ga and Sc) elemental variations in these olivines separates record the presence of hybrid pyroxenitic (olivine-poor) components in the Iceland mantle which are best sampled in South Iceland (Rasmussen *et al.*, 2020). This finding, coincided with a plume-derived $^{3}He/^{4}He$ fingerprint, indicating that the lithological heterogeneity present in the Icelandic mantle is a trait of the upwelling plume. Moreover, a lowering of $^{3}He/^{4}He_{ol}$ values from the initiation of the plume (60 Ma) until modern day was found to coincide with an increase in plume flux. This was suggested to reflect an increase in upwelling of lower mantle material carrying and entraining recycled oceanic lithosphere as represented by an overall coupled lowering in $^{3}He/^{4}He_{ol}$ and source-derived $\delta^{18}O_{ol}$ with time (Rasmussen *et al.*, *submitted*). Thus, the samples studied here offer an abundance of available data and pre-determined knowledge of mantle-derived variability in source lithology and origin of isotopic variations.

The data presented in this study is classified according to the volcanic regions defined in Figure 4.1 where ERZ (Eastern Rift Zone), WRZ (Western Rift Zone) and NRZ (Northern Rift Zone) constitutes the current rift axis. SIVZ (South Iceland Volcanic Zone) is a flank zone propagating southward from ERZ where transitional and alkalic magmas prevail similarly to the two other flank zones, ÖVZ (Öræfajökull Volcanic Zone) and SNS (Snæfellsnes). TER represents olivine from two Tertiary lavas from the West Fjords, while HRP (Hreppar formation) represents an isolated region with Plio-Pleistocene aged rocks, located between the WRZ and ERZ (Figure 4.1).

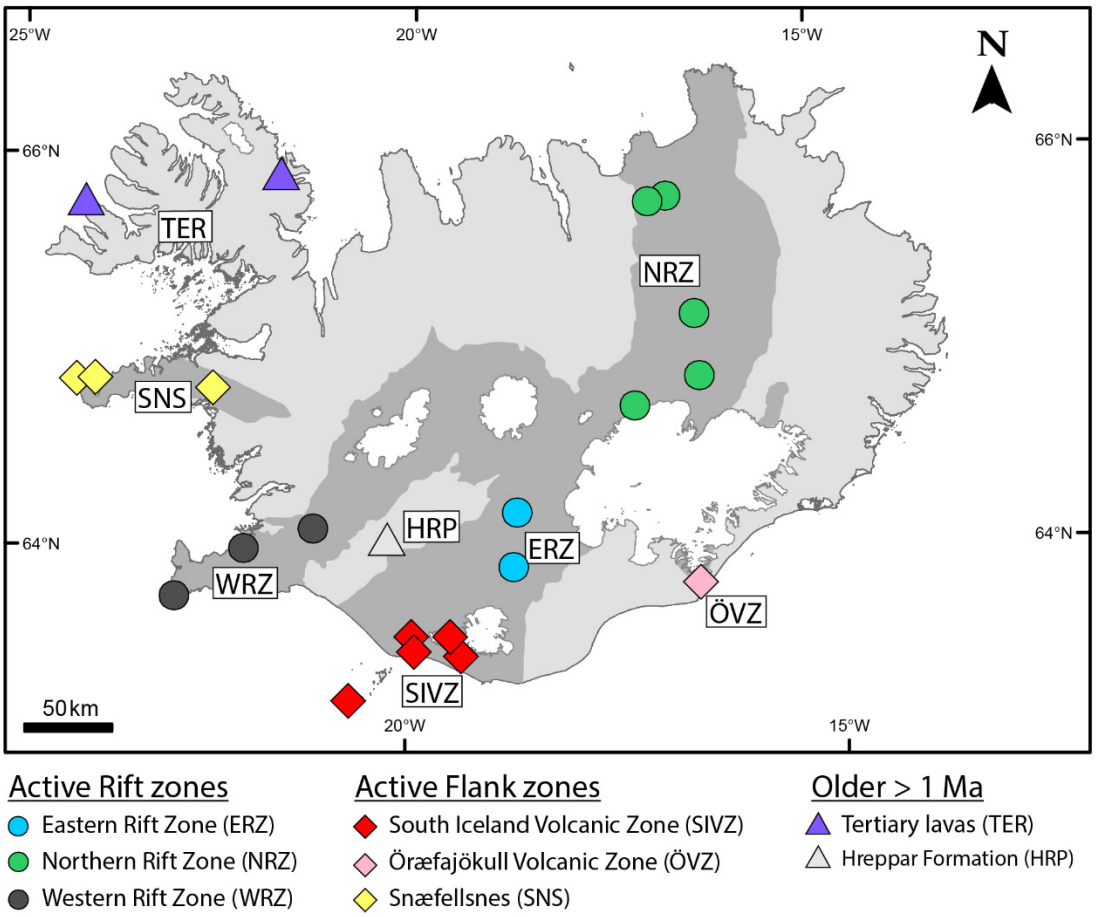

Figure 4.1 Map of sample localities targeted for this study. Abbreviations given in the legend and the symbols and colours assigned each region will be used throughout this manuscript.

4.3 Methods

The olivine crystals used for this study are different from the ones analysed in Rasmussen *et al.* (2020) and Rasmussen *et al.* (*submitted*) but are from the same sample separate, except for the case of FIM-GSV where, due to lack of material, olivine from new hand specimens from the same outcrop were used. The new crystals were first analysed for their major and minor elements by Electron Microprobe Analyser (EMPA) using a JEOL JXA-8230 electron microprobe at the Institute of Earth Sciences, University of Iceland. We used a high-precision method (Batanova *et al.*, 2015) involving an increased probe current (500 nA) and counting time that provides detection limits down to 4 ppm (2 standard errors) on minor and trace elemental contents in olivine. The specific analytical settings are identical to the ones presented in Rasmussen *et al.* (2020). A minimum of three points were analysed per crystal to cover any variation observed in the crystals and back scattered electron images were used to avoid grains that showed large degrees of forsterite zonation or contained obvious mineral or fluid inclusions and cracks. Following EMPA, the crystals targeted for digestion were separated from the epoxy buttons by heating and removal by tweezers under a binocular microscope. To directly match our results with trace element data from Rasmussen *et al.* (2020) and oxygen isotopic values from Rasmussen *et al.* (*submitted*), we only targeted

crystals displaying Fo, Ni and Mn contents similar to the olivine compositions presented in these studies. These crystals were then rinsed in acetone and MQ water prior to digestion. A minimum of 1 mg olivine (dependent on the inferred total Fe content) was digested for each sample and each data-point is based on bulk digestion of 1-5 olivine crystals with diameters ranging from 1-4.5 mm (see Table 4.1)

Aliquots from the same digested sample were used for both Mg and Fe purification, using methods described in Tipper *et al.* (2008) and Williams *et al.*, (2004); Williams *et al.*, (2005) respectively. Isotopic analyses of δ^{26}Mg and δ^{56}Fe were measured with a Thermo Neptune Plus multi-collector ICP-MS from solutions with ~ 2 ppm Mg in 2% HNO_3 and ~ 8.3 ppm Fe in 0.1M HNO_3 at the Department of Earth Sciences, University of Cambridge where the δ denotes the per mil deviation of the sample ratio relative to a standard which for Mg is defined according to equation 1 and for Fe defined according to equation 2

$$\delta^{26/24}Mg_{sample} = \left(\frac{^{26}Mg/^{24}Mg_{sample}}{^{26}Mg/^{24}Mg_{DSM3}} - 1\right) \cdot 10^3 \quad \text{equation 1}$$

$$\delta^{56/54}Fe_{sample} = \left(\frac{^{56}Fe/^{54}Fe_{sample}}{^{56}Fe/^{54}Fe_{IRMM14}} - 1\right) \cdot 10^3 \quad \text{equation 2}$$

For $\delta^{26}Mg_{ol}$ measurements, the sample was introduced using an APEX IR sample introduction system and an ESI PFA nebuliser. Beam voltages were matched to the beam intensity for ^{24}Mg for DSM-3 (8V) at medium resolution and Mg concentrations of 300 ppb. Instrumental drift and mass bias were corrected for by sample-standard bracketing of DSM-3 and the analytical precision of the analyses are based on 3 repeat measurements for each sample and is generally found to be better than ±0.12 ‰ for $\delta^{26}Mg_{ol}$ (except for one TER sample with 2σ of 0.19; 2σ, Table 4.1). Mass dependence and reproducibility of the δ^{26}Mg measurements were evaluated by using CAM-1 (δ^{26}Mg -2.63 ± 0.103‰ (2σ) *n* = 9) and Z1 (δ^{26}Mg -3.33 ± 0.107‰ (2σ) *n* = 12) while Z1 was also used to evaluate accuracy (δ^{26}Mg -3.28 ± 0.120‰ (2σ) *n* = 18).

For $\delta^{56}Fe_{ol}$ measurements, the sample was introduced using a PFA micro-concentric nebuliser and a quartz spray chamber by wet plasma mode. Beam voltages were matched to the beam for ^{56}Fe for IRMM-14 (to 10 %) at medium resolution (M/DeltaM <8000), Fe concentrations of 8.26 ppm and beam voltages between 33-48 V, dependent on the sensitivity of the instrument that day. Instrumental drift and mass bias were corrected for by sample-standard bracketing of IRMM-14 and the analytical precision of the analyses are based on 3 repeat measurements for each sample and is generally found to be better than ±0.049 ‰ for $\delta^{56}Fe_{ol}$ (2σ, Table 4.1). Mass dependence and reproducibility of the δ^{56}Fe measurements were evaluated by the use of an in-house FeCl standard (δ^{56}Fe of -0.72 ± 0.04‰, δ^{57}Fe of -1.07 ± 0.06 ‰ 2SD (2σ) *n* = 31) similarly analysed in other studies (e.g., Williams & Bizimis, 2014; Gleeson *et al.*, 2020). The accuracy of these measurements was evaluated using the external standards BHVO-2 (δ^{56}Fe of 0.08 ± 0.02‰, δ^{57}Fe of 0.13 ± 0.02 ‰ (2σ) *n* = 3) and BCR (δ^{56}Fe of 0.09 ± 0.05‰, δ^{57}Fe of 0.12 ± 0.02 ‰ (2σ) *n* = 3). Chemistry blanks possessed insignificant amounts of Fe compared to our samples (< 2.5 ng).

4.4 Results

Overall, the collected data (Table 4.1 and Figure 4.2) shows a variation in $\delta^{26}Mg_{ol}$ between -0.29 ± 0.04 and -0.08 ± 0.19 ‰ and are all, except for one analysis, within error of MORB glasses and whole rock measurements (-0.31 to -0.19 ‰; Teng *et al.*, 2010; Bourdon *et al.*, 2010). Published Icelandic $\delta^{26}Mg$ melt and olivine data is in good agreement with the variation recorded by the olivine analysed here (Figure 4.2).

We observe limited variation in $\delta^{26}Mg_{ol}$ independent of Fo content variation (Figure 4.3a). The only data point that, beyond the 2σ, plots with higher $\delta^{26}Mg_{ol}$ (-0.11 ‰) relative to the field defined by MORBs is the high-forsterite population (Fo_{85}) of three olivine populations from a single sample from Hamragarðaheiði with varying Fo contents (displayed as "HAMRA")

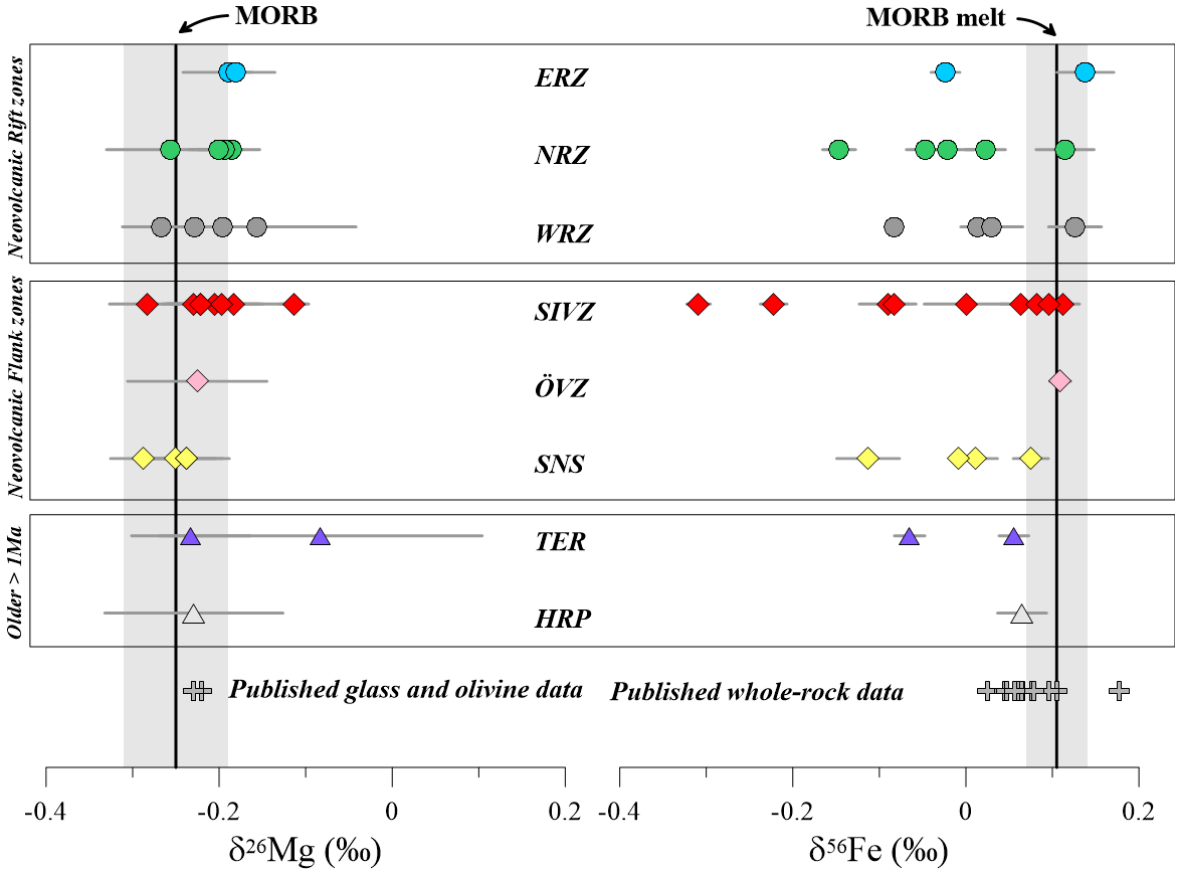

Figure 4.2 Results of Mg and Fe isotopic analysis for Iceland olivine. The grey fields represent that expected from MORB melts (and all MORB products for $\delta^{26}Mg$). Available data for Icelandic samples is plotted for comparison. The error bars represent the 2σ error based on three separate measurements of the same sample and varies between 0.01-0.07‰ for $\delta^{56}Fe$ and 0.01-0.19‰ for $\delta^{26}Mg$. The literature data on is sourced from Pogge von Strandmann et al. (2008); Schuessler et al. (2009) and Weyer and Ionov (2007).

Table 4.1 Mg and Fe isotopic data measured on Icelandic olivine along with the sizes and number of crystals digested for analysis. The points analysed refer to spots analysed by EMPA. The complete dataset along with previously published data for the same samples (and locations for Pb) can be found in the data supplements for Chapter 4.

Sample name	Locality	Fo content	±	Points analysed	$\delta^{26/24}$Mg	±2σ	$\delta^{25/24}$Mg	±2σ	$\delta^{56/54}$Fe	±2σ	$\delta^{57/54}$Fe	±2σ	Crystals digested	Max crystal diameter (mm)
ERZ														
ICE08R-20	Fontur, craters	88	0.13	*3*	-0.189	0.05	-0.121	0.02	0.138	0.03	0.174	0.03	*1*	*2.2*
A29	Hörðufell/Herðubreið	87	0.05	*3*	-0.181	0.02	-0.109	0.03	-0.024	0.02	-0.009	0.03	*1*	*1.9*
NRZ														
BORG-1	Borgarhraun	89	0.08	*6*	-0.185	0.01	-0.114	0.02	-0.021	0.03	-0.026	0.05	*2*	*1.6*
NAL 625	Vaðalda	85	0.01	*3*					0.023	0.02	0.049	0.02	*1*	*2.2*
NAL 611	Kistufell	89	0.17	*15*	-0.257	0.07	-0.150	0.05	0.115	0.03	0.164	0.03	*5*	*1.0*
Th29	Þeistareykir picrite	89	0.08	*3*	-0.194	0.04	-0.102	0.08	-0.147	0.02	-0.214	0.03	*1*	*3.2*
NAL 688	Eggert	90	0.02	*3*	-0.201	0.02	-0.104	0.02	-0.047	0.02	-0.059	0.01	*1*	*2.6*
WRZ														
BUR-1	Búrfellshraun	89	0.02	*3*	-0.196	0.12	-0.108	0.06	0.013	0.02	-0.012	0.04	*1*	*2.2*
D2	Háleyjabunga	89	0.04	*3*	-0.156	0.11	-0.101	0.03	0.126	0.03	0.189	0.06	*1*	*3.2*
MID-1	Miðfell	90	0.05	*3*	-0.267	0.03	-0.127	0.04	-0.083	0.01	-0.104	0.06	*1*	*2.6*
MID-1	Miðfell	90	0.08	*3*	-0.228	0.08	-0.118	0.03	0.030	0.04	0.034	0.04	*1*	*2.2*
SIVZ														
FIM-GSV	Fimmvörðuháls 2010	80	0.02	*6*	-0.284	0.04	-0.160	0.02	0.063	0.02	0.062	0.01	*2*	*1.0*
Surtsey 1967	Surtsey 1967 basalt	86	0.38	*9*	-0.205	0.06	-0.101	0.04	-0.222	0.02	-0.342	0.03	*3*	*1.0*
Surtsey 1967	Surtsey 1967 basalt	87	0.33	*15*	-0.183	0.08	-0.091	0.07	-0.309	0.01	-0.458	0.01	*5*	*1.0*
HVAMM-2	Hvammsmúli	88	0.01	*3*	-0.221	0.04	-0.093	0.02	-0.090	0.03	-0.129	0.06	*1*	*1.6*
HVAMM-2	Hvammsmúli	88	0.05	*3*					0.001	0.05	-0.038	0.03	*1*	*1.3*
HVIT-1	Hvítmaga	88	0.12	*3*	-0.229	0.01	-0.125	0.01	0.113	0.01	0.163	0.02	*1*	*2.6*
HAMRA-1	Hamragarðaheiði	78	0.20	*6*	-0.197	0.04	-0.122	0.02	0.082	0.01	0.114	0.03	*2*	*2.9*
HAMRA-1	Hamragarðaheiði	80	0.19	*6*	-0.222	0.04	-0.132	0.02	0.096	0.04	0.123	0.05	*2*	*2.6*
HAMRA-1	Hamragarðaheiði	85	0.23	*6*	-0.113	0.02	-0.088	0.04	-0.083	0.02	-0.108	0.04	*2*	*1.3*
ÖVZ														
SAL 688	Öræfajökull	86	0.04	*3*	-0.225	0.08	-0.117	0.04	0.109	0.01	0.159	0.03	*1*	*2.9*
SNS														
SNS 206	Nykurhraun	90	0.05	*9*	-0.250	0.05	-0.125	0.01	0.011	0.03	0.008	0.02	*3*	*2.2*
SNS 206	Nykurhraun	89	0.09	*6*	-0.238	0.04	-0.110	0.01	-0.008	0.01	-0.009	0.01	*2*	*2.2*
SNS 221	Bekkjahraun	82	0.02	*3*	-0.288	0.04	-0.140	0.04	0.075	0.02	0.098	0.00	*1*	*4.5*
SNS 214	Ólafsvíkurenni	89	0.21	*6*	-0.237	0.05	-0.126	0.01	-0.113	0.04	-0.153	0.03	*2*	*1.0*
TER														
ICE08R-02	Selárdalur	86	0.09	*6*	-0.083	0.19	-0.069	0.07	0.056	0.02	0.081	0.01	*2*	*1.9*
POI 07-01	Reykjafjörður syðri	87	0.03	*9*	-0.233	0.07	-0.120	0.02	-0.065	0.02	-0.088	0.03	*3*	*1.3*
HRP														
THJOR-1	Skeljafell	89	0.02	*3*	-0.229	0.10	-0.128	0.05	0.065	0.03	0.146	0.02	*1*	*3.5*

Values for $\delta^{56}Fe_{ol}$ vary between -0.31 ± 0.014 ‰ and are thus clearly resolvable from variations observed in MORB melts (+0.04 to +0.14 ‰; Teng *et al.*, 2013; Chen *et al.*, 2019; grey fields in Figure 4.2 and Figure 4.3). Following the regional grouping presented in Figure 4.1, the greatest variation appears to be found in olivine from the SIVZ with $\delta^{56}Fe_{ol}$ ranging from -0.31 to +0.11 ‰. Published $\delta^{56}Fe_{whole\text{-}rock}$ values are mirrored in the Icelandic olivine set, apart from values >MORB melts as displayed by a single whole rock data point from Heimaey (Figure 4.2; Schuessler *et al.*, 2009).

In contrast to $\delta^{26}Mg_{ol}$, we observe a large variation in $\delta^{56}Fe_{ol}$ across the Fo content range (Figure 4.3b). The largest variation in $\delta^{56}Fe_{ol}$ is found at Fo_{87} representing the entire variation

observed in our sample set. In general, we observe greater variation at high-forsterite contents (>Fo_{86}) which represent most of the olivine analysed here.

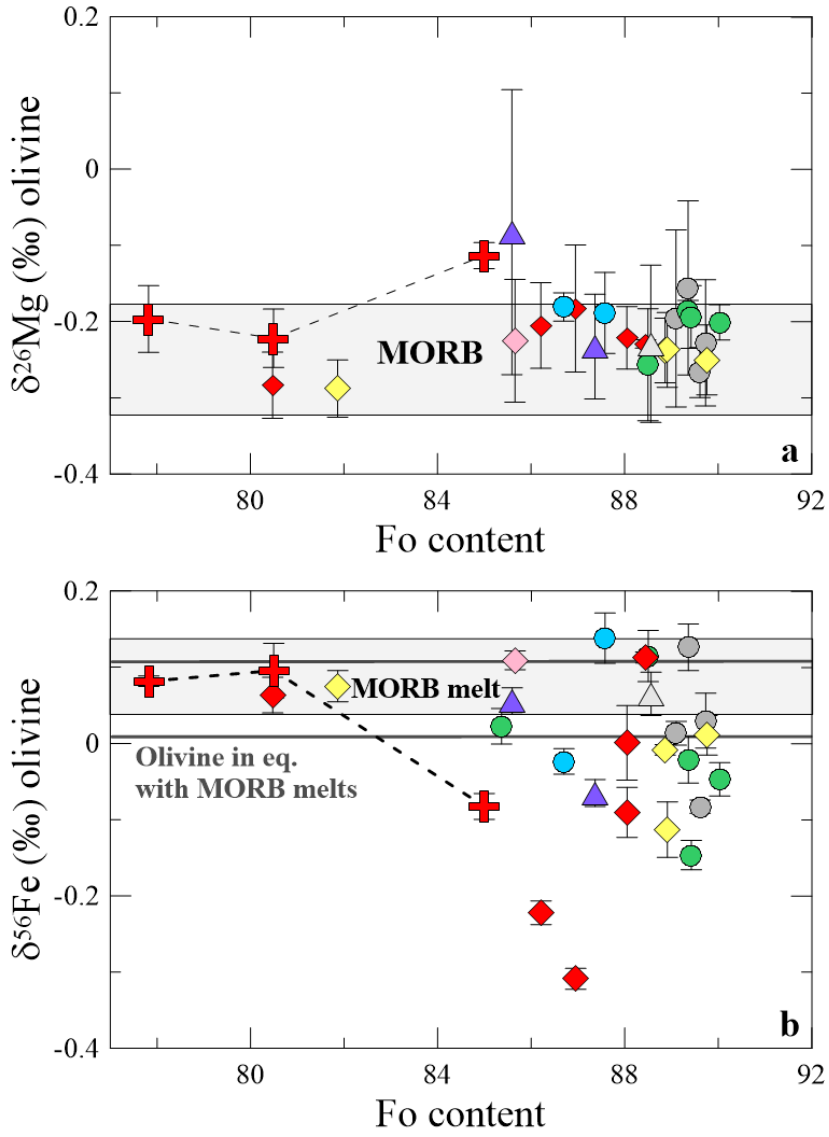

Figure 4.3 $\delta^{26}Mg$ and $\delta^{56}Fe$ values of Icelandic olivine with Fo_{78-91}. Variation in $\delta^{26}Mg_{ol}$ is mostly within the grey field defined by MORBs (Teng et al., 2013; Teng et al., 2010 and Chen et al 2019) while $\delta^{56}Fe_{ol}$ shows a variation between -0.31 and 0.14 ‰, clearly resolvable from the variation seen in MORB melts. The largest variation in $\delta^{56}Fe_{ol}$ is recorded in olivine with Fo>86. The grey lines in b represent predicted $\delta^{56}Fe$ values of olivine in equilibrium with a melt similar to MORBs with $D_{melt\text{-}olivine}$ between 0.027-0.037 (average 0.032). The red crosses represent three olivine populations from Hamragerði (HAMRA) with varying Fo contents. The symbols are the same as in Figure 4.1 and error bars are defined the same as for Figure 4.2.

4.5 Discussion

4.5.1 Assessing modifications resulting from magmatic processes

Equilibrium fractionation (partial melting and fractional crystallisation)

Studies on isotopic fractionation have demonstrated that at near-magmatic temperatures isotopic fractionation becomes near-insignificant (e.g., Urey, 1947; Chacko *et al.*, 2001). Indeed, this was previously shown to be the case for Mg isotopes during partial melting and fractional crystallisation (e.g., Teng *et al.*, 2007) as shown by uniform $\delta^{26}Mg$ values measured in volcanic products and individual mantle-minerals (Teng *et al.*, 2010; Handler *et al.*, 2009; Yang *et al.*, 2009). The homogenous $\delta^{26}Mg_{ol}$ values at variable Fo contents displayed by the olivines studied here supports this notion (Figure 4.3a) and allows us to adopt the measured $\delta^{26}Mg_{ol}$ value as representative of $\delta^{26}Mg$ value of the source material.

However, equilibrium fractionation of Fe isotopes between two mediums is a function of the difference in bond strength of Fe in the mediums, which in turn is controlled by bond lengths, oxidation state and the coordination of Fe, where stronger bonds favours the heavy isotope (Macris *et al.*, 2015; Young *et al.*, 2015; Dauphas *et al.*, 2014). Fe^{3+} acts like an incompatible element during mantle melting and as Fe^{3+} generates stronger and shorter Fe-O bonds than Fe^{2+}, and thus concentrates the heavy isotope, crystallisation of Fe^{2+}-bearing phases such as olivine, are predicted to result in differentiated melts with high $\delta^{56}Fe$ values (i.e., increasing $\delta^{56}Fe_{melt}$). Fractionation of Fe isotopes is therefore expected to occur both during melting (Weyer & Ionov, 2007) and subsequent fractional crystallisation. The effect of partial melting is, however, insignificant at the degree of melting observed in MORB and OIB settings (e.g., Dauphas *et al.*, 2009; Gleeson *et al.*, 2020). Consequently, to evaluate the $\delta^{56}Fe$ value of the melt crystallising the olivines presented in Figure 4.3b, we need to assess the effect of simple fractional crystallisation (Peters *et al.*, 2019). As the olivines presented here appear to be the product of melts crystallising dominantly olivine and clinopyroxene (Rasmussen *et al.*, 2020) we simply calculate the fractionation factor between a tholeiitic melt and olivine based on the bonding values presented in Dauphas *et al.* (2014).

At temperatures between 1150-1399°C, a reasonable crystallisation temperature for high-forsterite olivine in Iceland (Breddam, 2002; Caracciolo *et al.*, 2020; Hermes & Schilling, 1976; Spice *et al.*, 2016; Matthews *et al.*, 2016), and Fe^{3+}/Fe_{TOT} ratios between 0.14 and 0.17 (Novella *et al.*, 2020; Schipper & Moussallam, 2017) we find that the fractionation factor $\Delta_{melt\text{-}olivine}$ is between 0.037 at 1150 °C and 0.027 at 1399°C (Figure 4.4a), much lower than has been suggested characteristic for fractional crystallisation in more differentiated magmas (e.g., Teng *et al.*, 2008; Chen *et al.*, 2019). Thus, olivine with $\delta^{56}Fe_{ol}$ between 0.008-0.108 ‰ (grey line in Figure 4.3b) could result from their crystallisation from a MORB-like melt ($\delta^{56}Fe_{melt}$ between 0.04-0.14 ‰) at temperatures above 1150°C. Based on the models presented in Figure 4.4a, we see, that the fractionation factor decreases with an increase in temperature, and hence olivine with higher Fo contents should reflect $\delta^{56}Fe$ values closer to their source melt composition relative to olivine with lower Fo contents. However, we observe no correlation between $\delta^{56}Fe_{ol}$ and Ca/Al (Figure 4.4b), which in olivine can be utilised as a proxy for relative crystallisation temperatures. This lack of correlation suggests that the variations in $\delta^{56}Fe_{ol}$ we observe are not purely a result of temperature-dependent variations in the fractionation factor $\Delta_{melt\text{-}olivine}$ but must be caused in part by other processes.

Moreover, many olivines with >Fo$_{86}$ display δ^{56}Fe values much lower than predicted from high-temperature equilibrium fractionation from melts resulting from partial melting of even a depleted N-MORB mantle ($\delta^{56}Fe_{melt}$ = 0.04 ± 0.01 ‰, Chen *et al.*, 2019).

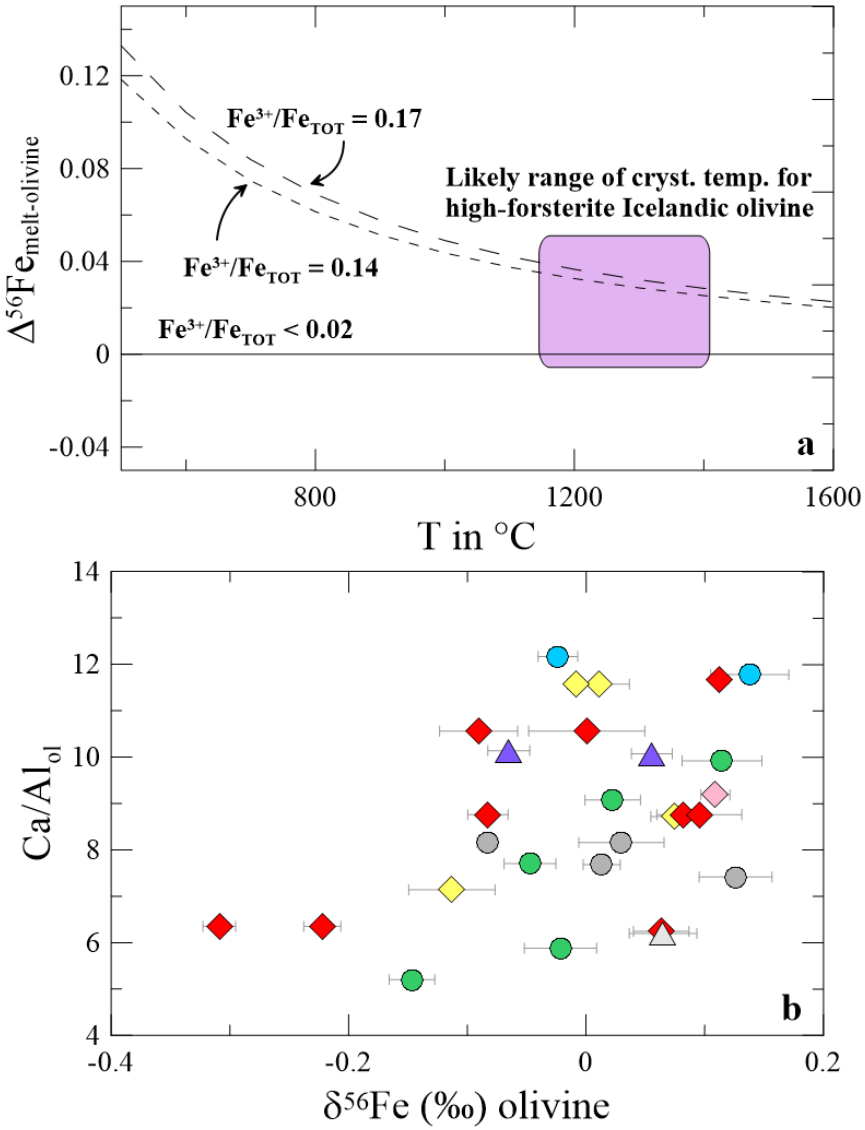

Figure 4.4 Temperature-controlled fractionation of δ^{56}Fe during olivine crystallisation. a) Fractionation factors as a function of temperature and ratio of Fe^{3+}/Fe_{TOT} from Dauphas et al. (2014). Within the expected temperature range for Icelandic magmas (purple field), the fractionation factor $\Delta_{melt\text{-}olivine}$ ranges between 0.027-0.037 in a melt with Fe^{3+}/Fe_{TOT} between 0.14-0.17 (Novella et al., 2020; Schipper & Moussallam, 2017). b) Ca/Al_{ol} values for the olivine studied here. A lack of correlation between Ca/Al_{ol}, which can act as a proxy for relative crystallisation temperatures, and $\delta^{56}Fe_{ol}$ suggests, that the variation in $\delta^{56}Fe_{ol}$ is not controlled by a change in $\Delta_{melt\text{-}olivine}$ as an effect of lowering crystallisation temperatures (increasing Ca/Al_{ol}). The symbols are the same as in Figure 4.1 and error bars are defined the same as for Figure 4.2.

Possible effects from crustal assimilation processes

Hydrothermal alteration of basaltic crust at varying temperatures has resulted in material with $\delta^{18}O$ values between +10 and -11 ‰ (Zakharov *et al.*, 2019), which can be readily assimilated by hot mantle-derived melts percolating through the crust. Assimilation of low $\delta^{18}O$ crust has indeed been shown to cause lowering of mantle-derived $\delta^{18}O$ values of >1 ‰, and magmas in the rift regions, with well-established mush zones, are especially vulnerable to such processes (Bindeman *et al.*, 2012; Bindeman *et al.*, 2008). The effect of assimilation on the $\delta^{18}O_{ol}$ values was shown to be significant in central Iceland where $\delta^{18}O_{ol}$ values down to 2.8 ‰ were found in olivine with Fo_{86} (Rasmussen *et al.*, *submitted*). Hydrothermal fluids preferentially fractionate lighter Fe isotopes (Rouxel *et al.*, 2003). Thus, hydrothermal sulfides and material overprinted by hydrothermal fluids present a reservoir for low $\delta^{56}Fe$ material that can theoretically be incorporated into mantle-derived melts through assimilation (Bilenker *et al.*, 2018; Johnson *et al.*, 2004). Following this notion, assimilation of significant amounts of hydrothermally-altered low-$\delta^{56}Fe$ crust should modify the Fe isotopic composition. As this crust is characterised by low-$\delta^{18}O$ values too, a shift to lower $\delta^{56}Fe$ values should correlate with a lowering in $\delta^{18}O$ values. However, such correlations are not displayed by the Icelandic olivines studied here (Figure 4.5), suggesting that despite the partial control that assimilation has on the $\delta^{18}O$ values, assimilation of hydrothermally altered crust has a negligible effect on the low measured $\delta^{56}Fe_{ol}$ values. Therefore, other processes, such as isotopic diffusion or mantle heterogeneity must be considered as potential explanations for the low $\delta^{56}Fe_{ol}$ values observed.

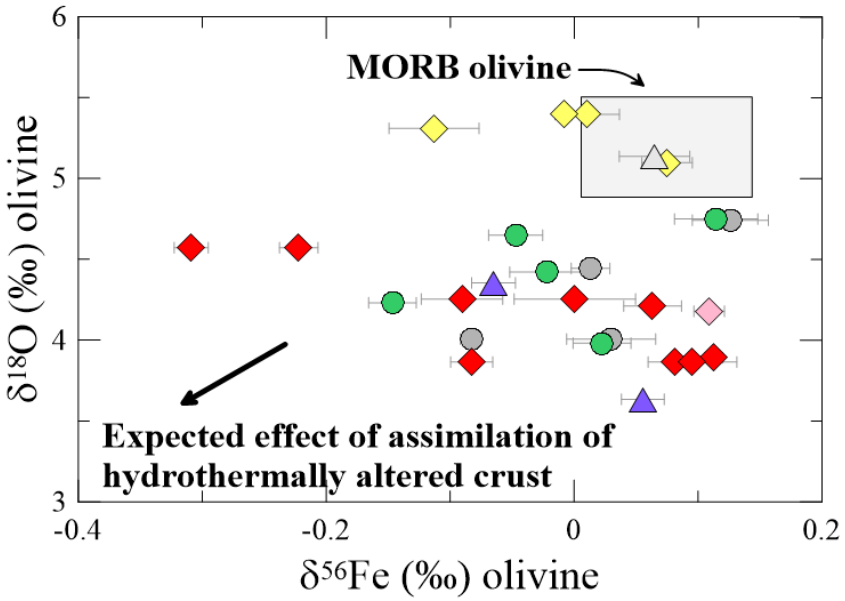

Figure 4.5 $\delta^{56}Fe_{ol}$ and $\delta^{18}O_{ol}$ values (Rasmssen et al.*,* submitted*) from the same olivine separates. Assimilation of low $\delta^{18}O$ crust has been shown to lower the $\delta^{18}O$ of Icelandic melts (e.g., Bindeman et al., 2008). As hydrothermal fluids are characterised by low Fe isotopes, hydrothermally altered material is characterised by low $\delta^{56}Fe$ values, and assimilation of this material could thus lead to coupled lowering of $\delta^{18}O_{ol}$ and $\delta^{56}Fe_{ol}$. However, this is not the case, which highlights, that assimilation cannot reproduce the low $\delta^{56}Fe$ values we measure in Icelandic olivine. The symbols are the same as in Figure 4.1 and error bars are defined the same as for Figure 4.2.*

Kinetic fractionation (diffusion-induced modifications)

High-forsterite Icelandic olivine is generally carried within more differentiated melts that are relatively rich in Fe (e.g., Thomson & Maclennan, 2013). With time, this compositional difference between cargo and carrier melt can cause diffusive exchange of Mg and Fe between the two, which in olivine has shown to result in coupled increase in $\delta^{26}Mg_{ol}$ and lowering of $\delta^{56}Fe_{ol}$ (e.g., Teng *et al.*, 2011; Dauphas *et al.*, 2010). As the rate of diffusion is controlled in part by the compositional difference, olivines with higher forsterite contents are more likely to be affected than those with Mg and Fe contents closer to the carrier melt composition. This effect is well displayed by measurements of three "HAMRA" populations with varying Fo contents, where the HAMRA-population with Fo_{85} display both higher $\delta^{26}Mg$ (-0.1‰) and lower $\delta^{56}Fe_{ol}$ values (~-0.1 ‰) relative to the two populations with Fo_{80} and Fo_{78} that display predicted MORB-like $\delta^{26}Mg_{ol}$ (-0.2‰) and $\delta^{56}Fe_{ol}$ values (+0.1 ‰, Figure 4.3).

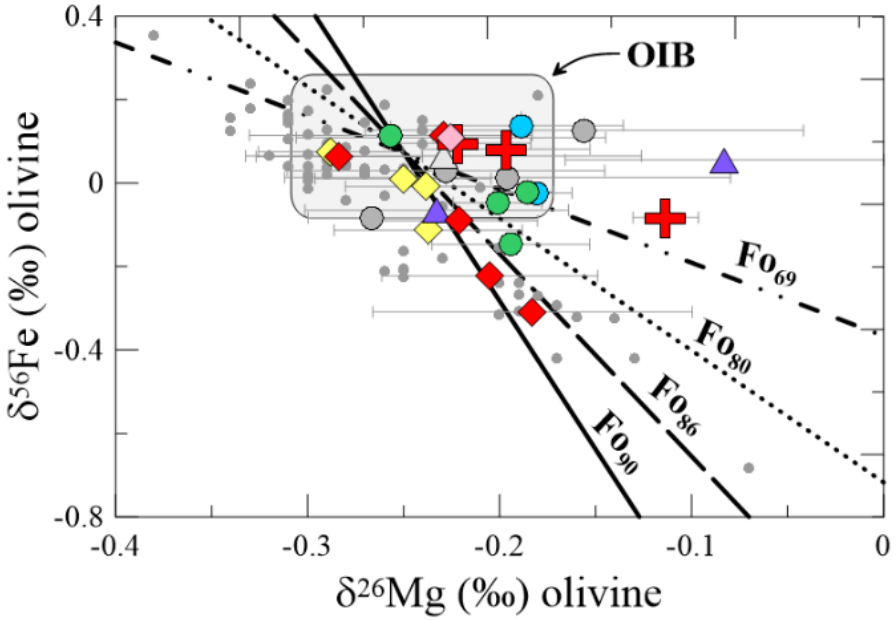

Figure 4.6 $\delta^{26}Mg_{ol}$-$\delta^{56}Fe_{ol}$ plot showing the effect of diffusion on the coupled $\delta^{56}Fe_{ol}$ and $\delta^{26}Mg_{ol}$ values. Coupled diffusion of Mg and Fe is expected to result in a linear relationship as shown above by olivine from Kilauea, Hawaii (Teng et al., 2011, marked by grey dots) and described by diffusion models for olivine with specific Fo contents (Dauphas et al., 2010). From this plot we find that olivine from SIVZ (Surtsey) clearly reflects $\delta^{26}Mg_{ol}$ and $\delta^{56}Fe_{ol}$ values consistent with binary diffusin of Mg and Fe diffusion in olivine with Fo_{86}. The high-forsterite HAMRA population (Fo_{85}) displays values consistent with binary diffusion of Mg and Fe olivine with Fo_{69}. This inconsistency might suggest that several processes are affecting these measured $\delta^{26}Mg_{ol}$ and $\delta^{56}Fe_{ol}$ values. However, the slope generated by the three HAMRA populations is in good agreement with the diffusion slope generated by olivine data with $Fo_{90\text{-}76}$ from Hawaii. The symbols are the same as in Figure 4.1 and error bars are defined the same as for Figure 4.2.

The effect of diffusion should thus generate a negative slope between the two isotopic ratios and the expected $\delta^{56}Fe_{ol}/\delta^{26}Mg_{ol}$ can be calculated for any given forsterite content (Dauphas

et al., 2010). As the absolute Fe/Mg content in high-forsterite olivines is low, the effect of diffusion is more prominent in δ^{56}Fe- than δ^{26}Mg space (e.g., Dauphas *et al.*, 2010; Oeser *et al.*, 2015). Indeed, this mass-dependent effect involving binary diffusion of Mg and Fe isotopes is reflected in an increasing expected $\delta^{56}Fe_{ol}/\delta^{26}Mg_{ol}$ ratio for increasing Fo contents (Figure 4.6).

Binary diffusion models, reflecting expected diffusion trends of Mg and Fe isotopes, can be generated at various Fo contents when the β value for Mg and Fe is known (Dauphas *et al.*, 2010). The β variable reflects the mass-dependent magnitude of fractionation of two isotopes of an element in a specific medium (Sio *et al.*, 2018; Richter *et al.*, 2009) and the definition for β varies according to the fractionation law describing equilibrium and kinetic fractionation. The change in β value thus controls the different slopes reflecting the expected results of equilibrium and kinetic fractions (see for example McCoy-West *et al.*, 2018; Young *et al.*, 2002). Here, we used $\beta_{Mg} = 0.09$ and $\beta_{Fe} = 0.16$, (Sio *et al.*, 2018) to calculate the expected slopes for diffusion associated with olivine with Fo_{69}, Fo_{80}, Fo_{86} and Fo_{90} as presented in Figure 4.6. Moreover, we added a field representing the range measured in oceanic basalts (represented by Hawaii whole rock data; Teng *et al.*, 2013; Teng *et al.*, 2010) along with Hawaiian olivine previously shown to be affected by diffusion of Mg and Fe (Teng *et al.*, 2011). The diffusion models show how the very low $\delta^{56}Fe_{ol}$ values found in SIVZ (down to -0.31 ‰) can indeed be explained by binary diffusion of Mg and Fe isotopes in olivine (Figure 4.6). Moreover, the slope, or $\delta^{56}Fe_{ol}/\delta^{26}Mg_{ol}$ generated by the HAMRA population is around -1.7 which is equal to the ratio expected for diffusion in an olivine with Fo_{69}, suggesting that diffusion has acted to lower initial $\delta^{56}Fe_{ol}$ but increase $\delta^{26}Mg_{ol}$ values of this olivine population (Dauphas *et al.*, 2010). The discrepancy in Fo contents (the high-forsterite HAMRA population is characterised by Fo_{85}) might be caused by simplified model assumptions or concurrent growth and diffusion processes. We note, however, that this slope is similar to the slope for diffusion controlled $\delta^{26}Mg_{ol}$ and $\delta^{56}Fe_{ol}$ values in olivine from Hawaii (displayed by grey dots in Figure 4.6; Teng *et al.*, 2011) supporting the expected dominant effect from coupled diffusion of Mg and Fe.

Based on these results, we cannot entirely rule out the presence of source-derived variability. Moreover, as these specific samples have previously been shown to preserve mantle-derived heterogeneity (e.g., Rasmussen *et al.*, 2020; Rasmussen *et al.*, *submitted*), this warrants a reflection on possible ways of distinguishing variations in δ^{56}Fe due to mantle heterogeneity.

4.5.2 Mantle-derived heterogeneity?

Previous work on the Icelandic sample set discussed in this study showed that olivine from especially SIVZ displayed signs of originating from pyroxenite-peridotite accumulated melts sourced from the underlying mantle plume (Rasmussen *et al.*, 2020). As the digested populations were chosen based on their major and minor elemental likeness to olivines studied in Rasmussen *et al.* (2020), this allows us to directly use the chemical fingerprints previously determined for each sample. The trace element dataset can aid in distinguishing enriched and depleted source components and evaluate how the minor and trace element fingerprints of pyroxenitic-derived melts is reflected in δ^{56}Fe in Icelandic olivine.

Olivine with low Mn/Fe (100Mn/Fe below ~1.5) was previously suggested to trace the contribution of pyroxenite-derived melts (e.g., Sobolev *et al.*, 2007) and combined with high Ga/Sc values was found to trace the presence of pyroxenitic components in the Icelandic

mantle (Rasmussen *et al.*, 2020). This negative relationship is also captured in the olivine populations analysed for this study, highlighting that the olivine populations targeted here reflect similar contributions of pyroxenite-derived melts as the olivines targeted previously (Figure 4.7a). Likewise, ratios of incompatible trace elements such as Ti_{ol} and Y_{ol} were previously shown to readily distinguish trace element enriched (high Ti/Y_{ol}) and depleted (low Ti/Y_{ol}) sources in olivine from WRZ (Neave *et al.*, 2018). We can evaluate the use of Ti/Y_{ol} as a tracer of enriched and depleted mantle components by the use of Pb isotopic data which is available for the majority of the locations studied here (Figure 4.7b; see references in figure caption). Indeed, we observe a positive correlation between Ti/Y_{ol} and Pb isotopes as would be expected if both tracers were controlled by mantle enrichment. Here we find that, as previously established (e.g., Kokfelt *et al.*, 2006), the off-rift zones of SNS and SIVZ are sourced by more enriched mantle components than what is dominant in the on-rift zones (ERZ, NRZ and WRZ) and ÖVZ. However, we see no traces of pyroxenite contributions in SNS, which supports previous findings, suggesting that the enriched component in SNS can be attributed to different enrichment processes than found in the SIVZ (Rasmussen *et al.*, 2020).

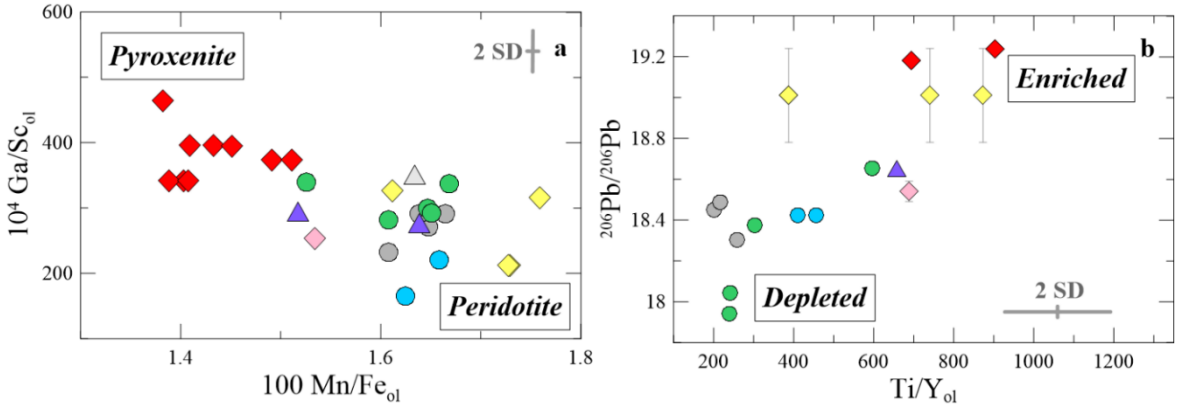

Figure 4.7 Trace elemental and Pb isotopic ratios tracing the presence of pyroxenitic and peridotitic mantle lithologies and radiogenic and trace element enriched (following referred to as simply enriched) and depleted mantle components. The olivine here does indeed sample both pyroxenitic and peridotitic lithologies which mostly corresponds to the sampling of enriched and depleted mantle components. An exemption to this, is the lack of pyroxenitic Mn/Fe and Ga/Sc compositions in olivine from SNS, supporting previous notions that the enrichment in SNS is decoupled to the presence of pyroxenite (Rasmussen et al., 2020). The symbols are the same as in Figure 4.1 and error bars are defined the same as for Figure 4.2. The trace elemental data is from Rasmussen et al. (2020) and the Pb isotopic data is compiled in data supplement for Chapter 4, T2 from the following literature: Hilton et al., (1999); Kokfelt et al. (2006); Manning and Thirlwall (2014); Halldórsson et al., (2018); Halldórsson et al., (2016); Peate et al., (2009); Peate et al., (2010); Thirlwall et al., (2004); Furman et al. (1991) and Jackson et al., (2020).

Several studies have recently shown that the mineral assembly of the mantle source can generate variations in the $\delta^{56}Fe$ values in the thereof derived basalts (e.g., Gleeson *et al.*, 2020, Konter *et al.*, 2016; Nebel *et al.*, 2019). As such, an accumulated pyroxenite-peridotite melt or the melting of a metasomatized lherzolite was proposed to be responsible for high $\delta^{56}Fe_{melt}$ values (up to 0.3 ‰, Konter *et al.*, 2016) observed in Samoan lavas, which is yet to

date the heaviest $\delta^{56}Fe_{melt}$ value measured in any OIB. A metasomatized source could not, however explain the high $\delta^{56}Fe_{melt}$ values displayed by basalts from plume-influenced segments of the Galapagos Spreading Centre and thus the presence of garnet-pyroxenite was proposed to control the high values measured here (up to 0.24 ‰, Gleeson *et al.*, 2020). Conversely, high-degree melts of depleted refractory (peridotitc-harzburgitic lithologies) components were proposed to be capable of producing melts with low $\delta^{56}Fe_{melt}$ values down to -0.1 ‰ ($\delta^{57}Fe_{melt}$ = -0.15 ‰; Williams & Bizimis, 2014). Recent evidence has suggested that mantle-core interaction through Soret diffusion of Fe can also result in the generation of high $\delta^{56}Fe$ domains entrained by deep-sourced mantle plumes (Lesher *et al.*, 2020), such as the Iceland plume. After having established the source-derived variabilities traced by minor and trace element ratios and Pb isotopes, we can use these to evaluate the prospect of a mantle-derived origin of the $\delta^{56}Fe_{ol}$ variation observed in Icelandic olivine.

If indeed the variations we observe in $\delta^{56}Fe$ from the Iceland plume are an effect of the preservation of pyroxenite-derived melts, we would expect to see a positive correlation between Ga/Sc_{ol} and $\delta^{56}Fe_{ol}$ values, excluding the very low $\delta^{56}Fe$ values displayed by olivine from HAMRA and Surtsey (Figure 4.6). This is not, however, the case, implying that the presence of pyroxenite is decoupled from the $\delta^{56}Fe$ variations displayed by Iceland olivine (Figure 4.8a). Similarly, $\delta^{56}Fe_{ol}$ values appear decoupled from Ti/Y_{ol} suggesting, that the variation we observe in $\delta^{56}Fe_{ol}$ is also decoupled to the entrainment of enriched or depleted mantle components (Figure 4.8b). Thus, based on trace element systematics in olivine we can deduce, that the $\delta^{56}Fe$ variation observed in Icelandic olivine is decoupled from mantle lithological variability and mantle-source enrichment.

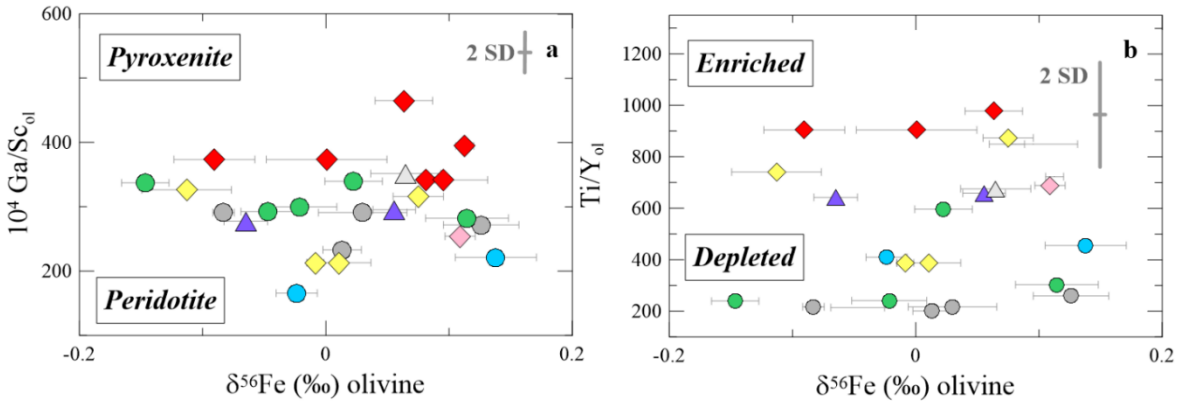

Figure 4.8 Evaluating the signature of $\delta^{56}Fe_{ol}$ variations using trace element ratios indicative of pyroxenite and/or enriched mantle components. Following the discussion in section 4.5.1, we have excluded three low $\delta^{56}Fe_{ol}$ values that reflect diffusion-controlled processes. As presented in Figure 4.7, the trace element ratios trace mantle-derived variability controlled by variations in mantle lithology and radiogenic and trace element enrichment. The lack of a relationship between these tracers and $\delta^{56}Fe_{ol}$ suggests, that the variation we observe in $\delta^{56}Fe_{ol}$ is decoupled from processes causing mantle enrichment. This decoupling implies that the variation we observe in $\delta^{56}Fe_{ol}$ is controlled by secondary processes occurring in the lithosphere and crust. The symbols are the same as in Figure 4.1 and error bars are defined the same as for Figure 4.2.

As recent evidence has suggested that diffusion across the mantle-core boundary can affect the $\delta^{56}Fe$ value of the lower mantle reservoir feeding deeply sourced plumes, we consider this process as a possible control on the $\delta^{56}Fe_{ol}$ values presented here, by evaluating the $^{3}He/^{4}He_{ol}$ values measured for the same samples (Harðardóttir *et al.*, 2018). Any effect of core contribution or core-mantle interaction would be expected to be preserved in olivine displaying the highest $^{3}He/^{4}He_{ol}$ values as these would represent the purest contribution from a lower mantle sourced plume. However, we see no evidence of systematic variations in $\delta^{56}Fe$ and $^{3}He/^{4}He_{ol}$ as would be expected if core-mantle interaction was controlling the $\delta^{56}Fe_{ol}$ values of Icelandic olivine.

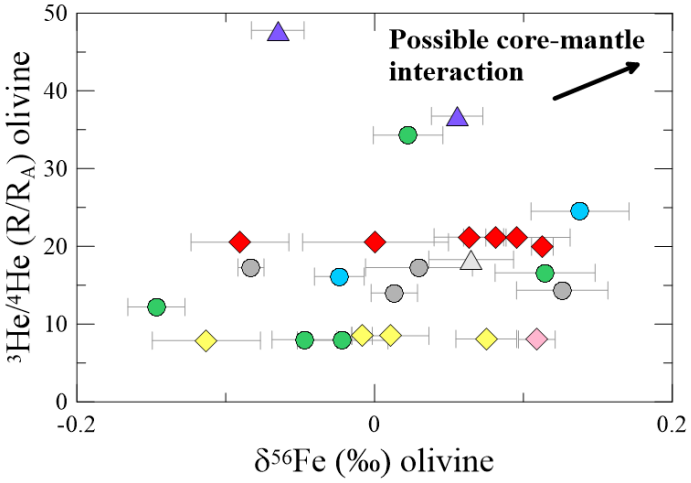

Figure 4.9 He isotope systematics and $\delta^{56}Fe_{ol}$ from the same olivine separates. High $^{3}He/^{4}He_{ol}$ reflects contribution of material from the lower mantle. If the variation observed in $\delta^{56}Fe_{ol}$ would reflect core-mantle interactions, we would expect the fingerprint of this interaction to be preserved in olivine with the highest $^{3}He/^{4}He_{ol}$ values. However, we observe no correlations, and we can thus exclude any effect that possible core-mantle processes would have on the $\delta^{56}Fe_{ol}$ measured here. The symbols are the same as in Figure 4.1 and error bars are defined the same as for Figure 4.2.

The lack of correlation between $\delta^{56}Fe_{ol}$ and several source-derived parameters suggests that the variations we observe in $\delta^{56}Fe_{ol}$ are dominantly controlled by magmatic processes such as diffusion which warrants a discussion on the implications that the preservation of diffusion patterns have for the magma transport timescales of olivine in the Icelandic crust.

4.5.3 Implications for timescales of magma transport

Diffusion is a kinetic process that occurs in magmatic crystals because of disequilibrium between the mineral and melt compositions and is thus a time-constrained process controlled by the diffusion rate of an element. Because of this, chemical zonation and inter-diffusion of Mg and Fe in olivine offers an exceptional tool for calculations of timescales for magma transport through the crust (e.g., Costa *et al.*, 2008). More reliable results have come from the combination of elemental Mg and Fe diffusion with diffusion patterns for $\delta^{26}Mg_{ol}$ and $\delta^{56}Fe_{ol}$ (Oeser *et al.*, 2015). However, these studies are usually carried out by *in-situ* isotopic measurements leading to spatial control on the diffusion patterns. As the analyses here were

done on a single crystal basis, or by combining up to 5 crystals, we do not have any spatial constraints. However, based on crystal sizes and degree of disequilibrium, represented by slightly high $\delta^{26}Mg_{ol}$ and notably low $\delta^{56}Fe_{ol}$, we can explore the relative importance of timescales for magma transport through the Icelandic crust of the various volcanic regions.

A relationship between crystal size and $\delta^{56}Fe_{ol}$ values was previously identified in olivine populations from Baffin Island. In this case, smaller crystals were shown to have re-equilibrated with their carrier melt before large crystals which resulted in a scenario where larger crystals were more likely to record diffusive patterns than smaller crystals (McCoy-West *et al.*, 2018). We measured the crystal diameters of the olivine digested for each sample and plotted the largest diameter measured for each sample along with the $\delta^{56}Fe_{ol}$ measured for the sample (Figure 4.10) and olivine from Baffin Island. We observe no negative correlation between crystal size and $\delta^{56}Fe_{ol}$ values and we also observe that Icelandic olivine display a much smaller range of $\delta^{56}Fe_{ol}$ values than what was observed in olivine from Baffin Island, despite digesting similar grain size olivines. Thus, the degree of diffusion appears to be controlled by varying residence time within the disequilibrium setting between the different volcanic systems rather than solely on the crystal size of the digested grains. To constrain the residence time likely to cause diffusion pattern as observed in Icelandic olivine, we recommend further work on modelling possible diffusion profiles for crystals of various sizes entrained in magmas at varying degrees of disequilibrium and temperatures and compare the modelled final olivine $\delta^{26}Mg$ and $\delta^{56}Fe$ values with the results we have presented in this study.

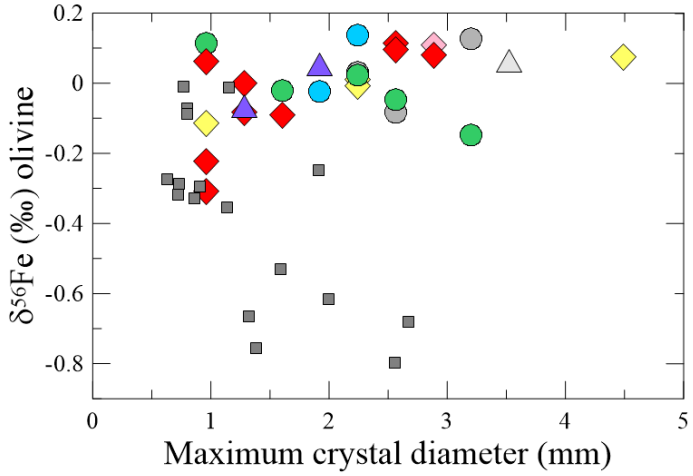

Figure 4.10 Figure displaying the maximum diameter or crystal size digested for each sample analysed for $\delta^{56}Fe_{ol}$. Based on olivine analyses from Baffin Island (McCoy-West et al., 2018), larger crystals are more likely to preserve disequilibrium patterns or signs of diffusion (low $\delta^{56}Fe_{ol}$) whereas smaller crystals are expected to re-equilibrate more rapidly with the carrier-melt and thus should be closer to the equilibrium melt value. This generates a negative correlation between maximum crystal diameter and $\delta^{56}Fe_{ol}$ which is clearly visible in olivine from Baffin Island (grey squares) However, we observe no such correlation suggesting that the timescales for magma transport, and thus the residence time for an olivine out of equilibrium with its carrier melt, is the main control on the degree of diffusion rather than crystal size of the digested crystals. The symbols are the same as in Figure 4.1 and error bars are defined the same as for Figure 4.2.

4.6 Conclusion

We studied the $\delta^{26}Mg$ and $\delta^{56}Fe$ systematics of previously well-characterised high-forsterite olivine from active rift and flank volcanic zones in Iceland and older Quaternary and Tertiary units. We observe measured $\delta^{26}Mg_{ol}$ values that mostly overlapped with a field defined by expected MORB $\delta^{26}Mg$ values whereas we observe a large spread in $\delta^{56}Fe_{ol}$ from -0.31 to 0.14 ‰ at $>Fo_{86}$. Part of the variation in $\delta^{56}Fe_{ol}$ space can be explained by equilibrium fractional crystallisation between MORB-like melts and olivine, however we show, that the majority of the variation in $\delta^{56}Fe_{ol}$ values are a result of coupled diffusive exchange of Fe and Mg between carrier melt and olivine. To constrain the resulting implications for magma transport in the Icelandic crust, future diffusion modelling must be performed for various crystal sizes, storage temperature and forsterite contents.

4.7 Acknowledgement

This work was funded by the Nordic Volcanological Center and the Icelandic Research Fund (Grant #196084-051). SAH further acknowledges support from the Icelandic Research Fund (Grant #196139-051). The authors would like to thank Tonny Thomsen, Mojagan Alaei and Thomas Kokfelt from the Geological Survey of Denmark and Greenland for assistance in preparing the samples for analysis. Thanks to Guðmundur Guðfinnsson for assistance with running the microprobe. Guðrun Sverrisdóttir is thanked for contributing and sharing her private FIM-GSV sample collection. Moreover, we thank Simon Matthews, Oliver Shorttle, Sally Gibson, Guðmundur Guðfinnsson, Edward Marshall and Eemu Ranta for fruitful discussions and suggestions and the entire lab at the Department of Earth Sciences, University of Cambridge for distillation of a record amount of concentrated acids.

4.8 References

Batanova, V. G., Sobolev, A. V., & Kuzmin, D. V. (2015). Trace element analysis of olivine: High precision analytical method for JEOL JXA-8230 electron probe microanalyser. *Chemical Geology, 419*, 149-157.

Bilenker, L. D., Weis, D., Scoates, J. S., & Perry, E. (2018). The application of stable Fe isotopes to magma sulfide systems: constraints on the Fe isotope composition of magmatic pyrrhotite. *Economic Geology, 113*(5), 1181-1192.

Bindeman, I., Gurenko, A., Carley, T., Miller, C., Martin, E., & Sigmarsson, O. (2012). Silicic magma petrogenesis in Iceland by remelting of hydrothermally altered crust based on oxygen isotope diversity and disequilibria between zircon and magma with implications for MORB. *Terra Nova, 24*(3), 227-232.

Bindeman, I., Gurenko, A., Sigmarsson, O., & Chaussidon, M. (2008). Oxygen isotope heterogeneity and disequilibria of olivine crystals in large volume Holocene basalts from Iceland: Evidence for magmatic digestion and erosion of Pleistocene hyaloclastites. *Geochimica et Cosmochimica Acta, 72*(17), 4397-4420.

Bjarnason, I. T., & Schmeling, H. (2009). The lithosphere and asthenosphere of the Iceland hotspot from surface waves. *Geophysical Journal International, 178*(1), 394-418.

Bourdon, B., Tipper, E. T., Fitoussi, C., & Stracke, A. (2010). Chondritic Mg isotope composition of the Earth. *Geochimica et Cosmochimica Acta, 74*(17), 5069-5083.

Breddam, K. (2002). Kistufell: primitive melt from the Iceland mantle plume. *Journal of Petrology, 43*(2), 345-373.

Caracciolo, A., Bali, E., Guðfinnsson, G. H., Kahl, M., Halldórsson, S. A., Hartley, M. E., & Gunnarsson, H. (2020). Temporal evolution of magma and crystal mush storage conditions in the Bárðarbunga-Veiðivötn volcanic system, Iceland. *Lithos, 352-353*, 105234.

Chacko, T., Cole, D. R., & Horita, J. (2001). Equilibrium oxygen, hydrogen and carbon isotope fractionation factors applicable to geologic systems. *Reviews in Mineralogy and Geochemistry, 43*(1), 1-81.

Chen, S., Niu, Y., Guo, P., Gong, H., Sun, P., Xue, Q., Duan, M., & Wang, X. (2019). Iron isotope fractionation during mid-ocean ridge basalt (MORB) evolution: Evidence from lavas on the East Pacific Rise at 10° 30′ N and its implications. *Geochimica et Cosmochimica Acta, 267*, 227-239.

Costa, F., Dohmen, R., & Chakraborty, S. (2008). Time scales of magmatic processes from modeling the zoning patterns of crystals. *Reviews in Mineralogy and Geochemistry, 69*(1), 545-594.

Dauphas, N., Craddock, P. R., Asimow, P. D., Bennett, V. C., Nutman, A. P., & Ohnenstetter, D. (2009). Iron isotopes may reveal the redox conditions of mantle melting from Archean to Present. *Earth and Planetary Science Letters, 288*(1-2), 255-267.

Dauphas, N., Roskosz, M., Alp, E., Neuville, D., Hu, M., Sio, C., Tissot, F., Zhao, J., Tissandier, L., & Médard, E. (2014). Magma redox and structural controls on iron isotope variations in Earth's mantle and crust. *Earth and Planetary Science Letters, 398*, 127-140.

Dauphas, N., Teng, F.-Z., & Arndt, N. T. (2010). Magnesium and iron isotopes in 2.7 Ga Alexo komatiites: Mantle signatures, no evidence for Soret diffusion, and identification of diffusive transport in zoned olivine. *Geochimica et Cosmochimica Acta, 74*(11), 3274-3291.

Furman, T., Frey, F. A., & Park, K.-H. (1991). Chemical constraints on the petrogenesis of mildly alkaline lavas from Vestmannaeyjar, Iceland: the Eldfell (1973) and Surtsey (1963–1967) eruptions. *Contributions to Mineralogy and Petrology, 109*(1), 19-37.

Gleeson, M. L. M., Gibson, S. A., & Williams, H. M. (2020). Novel insights from Fe-isotopes into the lithological heterogeneity of Ocean Island Basalts and plume-influenced MORBs. *Earth and Planetary Science Letters, 535*, 116114.

Halldórsson, S. A., Bali, E., Hartley, M. E., Neave, D. A., Peate, D. W., Guðfinnsson, G. H., Bindeman, I., Whitehouse, M. J., Riishuus, M. S., Pedersen, G. B. M., Jakobsson, S., Askew, R., Gallagher, C. R., Guðmundsdóttir, E. R., Gudnason, J., Moreland, W. M., Óskarsson, B. V., Nikkola, P., Reynolds, H. I., Schmith, J., & Thordarson, T. (2018). Petrology and geochemistry of the 2014–2015 Holuhraun eruption, central Iceland: compositional and mineralogical characteristics, temporal variability and magma storage. *Contributions to Mineralogy and Petrology, 173*(8), 64.

Halldórsson, S. A., Barnes, J. D., Stefánsson, A., Hilton, D. R., Hauri, E. H., & Marshall, E. W. (2016). Subducted lithosphere controls halogen enrichments in the Iceland mantle plume source. *Geology, 44*(8), 679-682.

Handler, M. R., Baker, J. A., Schiller, M., Bennett, V. C., & Yaxley, G. M. (2009). Magnesium stable isotope composition of Earth's upper mantle. *Earth and Planetary Science Letters, 282*(1-4), 306-313.

Harðardóttir, S., Halldórsson, S. A., & Hilton, D. R. (2018). Spatial distribution of helium isotopes in Icelandic geothermal fluids and volcanic materials with implications for location, upwelling and evolution of the Icelandic mantle plume. *Chemical Geology*.

Hermes, O. D., & Schilling, J.-G. (1976). Olivine from Reykjanes Ridge and Iceland tholeiites, and its significance to the two-mantle source model. *Earth and Planetary Science Letters, 28*(3), 345-355.

Hilton, D. R., Grönvold, K., Macpherson, C. G., & Castillo, P. R. (1999). Extreme $^{3}He/^{4}He$ ratios in northwest Iceland: constraining the common component in mantle plumes. *Earth and Planetary Science Letters, 173*(1-2), 53-60.

Hofmann, A. W. (1997). Mantle geochemistry: the message from oceanic volcanism. *Nature, 385*(6613), 219-229.

Hofmann, A. W., & White, W. M. (1982). Mantle plumes from ancient oceanic crust. *Earth and Planetary Science Letters, 57*(2), 421-436.

Jackson, M. G., Blichert-Toft, J., Halldórsson, S. A., Mundl-Petermeier, A., Bizimis, M., Kurz, M. D., Price, A. A., Harðardóttir, S., Willhite, L. N., Breddam, K., Becker, T. W., & Fischer, R. A. (2020). Ancient helium and tungsten isotopic signatures preserved in mantle domains least modified by crustal recycling. *Proceedings of the National Academy of Sciences*, 202009663. doi:10.1073/pnas.2009663117

Johnson, C. M., Beard, B. L., & Albarède, F. (2004). *Geochemistry of non-traditional stable isotopes* (Vol. 55): Walter de Gruyter GmbH & Co KG.

Kokfelt, T. F., Hoernle, K., Hauff, F., & Fiebig, J. (2006). Combined Trace Element and Pb-Nd-Sr-O Isotope Evidence for Recycled Oceanic Crust (Upper and Lower) in the Iceland Mantle Plume. *Journal of Petrology, 47*(9), 1705-1749.

Konter, J. G., Pietruszka, A. J., Hanan, B. B., Finlayson, V. A., Craddock, P. R., Jackson, M. G., & Dauphas, N. (2016). Unusual $\delta^{56}Fe$ values in Samoan rejuvenated lavas generated in the mantle. *Earth and Planetary Science Letters, 450*, 221-232.

Lesher, C. E., Dannberg, J., Barfod, G. H., Bennett, N. R., Glessner, J. J., Lacks, D. J., & Brenan, J. M. (2020). Iron isotope fractionation at the core–mantle boundary by thermodiffusion. *Nature Geoscience, 13*(5), 382-386.

Liu, F., Li, X., Wang, G., Liu, Y., Zhu, H., Kang, J., Huang, F., Sun, W., Xia, X., & Zhang, Z. (2017). Marine Carbonate Component in the Mantle Beneath the Southeastern Tibetan Plateau: Evidence From Magnesium and Calcium Isotopes. *Journal of Geophysical Research: Solid Earth, 122*(12), 9729-9744.

Maclennan, J. (2008). Concurrent mixing and cooling of melts under Iceland. *Journal of Petrology, 49*(11), 1931-1953.

Macris, C. A., Manning, C. E., & Young, E. D. (2015). Crystal chemical constraints on inter-mineral Fe isotope fractionation and implications for Fe isotope disequilibrium in San Carlos mantle xenoliths. *Geochimica et Cosmochimica Acta, 154*, 168-185.

Mallik, A., & Dasgupta, R. (2012). Reaction between MORB-eclogite derived melts and fertile peridotite and generation of ocean island basalts. *Earth and Planetary Science Letters, 329*, 97-108.

Manning, C. J., & Thirlwall, M. F. (2014). Isotopic evidence for interaction between Öræfajökull mantle and the Eastern Rift Zone, Iceland. *Contributions to Mineralogy and Petrology, 167*(1), 959.

Matthews, S., Shorttle, O., & Maclennan, J. (2016). The temperature of the Icelandic mantle from olivine-spinel aluminum exchange thermometry. *Geochemistry, Geophysics, Geosystems, 17*(11), 4725-4752.

McCoy-West, A. J., Fitton, J. G., Pons, M.-L., Inglis, E. C., & Williams, H. M. (2018). The Fe and Zn isotope composition of deep mantle source regions: Insights from Baffin Island picrites. *Geochimica et Cosmochimica Acta, 238*, 542-562.

Neave, D. A., Shorttle, O., Oeser, M., Weyer, S., & Kobayashi, K. (2018). Mantle-derived trace element variability in olivines and their melt inclusions. *Earth and Planetary Science Letters, 483*, 90-104.

Nebel, O., Sossi, P. A., Bénard, A., Arculus, R. J., Yaxley, G. M., Woodhead, J. D., Rhodri Davies, D., & Ruttor, S. (2019). Reconciling petrological and isotopic mixing mechanisms in the Pitcairn mantle plume using stable Fe isotopes. *Earth and Planetary Science Letters, 521*, 60-67.

Novella, D., Maclennan, J., Shorttle, O., Prytulak, J., & Murton, B. J. (2020). A multi-proxy investigation of mantle oxygen fugacity along the Reykjanes Ridge. *Earth and Planetary Science Letters, 531*, 115973.

Oeser, M., Dohmen, R., Horn, I., Schuth, S., & Weyer, S. (2015). Processes and time scales of magmatic evolution as revealed by Fe–Mg chemical and isotopic zoning in natural olivines. *Geochimica et Cosmochimica Acta, 154*, 130-150.

Peate, D. W., Baker, J. A., Jakobsson, S. P., Waight, T. E., Kent, A. J. R., Grassineau, N. V., & Skovgaard, A. C. (2009). Historic magmatism on the Reykjanes Peninsula, Iceland: a snap-shot of melt generation at a ridge segment. *Contributions to Mineralogy and Petrology, 157*(3), 359.

Peate, D. W., Breddam, K., Baker, J. A., Kurz, M. D., Barker, A. K., Prestvik, T., Grassineau, N., & Skovgaard, A. C. (2010). Compositional Characteristics and Spatial Distribution of Enriched Icelandic Mantle Components. *Journal of Petrology, 51*(7), 1447-1475.

Peters, B. J., Shahar, A., Carlson, R. W., Day, J. M., & Mock, T. D. (2019). A sulfide perspective on iron isotope fractionation during ocean island basalt petrogenesis. *Geochimica et Cosmochimica Acta, 245*, 59-78.

Pogge von Strandmann, P. A. E., Burton, K. W., James, R. H., van Calsteren, P., Gislason, S. R., & Sigfússon, B. (2008). The influence of weathering processes on riverine magnesium isotopes in a basaltic terrain. *Earth and Planetary Science Letters, 276*(1), 187-197.

Polyakov, V. B., & Mineev, S. D. (2000). The use of Mössbauer spectroscopy in stable isotope geochemistry. *Geochimica et Cosmochimica Acta, 64*(5), 849-865.

Rasmussen, M. B., Halldórsson, S. A., Gibson, S. A., & Guðfinnsson, G. H. (2020). Olivine chemistry reveals compositional source heterogeneities within a tilted mantle plume beneath Iceland. *Earth and Planetary Science Letters, 531*, 116008.

Rasmussen, M. B., Halldórsson, S. A., Jackson, M. G., Bindeman, I. N., & Whitehouse, M. J. (*submitted).* Formation of the Iceland Plateau by enhanced plume flux and entrainment of deeply-stored domains.

Richter, F. M., Watson, E. B., Mendybaev, R., Dauphas, N., Georg, B., Watkins, J., & Valley, J. (2009). Isotopic fractionation of the major elements of molten basalt by chemical and thermal diffusion. *Geochimica et Cosmochimica Acta, 73*(14), 4250-4263.

Roskosz, M., Sio, C. K. I., Dauphas, N., Bi, W., Tissot, F. L. H., Hu, M. Y., Zhao, J., & Alp, E. E. (2015). Spinel–olivine–pyroxene equilibrium iron isotopic fractionation and applications to natural peridotites. *Geochimica et Cosmochimica Acta, 169*, 184-199.

Rouxel, O., Dobbek, N., Ludden, J., & Fouquet, Y. (2003). Iron isotope fractionation during oceanic crust alteration. *Chemical Geology, 202*(1), 155-182.

Rudge, J. F., Maclennan, J., & Stracke, A. (2013). The geochemical consequences of mixing melts from a heterogeneous mantle. *Geochimica et Cosmochimica Acta, 114*, 112-143.

Schipper, C. I., & Moussallam, Y. (2017). Temporal redox variation in basaltic tephra from Surtsey volcano (Iceland). *Bulletin of Volcanology, 79*(10), 71. doi:10.1007/s00445-017-1156-2

Schuessler, J. A., Schoenberg, R., & Sigmarsson, O. (2009). Iron and lithium isotope systematics of the Hekla volcano, Iceland — Evidence for Fe isotope fractionation during magma differentiation. *Chemical Geology, 258*(1-2), 78-91.

Shahar, A., Young, E. D., & Manning, C. E. (2008). Equilibrium high-temperature Fe isotope fractionation between fayalite and magnetite: An experimental calibration. *Earth and Planetary Science Letters, 268*(3), 330-338.

Sio, C. K., Roskosz, M., Dauphas, N., Bennett, N. R., Mock, T., & Shahar, A. (2018). The isotope effect for Mg-Fe interdiffusion in olivine and its dependence on crystal orientation, composition and temperature. *Geochimica et Cosmochimica Acta, 239*, 463-480.

Sio, C. K. I., Dauphas, N., Teng, F.-Z., Chaussidon, M., Helz, R. T., & Roskosz, M. (2013). Discerning crystal growth from diffusion profiles in zoned olivine by in situ Mg–Fe isotopic analyses. *Geochimica et Cosmochimica Acta, 123*, 302-321.

Sobolev, A. V., Hofmann, A. W., Kuzmin, D. V., Yaxley, G. M., Arndt, N. T., Chung, S. L., Danyushevsky, L. V., Elliott, T., Frey, F. A., Garcia, M. O., Gurenko, A. A., Kamenetsky, V. S., Kerr, A. C., Krivolutskaya, N. A., Matvienkov, V. V., Nikogosian, I. K., Rocholl, A., Sigurdsson, I. A., Sushchevskaya, N. M., & Teklay, M. (2007). The amount of recycled crust in sources of mantle-derived melts. *Science, 316*(5823), 412-417.

Sobolev, A. V., Hofmann, A. W., Sobolev, S. V., & Nikogosian, I. K. (2005). An olivine-free mantle source of Hawaiian shield basalts. *Nature, 434*(7033), 590-597.

Soderman, C. R., Matthews, S., Shorttle, O., Jackson, M. G., Ruttorc, S., Nebel, O., Turner, S., Beiere, C., Millet, M.-A., Widom, E., Humayun, M., & Williams, H. M. (2020). Heavy δ^{57}Fe in ocean island basalts: a non-unique signature of processes and source lithologies in the mantle. *Geochimica et Cosmochimica Acta*, *292*(1), 309-332.

Spice, H. E., Fitton, J. G., & Kirstein, L. A. (2016). Temperature fluctuation of the Iceland mantle plume through time. *Geochemistry, Geophysics, Geosystems, 17*(2), 243-254.
Stracke, A., Genske, F., Berndt, J., & Koornneef, J. M. (2019). Ubiquitous ultra-depleted domains in Earth's mantle. *Nature Geoscience, 12*(10), 851-855.
Teng, F.-Z., Dauphas, N., & Helz, R. T. (2008). Iron Isotope Fractionation During Magmatic Differentiation in Kilauea Iki Lava Lake. *Science, 320*(5883), 1620-1622.
Teng, F.-Z., Dauphas, N., Helz, R. T., Gao, S., & Huang, S. (2011). Diffusion-driven magnesium and iron isotope fractionation in Hawaiian olivine. *Earth and Planetary Science Letters, 308*(3-4), 317-324.
Teng, F.-Z., Dauphas, N., Huang, S., & Marty, B. (2013). Iron isotopic systematics of oceanic basalts. *Geochimica et Cosmochimica Acta, 107*, 12-26.
Teng, F.-Z., Hu, Y., & Chauvel, C. (2016). Magnesium isotope geochemistry in arc volcanism. *Proceedings of the National Academy of Sciences, 113*(26), 7082-7087.
Teng, F.-Z., Li, W.-Y., Ke, S., Marty, B., Dauphas, N., Huang, S., Wu, F.-Y., & Pourmand, A. (2010). Magnesium isotopic composition of the Earth and chondrites. *Geochimica et Cosmochimica Acta, 74*(14), 4150-4166.
Teng, F.-Z., Wadhwa, M., & Helz, R. T. (2007). Investigation of magnesium isotope fractionation during basalt differentiation: Implications for a chondritic composition of the terrestrial mantle. *Earth and Planetary Science Letters, 261*(1–2), 84-92.
Thirlwall, M. F., Gee, M. A. M., Taylor, R. N., & Murton, B. J. (2004). Mantle components in Iceland and adjacent ridges investigated using double-spike Pb isotope ratios. *Geochimica et Cosmochimica Acta, 68*(2), 361-386.
Thomson, A., & Maclennan, J. (2013). The distribution of olivine compositions in Icelandic basalts and picrites. *Journal of Petrology, 54*(4), 745-768.
Tipper, E. T., Louvat, P., Capmas, F., Galy, A., & Gaillardet, J. (2008). Accuracy of stable Mg and Ca isotope data obtained by MC-ICP-MS using the standard addition method. *Chemical Geology, 257*(1), 65-75.
Urey, H. C. (1947). The thermodynamic properties of isotopic substances. *Journal of the Chemical Society (Resumed)*(0), 562-581.
Wang, X.-J., Chen, L.-H., Hofmann, A. W., Hanyu, T., Kawabata, H., Zhong, Y., Xie, L.-W., Shi, J.-H., Miyazaki, T., Hirahara, Y., Takahashi, T., Senda, R., Chang, Q., Vaglarov, B. S., & Kimura, J.-I. (2018). Recycled ancient ghost carbonate in the Pitcairn mantle plume. *Proceedings of the National Academy of Sciences of the United States of America, 115*(35), 8682-8687.
Weyer, S., & Ionov, D. A. (2007). Partial melting and melt percolation in the mantle: The message from Fe isotopes. *Earth and Planetary Science Letters, 259*(1-2), 119-133.
Wieser, P. E., Edmonds, M., Maclennan, J., Jenner, F. E., & Kunz, B. E. (2019). Crystal scavenging from mush piles recorded by melt inclusions. *Nature Communications, 10*(1), 5797.
Williams, H., Peslier, A., McCammon, C., Halliday, A., Levasseur, S., Teutsch, N., & Burg, J. (2005). Systematic iron isotope variations in mantle rocks and minerals: The effects of partial melting and oxygen fugacity. *Earth and Planetary Science Letters, 235*(1-2), 435-452.
Williams, H. M., & Bizimis, M. (2014). Iron isotope tracing of mantle heterogeneity within the source regions of oceanic basalts. *Earth and Planetary Science Letters, 404*, 396-407.
Williams, H. M., McCammon, C. A., Peslier, A. H., Halliday, A. N., Teutsch, N., Levasseur, S., & Burg, J.-P. (2004). Iron isotope fractionation and the oxygen fugacity of the mantle. *Science, 304*(5677), 1656-1659.

Yang, W., Teng, F.-Z., & Zhang, H.-F. (2009). Chondritic magnesium isotopic composition of the terrestrial mantle: a case study of peridotite xenoliths from the North China craton. *Earth and Planetary Science Letters, 288*(3-4), 475-482.

Young, E. D., Galy, A., & Nagahara, H. (2002). Kinetic and equilibrium mass-dependent isotope fractionation laws in nature and their geochemical and cosmochemical significance. *Geochimica et Cosmochimica Acta, 66*(6), 1095-1104.

Young, E. D., Manning, C. E., Schauble, E. A., Shahar, A., Macris, C. A., Lazar, C., & Jordan, M. (2015). High-temperature equilibrium isotope fractionation of non-traditional stable isotopes: Experiments, theory, and applications. *Chemical Geology, 395*, 176-195.

Zakharov, D. O., Bindeman, I. N., Tanaka, R., Friðleifsson, G. Ó., Reed, M. H., & Hampton, R. L. (2019). Triple oxygen isotope systematics as a tracer of fluids in the crust: A study from modern geothermal systems of Iceland. *Chemical Geology, 530*, 119312.

Zindler, A., & Hart, S. (1986). Chemical geodynamics. *Annual review of earth and planetary sciences, 14*, 493-571.

Zindler, A., Jagoutz, E., & Goldstein, S. (1982). Nd, Sr and Pb isotopic systematics in a three-component mantle: a new perspective. *Nature, 298*(5874), 519-523.

5 Supplementary material for Chapter 2

5.1 Analytical Techniques

5.1.1 Electron Microprobe Analyser (EMPA) – external standard reproducibility

The San Carlos olivine standard (NMNH 111312-44) supplied by the Smithsonian Institute, Washington DC to the University of Iceland acted as internal and external reference standard. To ensure stability, San Carlos olivine was analysed as an external standard regularly throughout each of five analytical sessions between real unknowns. The mean and repeatability or relative standard deviation (RSD) is based on the total analysis performed over these sessions and is presented in Table 5.1. The accuracy is based on the values presented in Batanova *et al*. (2015). The oxides marked by a star have fewer analysis included for evaluation of instrumental effects due to a software glitch.

Table 5.1 EMPA results for San Carlos olivine (NMNH-111312-44)

Oxide	Mean	*n*	RSD%	Accuracy %
SiO_2	41	*48*	0.46	99
TiO_2	0.010	*48*	4.9	244
Al_2O_3	0.037	*46*	2.6	112
FeO	9.8	*48*	0.25	103
MnO	0.14	*48*	0.81	101
MgO	49	*48*	0.50	99
CaO	0.093	*48*	1.0	100
Na_2O	0.009	*48*	8.7	101
P_2O_5*	0.005	*41*	20	107
Cr_2O_3*	0.017	*35*	14	113
CoO*	0.018	*38*	3.2	97
NiO	0.37	*47*	0.72	99
ZnO*	0.0076	*39*	12	108

5.1.2 Laser Ablation Inductively Coupled Plasma Mass Spectrometry (LA ICP-MS)

The olivine trace element data was retrieved through LA-ICP-MS as described in section 3.2. We used four international standards as unknowns: NIST 612, NIST 614, BIR-1G and a University of Cambridge in-house San Carlos olivine standard (BD4074OL) which has been well-characterised in previous work by Jackson & Gibson (2018). The exact composition of BD4074OL has been determined using EMPA and solution mode analysis and further analysed by *in-situ* methods to check for heterogeneity and was found to be slightly different from the Smithsonian standard. The accuracy of each element for each of the standards is presented in *Table 5.2-5.4*. The SiO_2 content measured by EMPA was used to calibrate the LA ICP-MS results and any drift was corrected using the *GLITTER* software.

Table 5.2 LA-ICP-MS results for in-house San Carlos olivine BD4074OL

Element	Mean	*n*	SD	RSD%	Reference values	Accuracy %
Li7	1.4	*38*	0.2	16	1.53	90
B11	15	*39*	6.2	42	0.41	3595
Na23	39	*38*	2.6	6.67	127	31
Mg25	-	-	-	-	-	-
Al27	70	*31*	3.4	4.87	78	89
Si29	-	-	-	-	-	-
P31	19	*29*	4.2	22	22	90
Ca43	386	*34*	105	27	447	86
Sc45	3.1	*37*	0.15	4.9	3.6	88
Ti47	14	*36*	1.1	8.1	17	83
V51	3.2	*36*	0.10	3.0	3.2	99
Cr53	122	*34*	2.3	1.9	131	93
Mn55	1013	*39*	16	1.5	1025	99
Fe57	71346	*39*	2166	3.0	75865	94
Co59	146	*37*	3.6	2.5	148	98
Ni60	2816	*39*	75	2.6	2909	97
Cu65	2.7	*38*	0.24	9.0	2.7	101
Zn66	71	*39*	3.5	5.0	72	99
Ga69	0.05	*33*	0.01	22	0.05	103
Ge72	0.7	*30*	0.09	14	0.87	77
Y89	0.02	*37*	0.004	24	0.02	111
Zr90	0.01	*27*	0.004	31	0.01	91
Nb93	0.05	*7*	0.09	190	0.02	296
Sn120	0.90	*39*	0.10	11	1.1	79
Pb208	0.05	*25*				

Table 5.3 LA-ICP-MS results for NIST 614

Element	Mean	*n*	SD	RSD%	Reference values	Accuracy %
Li7	1.61	*12*	0.27	17	1.7	95
B11	18.06	*13*	11	59	1.5	-
Na23	102029	*13*	4610	5	101634	100
Mg25	-	-	-	-	-	-
Al27	10895	*13*	358	3.3	1080	1009
Si29	-	-	-	-	-	-
P31	21	*11*	6	27	11	187
Ca43	85613	*13*	3904	4.6	8505	1007
Sc45	1.7	*13*	0.35	21	0.74	232
Ti47	3.8	*13*	0.69	19	3.6	104
V51	1.0	*13*	0.05	4.9	1.0	99
Cr53	1.0	*12*	0.24	23	1.2	88
Mn55	1.4	*13*	0.04	3.2	1.4	99
Fe57	16	*13*	2.48	15	19	86
Co59	0.72	*13*	0.04	5.5	0.79	91
Ni60	0.94	*13*	0.11	12	1.1	85
Cu65	1.3	*12*	0.14	11	1.4	92
Zn66	2.3	*13*	0.19	8.1	2.8	84
Ga69	1.2	*13*	0.05	4.1	1.3	93
Ge72	0.84	*13*	0.15	18	0.9	89
Y89	0.78	*13*	0.05	6.2	0.8	99
Zr90	0.86	*13*	0.05	5.5	0.8	101
Nb93	0.82	*13*	0.03	3.5	0.8	99
Sn120	2.3	*13*	0.17	7.6	1.7	136
Pb208	2.3	*13*	0.11	4.7	2.3	100

Table 5.4 LA-ICP-MS results for BIR-1G

Element	Mean	*n*	SD	RSD%	Reference values	Accuracy %
Li7	2.8	*12*	0.14	5.1	3.0	94
B11	17	*12*	11	61	-	
Na23	13514	*12*	731	5.4	13724	98
Mg25	-	-	-	-	-	-
Al27	83586	*12*	4057	4.9	82034	102
Si29	-	-	-	-	-	-
P31	84	*12*	12	15	118	71
Ca43	94420	*12*	2696	2.9	95054	99
Sc45	43	*11*	1.0	2.4	43	99
Ti47	6052	*12*	216	3.6	5400	112
V51	339	*12*	9.1	2.7	326	104
Cr53	399	*12*	11	2.8	392	102
Mn55	1293	*11*	26	2.0	1471	88
Fe57	73096	*12*	2460	3.4	80840	90
Co59	54	*12*	2.0	3.7	52	104
Ni60	180	*12*	7.2	4.0	178	101
Cu65	122	*12*	5.5	4.5	119	103
Zn66	100	*12*	9.4	9.4	78	128
Ga69	15	*12*	0.75	4.8	15	103
Ge72	1.4	*12*	0.23	16	1.2	119
Y89	13	*12*	0.81	6.0	14	94
Zr90	13	*12*	0.83	6.4	14	93
Nb93	0.52	*12*	0.03	5.8	0.52	100
Sn120	1.7	*12*	0.10	6.1	2.3	74
Pb208	3.7	*12*	0.37	9.9	3.7	100

5.2 Modelling parameters

Forward modelling involved the software Petrolog (Danyushevsky & Plechov, 2011). The initial melt compositions were taken from Walter (1998) and Sobolev *et al.* (2007) and are presented in Table S5, while the initial oxidation fugacity state for both melts were based on the Borisov & Shapkin (1990) quartz-fayalite-magnetite (QFM) buffer. The crystallisation pressure was set to 7kbar based on best model fit and the upper estimated pressure for the Eyjafjallajökull 2010 eruption from Keiding & Sigmarsson (2012). Clinopyroxene and plagioclase were allowed to crystallise following the model for MORB melts (mostly anhydrous) by Danyushevsky (2001) while olivine was set to crystallise following the model by Herzberg & O'Hara (2002). The partitioning of Ni in olivine was controlled by the model from Herzberg & O'Hara (2002), while the partitioning of Ni into clinopyroxene was at a constant value of 3 based on the findings of Le Roux *et al*. (2011).

Table 5.5 End-member melt compositions used in the forward modelling for olivine compositions from a pyroxenitic and peridotitic-derived source. The peridotitic composition is based on run 30.14 from Walter (1998) and Ni content calculated by Sobolev et al. (2007) while the pyroxenitic melt composition is from Sobolev et al. (2007).

Lithology	SiO_2	TiO_2	Al_2O_3	FeO	MnO	MgO	CaO	Na_2O	K_2O	Cr_2O_3	Ni in ppm
Peridotite	46.91	0.64	12.46	8.86	0.17	18.22	10.86	0.82	0.34	0.43	642
Pyroxenite	52.56	1.07	13.71	8.24	0.117	13.32	8.72	1.79	0.10	0.16	830

5.3 Evaluation of secondary effects on the $^{3}He/^{4}He$ isotopic composition in olivine

We tested for possible helium isotope modifications via secondary (crustal) processes in the suite of samples used for this study to ensure that the variations observed are source controlled rather than secondary. Melts which have experienced degassing and subsequent loss of helium, become more susceptible to contamination from radiogenic ^{4}He, either via crustal contamination or radiogenic in-growth. Addition of atmospheric-derived helium, which would decrease the $^{3}He/^{4}He$, to melts that have undergone significant degree of degassing is also possible (e.g., Harðardóttir *et al.*, 2018). We tested for possible modifications following magmatic evolution by plotting the $^{3}He/^{4}He$ isotopic composition of the olivines used in this study (from Harðardóttir *et al.,* 2018) with their respective Fo content, analysed here for the same sample set (Figure 5.1). Importantly, the lack of any correlation confirms, that any variation recorded in $^{3}He/^{4}He$ is unlikely to be affected by secondary magmatic processes such as fractional crystallisation, here represented by a lowering in Fo content.

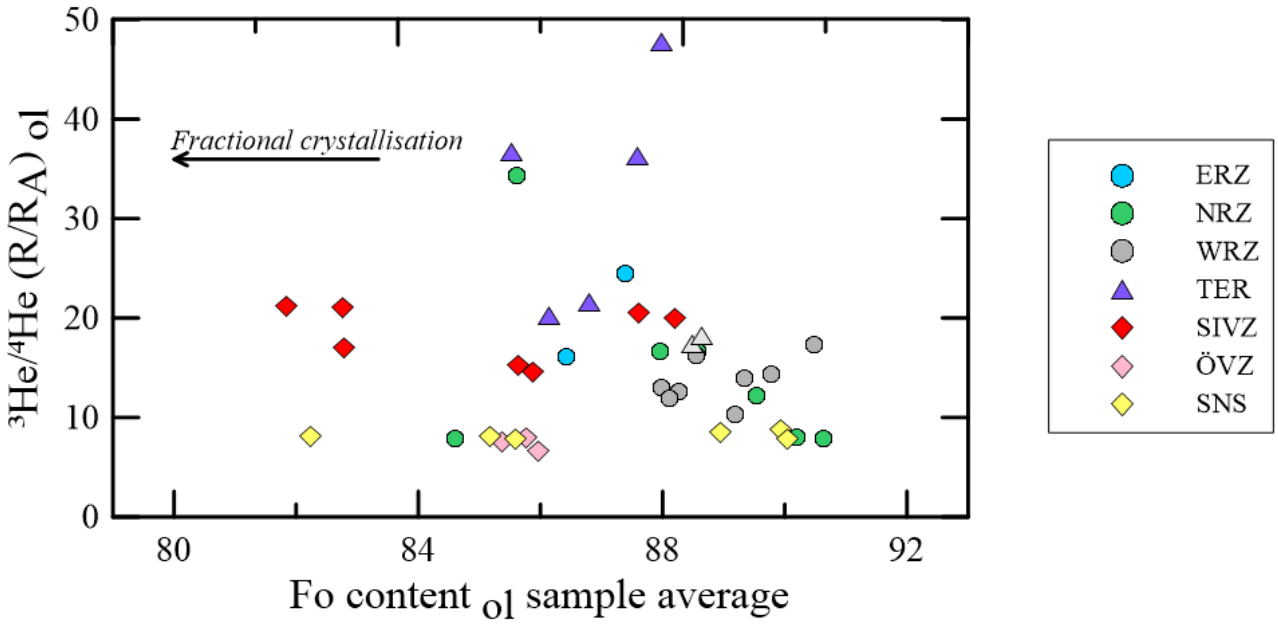

Figure 5.1 A plot of Fo content versus their respective $^{3}He/^{4}He$ for olivines from across Iceland. A lack of correlation confirms that measured $^{3}He/^{4}He$ in the olivine used in this study are unaffected by magmatic processes and rather represent primary mantle-derived variations.

We further evaluated possible effects of degassing on the $^{3}He/^{4}He$ for the specific samples of olivine used in this study by plotting helium concentrations versus $^{3}He/^{4}He$ (similar to Harðardottir *et al*., 2018; Figure 5.2). Again, we observe no correlations between measured $^{3}He/^{4}He$ and He concentration confirming that degassing, which would lower the He concentration, does not affect the He isotope systematics of the olivine targeted in this study. This is in line with the observations by Harðardóttir *et al.*, (2018) for Icelandic olivine.

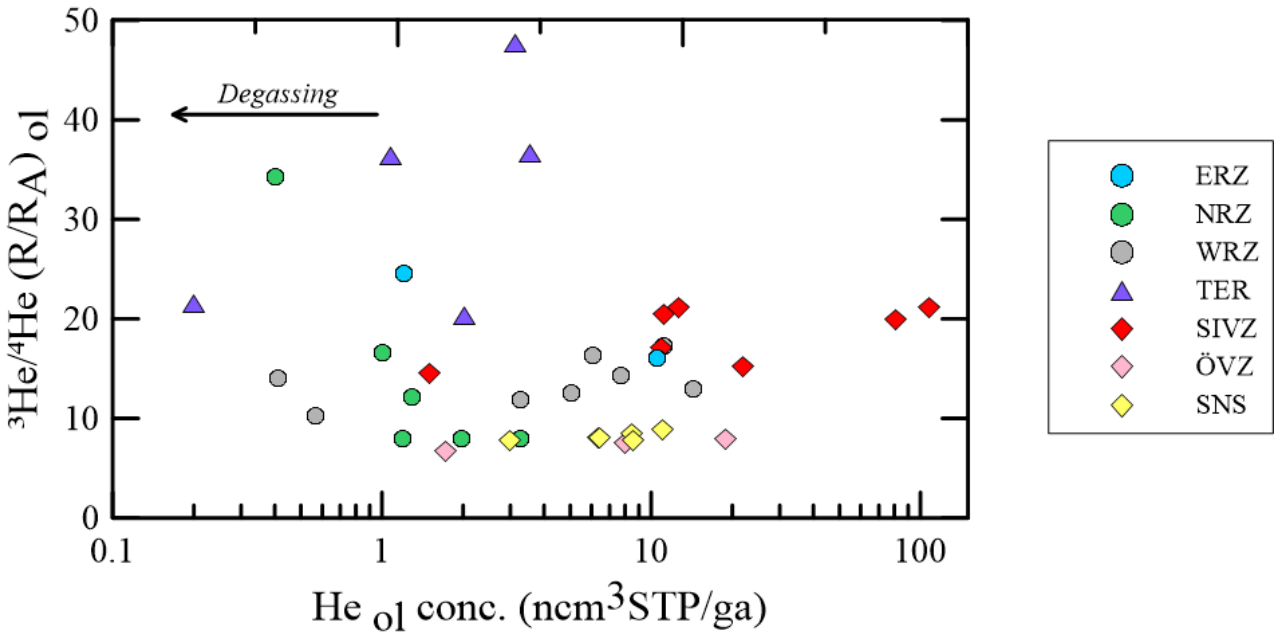

Figure 5.2 A plot of helium concentrations versus $^3He/^4He$ with data compiled by Harðardottir et al. (2018). A lack of correlation suggests that degassing plays no role in controlling the helium isotopes measured in the sample suite used in this study.

5.4 References

Batanova, V. G., Sobolev, A. V., & Kuzmin, D. V. (2015). Trace element analysis of olivine: High precision analytical method for JEOL JXA-8230 electron probe microanalyser. *Chemical Geology, 419*, 149-157.

Borisov, A. A., & Shapkin, A. I. (1990). A new empirical equation rating Fe^{3+}/Fe^{2+} in magmas to their composition, oxygen fugacity, and temperature. *Geochem. Int*, 27(1), 111-116.

Dan yushevsky, L. V. (2001). The effect of small amounts of H_2O on crystallisation of mid-ocean ridge and backarc basin magmas. *Journal of Volcanology and Geothermal Research*, 110(3-4), 265-280.

Danyushevsky, L. V., & Plechov, P. (2011). Petrolog3: Integrated software for modeling crystallization processes. *Geochemistry, Geophysics, Geosystems*, 12(7).

Harðardóttir, S., Halldórsson, S. A., & Hilton, D. R. (2018). Spatial distribution of helium isotopes in Icelandic geothermal fluids and volcanic materials with implications for location, upwelling and evolution of the Icelandic mantle plume. *Chemical Geology*, 480, 12-27.

Herzberg, C., & O'Hara, M. (2002). Plume-associated ultramafic magmas of Phanerozoic age. *Journal of Petrology*, 43(10), 1857-1883.

Jackson, C. G., & Gibson, S. A. (2018). Preservation of systematic Ni and Cr heterogeneity in otherwise homogeneous mantle olivine: Implications for timescales of post-metasomatism re-equilibration. *Lithos,* 318, 448-463.

Keiding, J. K., & Sigmarsson, O. (2012). Geothermobarometry of the 2010 Eyjafjallajökull eruption: New constraints on Icelandic magma plumbing systems. *Journal of Geophysical Research: Solid Earth*, *117*(B9).

Le Roux, V., Dasgupta, R., & Lee, C. T. (2011). Mineralogical heterogeneities in the Earth's mantle: constraints from Mn, Co, Ni and Zn partitioning during partial melting. *Earth and Planetary Science Letters*, *307*(3-4), 395-408.

Sobolev, A. V., Hofmann, A. W., Kuzmin, D. V., Yaxley, G. M., Arndt, N. T., Chung, S. L., Danyushevsky, L. V., Elliott, T., Frey, F. A., Garcia, M. O., Gurenko, A. A., Kamenetsky, V. S., Kerr, A. C., Krivolutskaya, N. A., Matvienkov, V. V., Nikogosian, I. K., Rocholl, A., Sigurdsson, I. A., Sushchevskaya, N. M., & Teklay, M. (2007). The amount of recycled crust in sources of mantle-derived melts. *Science, 316*(5823), 412-417.

Walter, J. M. (1998). Melting of Garnet Peridotite and the Origin of Komatiite and Depleted Lithosphere. *Journal of Petrology*, *39*(1), 29-60

6 Supplementary material for Chapter 3

6.1 Analytical details and data treatment

6.1.1 New EMPA analysis of olivine crystals for bulk laser fluorination $\delta^{18}O$ measurements

A new subset of olivines (i.e., not the same samples used in [Rasmussen *et al.*, 2020]) from the Vestfirðir were placed in crystal mounts and polished for Electron Microprobe Analysis (EMPA). 19 to 54 different olivine crystals (targeting the cores of each crystal) from each sample were characterised for their major and minor element compositions using the Cameca SX-100 electron microprobe (equipped with 5 tunable wavelength dispersive spectrometers) housed at UC Santa Barbara. Operating conditions involved a 40 degree take-off angle, and a beam energy of 20keV. The beam current was 40nA, and the beam diameter was 5 μm. The standards used included MnO synthetic for Mn, Fe_2SiO_4 (synthetic fayalite) for Fe, Ni_2SiO_4 (synthetic) for Ni, Mg_2SiO_4 (magnesium olivine) synthetic for Mg, Si, Diopside (Chesterman) for Ca, Orthoclase MAD-10 for Al, and Chromite (UC # 523-9) for Cr. Oxygen was calculated by cation stoichiometry and was included in the matrix correction. The matrix correction method was ZAF or Phi-Rho-Z Calculations and the mass absorption coefficients dataset was FFAST.

Moreover, seven new sets of crystals from samples from ERZ, SIVZ, NRZ and TER (i.e., crystals not analysed by SIMS or previous high-precision EMPA) were further analysed by EMPA to cover the complete variation of Fo represented within these samples. The measurements were performed using a JEOL JXA-8230 electron microprobe at the Institute of Earth Sciences, University of Iceland on 10-17 crystals from each sample. This instrument has five wavelength-dispersive spectrometers and an energy-dispersive spectrometer with a silicon-drift detector and the electron gun consists of a LaB_6 electron emitter. Springwater Meteorite Olivine (SMO, USNM 2566) was used as an internal standard. The analytical uncertainty for Fo content is based on external measurements of SMO and San Carlos olivine (NMNH 111312-44) and 1SD is less than Fo content ±0.1.

6.1.2 Oxygen isotopic analysis of olivine crystals by Secondary Ion Mass Spectrometry

Instrumental techniques

The *in-situ* $\delta^{18}O_{ol}$ was measured using a CAMECA IMS1280 Secondary Ion Mass Spectrometry (SIMS) instrument at the NordSIMS facility at the Swedish Museum of Natural History in three sessions from the 10-11th of May 2017. Prior to the SIMS measurements, the exact same spots were analysed by high-precision Electron Microprobe Probe Analyser (EMPA, for details see [Rasmussen *et al.*, 2020]). Based on the major and minor element variability (Figure 6.1 and section "Major- and minor elemental variability"), 1-3 grains were analysed for every sample with a minimum of 2-point measurements per crystal (found in data supplement for Chapter 3, T2). Between EMPA and SIMS analysis, the carbon coating used for EMPA measurements was replaced by gold coating (30 nm) following fine 1μm repolishing. The oxygen isotopic values presented in this study are reported relative to V-SMOW in standard delta notation (δ) following equation 3:

$$\delta = \left[\frac{\frac{^{18}O}{^{16}O}_{sample}}{\frac{^{18}O}{^{16}O}_{V-SMOW}} - 1 \right] \cdot 1000 \qquad \text{equation 3}$$

A $^{133}Cs+$ primary beam with an incident energy of 20 keV and current of 2.5 nA was used to sputter secondary ions from the olivine. A small raster (10 μm) was used throughout the analysis to homogenise the critically focussed beam and a low-energy normal incidence electron gun minimised sample charging. Measurement of secondary ions was performed at a mass resolution of 2500 (M/ΔM) using multicollection on Faraday detectors connected to low-noise amplifiers housed in a thermally stabilised, evacuated chamber. The magnetic field was locked with high precision using an NMR field sensor. During the fully automated analytical sessions, reference analyses were carried out regularly following the analyses of six unknowns. Each individual analysis comprised a pre-sputter to remove the Au coat, beam centering, and 64 seconds of data acquisition.

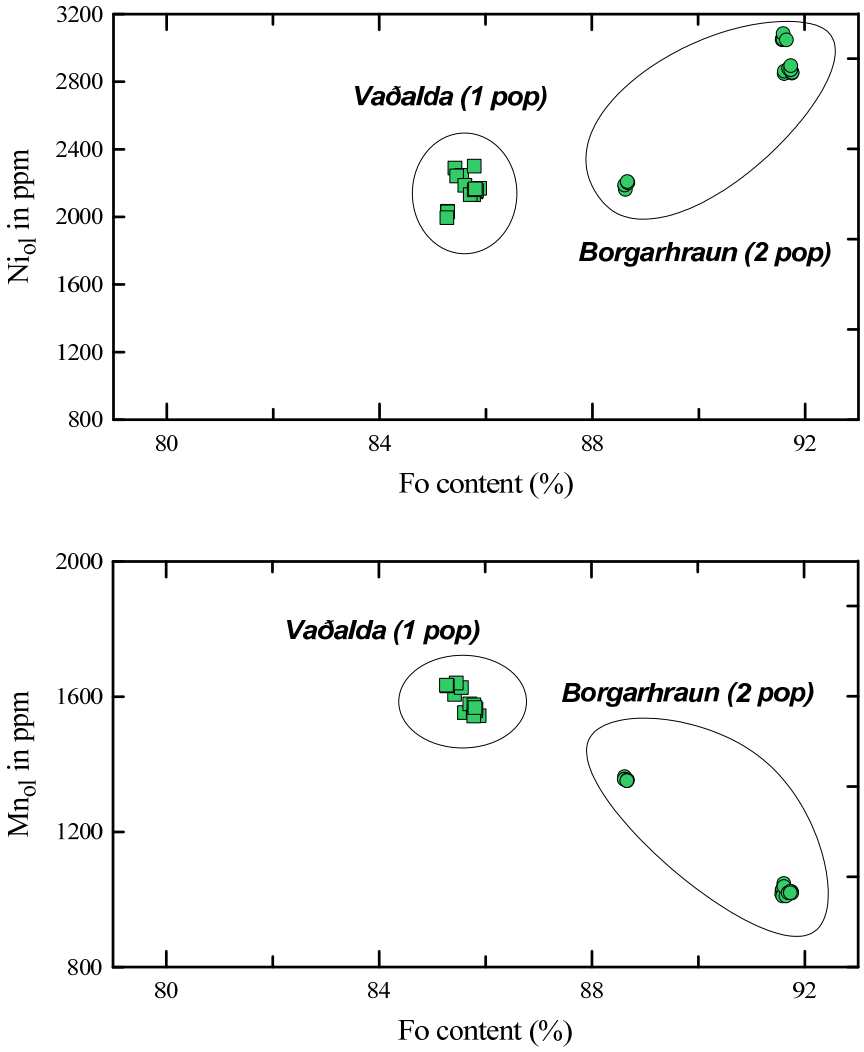

Figure 6.1 Example of sample variability evaluation. Each point represents one analysis. Olivine from Vaðalda indicates that the olivine crystals targeted in this study are homogenous (1 population) whereas olivine from Borgarhraun indicate, that the olivine crystals targeted here represent two chemically distinct populations. This was used to determine the minimum number of in-situ *analyses necessary to represent each sample.*

Standards and standard reproducibility

To avoid the effect of matrix effects, it is important to use olivine with an Fo content similar to that of the unknown samples, although it has recently been shown that there is negligible variation in instrumental mass bias across a range of compositions above Fo_{80} (Isa *et al.*, 2017, Eiler *et al.*, 1997). Corrections for instrumental mass fractionation were made using splits of a San Carlos olivine, supplied by Drs. Jaime Barnes and Edward Marshall, with $Fo_{90.6}$ (determined by EMPA). Importantly, this San Carlos standard has a $\delta^{18}O_{ol}$ value of 5.25‰, determined by laser fluorination, and is thus the same composition as the San Carlos standards used by most other labs (e.g., Bindeman *et al.*, 2008, Eiler *et al.*, 1995). The standard deviation of the San Carlos $\delta^{18}O_{ol}$ value varied slightly between the three sessions, and the external error – reflecting the repeatability for each data point and drift corrections based on regular spaced standard measurements – presented in Table 6.1 is therefore based upon an average of the three sessions.

Table 6.1 Analytical details for San Carlos standard used for SIMS analysis. The average result from three sessions is reported first, followed by individual session standard averages.

$\delta^{18}O_{ol}$ in ‰	**Mean**	***N***	**External error (1SD)**	**Average instrumental error (1SD)**	**Reference value (From [Eiler *et al.*, 1995])**
San Carlos olivine	5.28	*97*	0.14	0.17	5.25
San Carlos olivine first session	5.30	*14*	0.12	0.16	
San Carlos olivine second session	5.25	*35*	0.13	0.16	
San Carlos olivine third session	5.30	*48*	0.15	0.18	

Intra-crystal variability

Overall, very little intra-crystal variability in $\delta^{18}O$ was recorded in the sample suite targeted here. This is reflected in the fact that the average instrumental error is larger than the average intra-crystal variability (0.17 vs 0.14) noted as 1SD (Figure 6.2). The largest intra-crystal variation is recorded in olivine from SNS (up to 0.53 at Fo_{89}) which is related to uniquely more positive $\delta^{18}O_{ol}$ (up to 6.1 ‰). More commonly, however, 1SD varies between 0.1-0.15 (Figure 6.2). As the average instrumental error is larger than the average intra-crystal variation, the instrumental error is used on the individual *in-situ* analysis. Larger variation is recorded within individual samples and so individual intra-sample variation is used as 1SD in Figure 3.3.

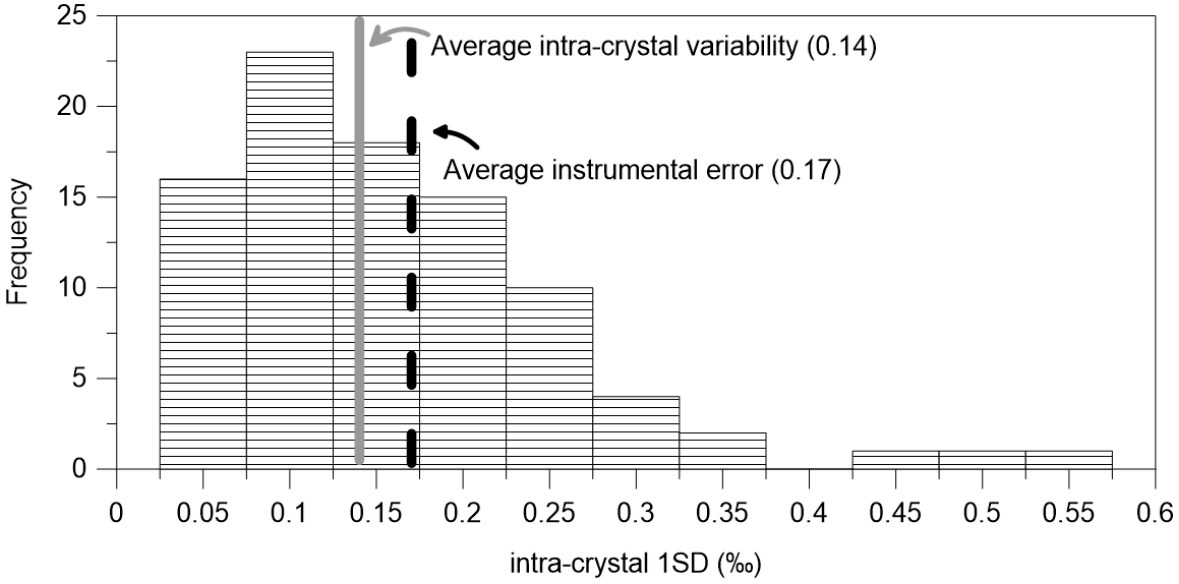

Figure 6.2 Histogram showing the intra-crystal variability in $\delta^{18}O_{ol}$ as 1SD. The high frequency of 1SD well below the average instrumental error (0.17) results in an intra-crystal 1SD below the instrumental error (0.14).

Major- and minor elemental variability

Following *in-situ* measurements of major and minor element compositions, the variations recorded in the olivine populations were evaluated to determine sample homogeneity prior to SIMS analysis. For samples that showed multiple chemical populations, crystals representative of each population were targeted to capture the entire variability. An example of this screening process is shown in Figure 6.1, where olivine from Vaðalda shows little chemical variability whereas olivine from Borgarhraun lavas contain at least two populations with variable Fo content. In both cases, there were no signs of any alteration of the crystal surface. Accordingly, one representative crystal was analysed for Vaðalda with SIMS whereas two crystals were analysed for Borgarhraun, representing both populations.

6.1.3 Oxygen isotopic analysis of olivine crystals by laser fluorination

A subset of samples from NW-Iceland (Vestfirðir), SIVZ, NRZ and ERZ were selected for oxygen isotopic analyses of host olivines by laser fluorination (LF) in the Stable Isotope Laboratory at the University of Oregon. This was done over four analytical sessions. All samples have two to five replicate oxygen isotopic analyses, where different olivines were selected from a sample for each replicate analysis (data supplement for Chapter 3, T3).

Olivine crystals from each sample, some previously crushed to sizes of 500-850 µm, were hand-picked under a binocular microscope. Care was taken to avoid crystals with any visible surface alteration, adhering groundmass or visible crystals/melt inclusions. As indicated in T3 (data supplemental for Chapter 3), most oxygen isotopic analyses consisted of multiple (≥4) olivine crystals being pooled for a single measurement, but some analyses consisted of either just three olivine crystals, two olivine crystals, or even a single olivine crystal. Total olivine masses analysed ranged from 0.80 to 2.11 mg. Prior to analysis, some samples from the Vestfirðir were leached in ~20% HF acid at room temperature for 10-30 min to remove any alteration products or hourglass melt inclusions not visible under binocular microscope. Methods for oxygen isotopic analyses of olivines follow Bindeman *et al*. (2008). Olivines were reacted with BrF_5 to release oxygen, and a 35W CO_2 laser was used. Gas purification followed a cryogenic method using liquid N_2, and a Hg-diffusion pump was used to eliminate any remaining F_2 from the fluorination process. Platinum-graphite was used to convert oxygen to CO_2 for analysis on a MAT253 mass spectrometer. Yields were measured using a baratron gauge, and ranged from 12.63 to 13.8 µmols O_2/mg. San Carlos olivine ($\delta^{18}O$ = 5.25 ‰), Gore Mt Garnet (UWG2, $\delta^{18}O$ = 5.80 ‰, [Valley *et al.*, 1995]), and the University of Oregon Garnet (OUG, $\delta^{18}O$ = 6.52 ‰) were used as standards. The data is reported relative to San Carlos Olivine (SCO) and precision of the measurements is estimated by concurrently running SCO along with the unknowns and recording the variability of this standard. This results in a precision of ± 0.07‰ (1SD) or better based on 4 standards measurements.

6.1.4 Comparison of *in-situ* and laser fluorination $\delta^{18}O$ data

Previous studies clearly established that bulk $\delta^{18}O$ analysis of olivine can skew the overall $\delta^{18}O$ towards values affected by secondary crustal processes, such as assimilation (Bindeman *et al.*, 2008). Therefore, *in-situ* methods are crucial to distinguish intra-crystal variations and target mineral cores unaffected by crustal processes.

The pairing of the methods is especially useful to identify sample heterogeneity. Therefore, we analysed some of the samples by both LF and SIMS and the results are shown in Figure 6.3 and Figure 6.4. Two samples show a significant difference between SIMS and LF measurements (HVIT-1 and HVAMM-2) which likely highlights the heterogeneity present in these two samples.

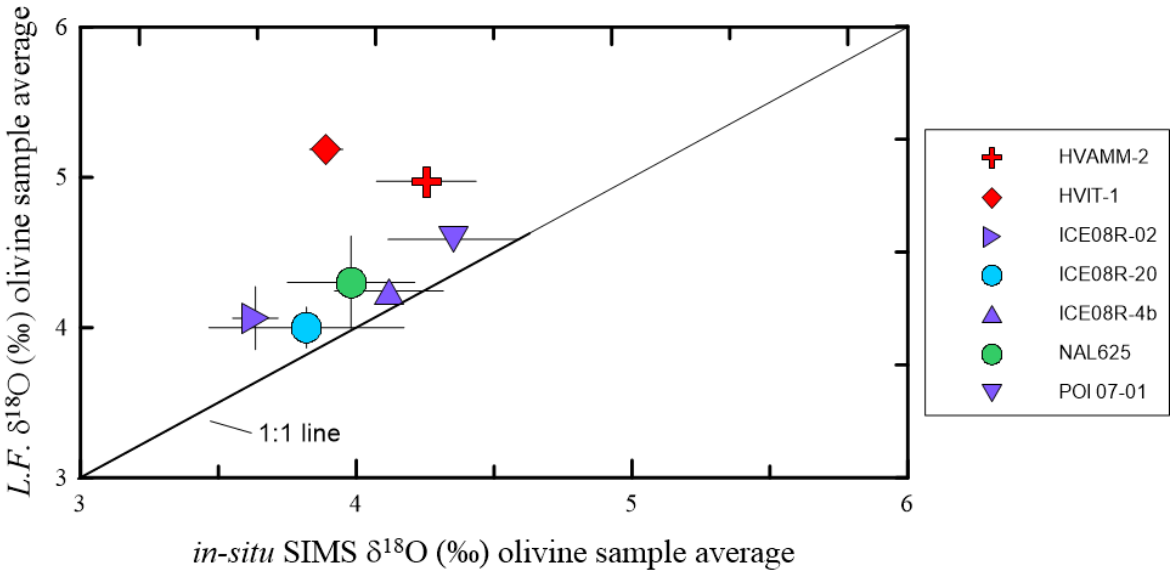

Figure 6.3 Same sample comparison between in-situ and LF-derived data. There is a slight offset between SIMS and LF-derived data which likely reflects heterogeneity within the samples analysed. The 1:1 line is drawn for comparison.

Additional olivines from three locations in the Vestfirðir (TER) were analysed by LF and are presented versus Fo content along with corresponding SIMS measurements in Figure 6.4a. We note here that only two out of 53 measurements reveal olivine compositions that overlap with DMM-derived olivine. These represent two out of 12 measurements performed on olivine from Búrfell that is otherwise characterised by $\delta^{18}O_{ol}$ 4.6 ± 0.1 ‰ (see data supplement for Chapter 3, T3). The variation captured by *in-situ* analysis is larger, suggesting that there is more heterogeneity in these samples than what is reflected by bulk LF data. Therefore, these independent methods of analysing oxygen isotopes, both confirm that low $\delta^{18}O$ values are indeed characteristics for the high-Fo olivine crystals targeted here.

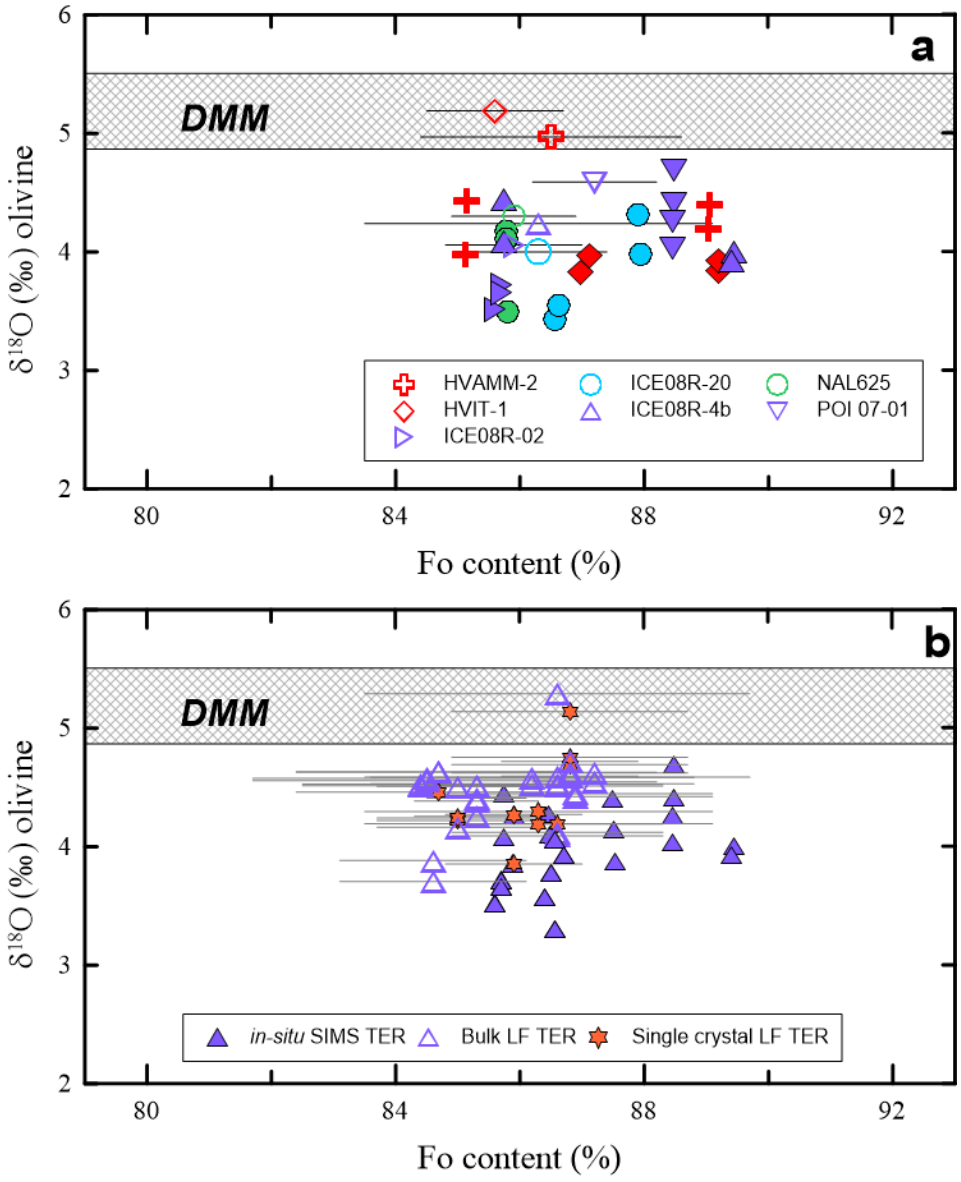

Figure 6.4 Fo content versus laser fluorination and SIMS $\delta^{18}O_{ol}$ measurements. a) A figure compiling the LF and SIMS measurements performed on the same sample separates. The unfilled symbols represent LF-derived data, and the filled symbols represent the SIMS-derived data from the same samples. All LF data points are based on single-crystal measurements except for POI-07-01 where both measurements are based on bulk analysis (see data supplement for Chapter 3). b) A figure compiling all Tertiary (TER) SIMS and LF data that is further divided into bulk and single-crystal LF analysis. Both methods confirm that low $\delta^{18}O$ values are indeed characteristics for the high-Fo olivine crystals targeted here

6.2 Evaluating the effects of crustal processes on $\delta^{18}O_{ol}$

6.2.1 Evidence for oxygen isotope zonation

To test for possible effects on $\delta^{18}O_{ol}$ resulting from combined assimilation and fractional crystallisation (AFC), we analysed two crystals (from ISO1-6 and A29-3) along a transect perpendicular to their core-to-rim forsterite-zonation pattern (Figure 6.5). Sample A29 comes from Hörðufell in the ERZ where there is strong evidence for crustal contamination (Bindeman *et al*., 2008). Similar SIMS analyses were performed by Bindeman *et al*., (2008) who found a positive correlation between $\delta^{18}O_{ol}$ and Fo content caused by AFC processes, and this data is also plotted in Figure 6.5. We observe no such correlation in our transects. The lack of correlation between a lowering of Fo content (down to Fo_{81}) and $\delta^{18}O_{ol}$ in the two selected transects suggests that AFC processes are thus not important for these samples. However, as diffusion of Mg and Fe is several orders of magnitude faster than O (Gérard & Jaoul, 1989; Spandler & O'Neill, 2010), corresponding zonation patterns could also be generated by diffusion rather than melt evolution, in which case we would not expect to see the coupled decrease in $\delta^{18}O_{ol}$ with Fo.

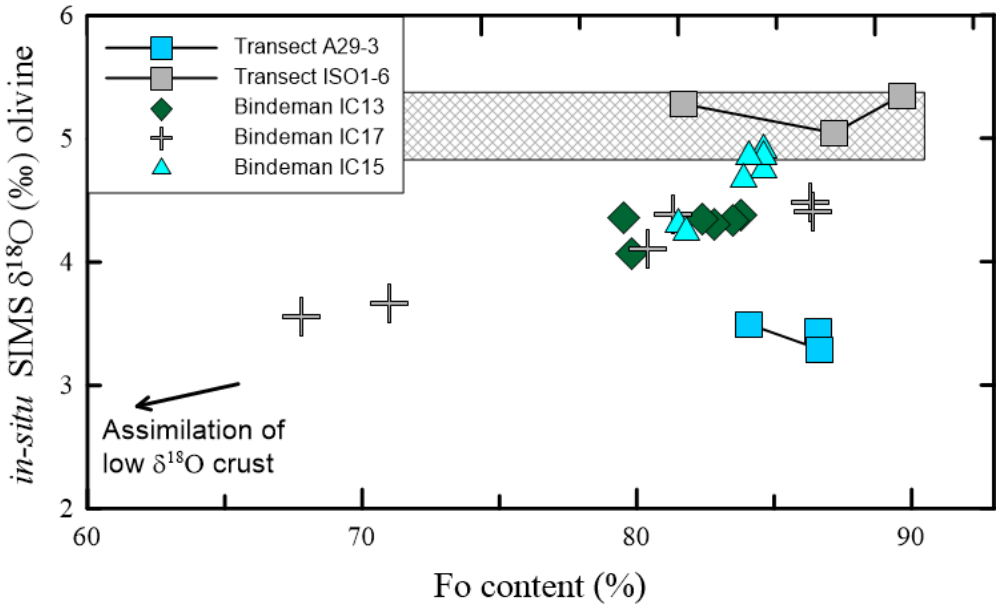

Figure 6.5 Transect analysis of crystals with zoned Fo contents (from this study and Bindeman et al. [2008]). The lack of positive correlation in the new dataset implies that coupled fractional crystallisation and assimilation play a minor role in the $\delta^{18}O_{ol}$ variation captured in this study.

6.3 Integrity of helium isotope data

Radiogenic ingrowth of ^{4}He occurs with time, i.e. as the heavy radiogenic parents (e.g., ^{238}U, ^{235}U, ^{232}Th, ^{147}Sm) undergo alpha-decay. Hence, radiogenic ingrowth of ^{4}He following eruption would result in a lowering of $^{3}He/^{4}He$. Because of this, measuring $^{3}He/^{4}He$ in old samples, where radiogenic ingrowth has occurred over a significant amount of time, can result in $^{3}He/^{4}He$ values that underestimate the actual source $^{3}He/^{4}He$.

The $^{3}He/^{4}He$ values in neovolcanic basalts from Iceland can be attributed a primary source control as these samples are too young for radiogenic ingrowth of ^{4}He to have a significant effect in most samples. However, this is not necessarily the case for $^{3}He/^{4}He$ values of Miocene basalts. To evaluate the effect that post-eruptive radiogenic ingrowth has had on the TER samples analysed in this study, we have compiled the literature data that measures the $[^{4}He^{*}]/[^{4}He]_{crushed}$ (where $[^{4}He^{*}]=[^{4}He]_{melt}$ $1\text{-}R_{melt}R_{crush}$, Graham *et al.*, 1998) along with the $^{3}He/^{4}He$ values, as these distinguish ^{4}He trapped in fluid- and melt inclusions ($[^{4}He]_{crushed}$) and He produced by radiogenic ingrowth in the matrix ($[^{4}He^{*}]$) (see methods in [Hilton *et al.*, 1999]). Only TER samples with previously determined $[^{4}He^{*}]/[^{4}He]_{crushed}$ below 20 were used in Figure 3.3. The source literature along with the $[^{4}He^{*}]/[^{4}He]_{crushed}$ is listed in data supplement for Chapter 3, T3.

6.4 References

Bindeman, I., Gurenko, A., Sigmarsson, O., & Chaussidon, M. (2008). Oxygen isotope heterogeneity and disequilibria of olivine crystals in large volume Holocene basalts from Iceland: Evidence for magmatic digestion and erosion of Pleistocene hyaloclastites. *Geochimica et Cosmochimica Acta, 72*(17), 4397-4420.

Eiler, J. M., Farley, K. A., Valley, J. W., Stolper, E. M., Hauri, E. H., & Craig, H. (1995). Oxygen isotope evidence against bulk recycled sediment in the mantle sources of Pitcairn Island lavas. *Nature, 377*(6545), 138-141.

Eiler, J. M., Graham, C., & Valley, J. W. (1997). SIMS analysis of oxygen isotopes: matrix effects in complex minerals and glasses. *Chemical Geology, 138*(3), 221-244.

Gérard, O., & Jaoul, O. (1989). Oxygen diffusion in San Carlos olivine. *Journal of Geophysical Research: Solid Earth, 94*(B4), 4119-4128.

Graham, D. W., Larsen, L. M., Hanan, B. B., Storey, M., Pedersen, A. K., & Lupton, J. E. (1998). Helium isotope composition of the early Iceland mantle plume inferred from the Tertiary picrites of West Greenland. *Earth and Planetary Science Letters, 160*(3), 241-255.

Hilton, D. R., Grönvold, K., Macpherson, C. G., & Castillo, P. R. (1999). Extreme $^{3}He/^{4}He$ ratios in northwest Iceland: constraining the common component in mantle plumes. *Earth and Planetary Science Letters, 173*(1-2), 53-60.

Isa, J., Kohl, I., Liu, M.-C., Wasson, J., Young, E., & McKeegan, K. (2017). Quantification of oxygen isotope SIMS matrix effects in olivine samples: Correlation with sputter rate. *Chemical Geology, 458*, 14-21.

Rasmussen, M. B., Halldórsson, S. A., Gibson, S. A., & Guðfinnsson, G. H. (2020). Olivine chemistry reveals compositional source heterogeneities within a tilted mantle plume beneath Iceland. *Earth and Planetary Science Letters, 531*, 116008.

Spandler, C., & O'Neill, H. S. C. (2010). Diffusion and partition coefficients of minor and trace elements in San Carlos olivine at 1,300 C with some geochemical implications. *Contributions to Mineralogy and Petrology, 159*(6), 791-818.

Valley, J. W., Kitchen, N., Kohn, M. J., Niendorf, C. R., & Spicuzza, M. J. (1995). UWG-2, a garnet standard for oxygen isotope ratios: strategies for high precision and accuracy with laser heating. *Geochimica et Cosmochimica Acta, 59*(24), 5223-5231.